PB81-205957

A Lidar Polarimeter Technique for Measuring Suspended Solids in Water

Texas A and M Univ., College Station

Prepared for

Environmental Monitoring Systems Lab.
Las Vegas, NV

May 81

U.S. Department of Commerce
National Technical Information Service
NTIS

TYPING GUIDE SHEET
BEGIN FIRST LINE OF TEXT HERE
CENTER OF PAGE
TOP OF IMAGE AREA
DROPPED HEAD BEGIN SECTIONS HERE

EPA-600/4-81-036
May 1981

PB81-205957

A LIDAR POLARIMETER TECHNIQUE FOR MEASURING SUSPENDED SOLIDS IN WATER

by

D. W. Presley and R. W. Newton
Remote Sensing Center
Texas A&M University
College Station, Texas 77843

Grant No. R 806351010

Project Officer

D. T. Wruble
Advanced Monitoring Systems Division
Environmental Monitoring Systems Laboratory
Las Vegas, Nevada 89114

ENVIRONMENTAL MONITORING SYSTEMS LABORATORY
OFFICE OF RESEARCH AND DEVELOPMENT
U.S. ENVIRONMENTAL PROTECTION AGENCY
LAS VEGAS, NEVADA 89114

BEGIN LAST LINE OF TEXT
BOTTOM OF IMAGE AREA OUTSIDE DIMENSION FOR TABLES AND ILLUSTRATIONS
3/8"

PRODUCT OF:
NATIONAL TECHNICAL INFORMATION SERVICE
U.S. DEPARTMENT OF COMMERCE
SPRINGFIELD, VA. 22161

EPA-287 (Cin.)
(4-76)

DISCLAIMER

This report has been reviewed by the Environmental Monitoring Systems Laboratory, U.S. Environmental Protection Agency, and approved for publication. Approval does not signify that the contents necessarily reflect the views and policies of the U.S. Environmental Protection Agency, nor does mention of trade names or commercial products constitute endorsement or recommendation for use.

TECHNICAL REPORT DATA

(Please read Instructions on the reverse before completing)

1. REPORT NO. EPA-600/4-81-036	2.	3. RECIPIENT'S ACCESSION NO. PB81 205957
4. TITLE AND SUBTITLE A LIDAR POLARIMETER TECHNIQUE FOR MEASURING SUSPENDED SOLIDS IN WATER		5. REPORT DATE May 1981 6. PERFORMING ORGANIZATION CODE
7. AUTHOR(S) D. W. Presley and R. W. Newton		8. PERFORMING ORGANIZATION REPORT NO.
9. PERFORMING ORGANIZATION NAME AND ADDRESS Remote Sensing Center Texas A&M University College Station, Texas 77843		10. PROGRAM ELEMENT NO. 11. CONTRACT/GRANT NO. R 806351010
12. SPONSORING AGENCY NAME AND ADDRESS U.S. Environmental Protection Agency--Las Vegas, NV Office of Research and Development Environmental Monitoring Systems Laboratory Las Vegas, NV 89114		13. TYPE OF REPORT AND PERIOD COVERED Final 14. SPONSORING AGENCY CODE EPA/600/07

15. SUPPLEMENTARY NOTES

D. T. Wruble, Advanced Monitoring Division, Environmental Monitoring Systems Laboratory, Las Vegas, NV 89114, Project Officer

16. ABSTRACT

This study investigates the capability of the lidar polarimeter to measure the concentration of suspended solids in water for a variety of measurement conditions. Previous laboratory and field measurements have demonstrated the potential of the system to measure turbidity, transmittance and suspended solids under field conditions. The instrument measures two orthagonally polarized components of laser energy back-scattered from a scene which in this study is sediment-laden water.

The results of the data analysis show the direct dependence of the back-scattered measurements to scattering particle concentration for all of the measurement conditions examined. This direct dependence confirms the ability of the lidar polarimeter to measure suspended solids in water. However, further laboratory measurements and field experiments to better determine particular particle effects are recommended.

17. KEY WORDS AND DOCUMENT ANALYSIS

a. DESCRIPTORS	b. IDENTIFIERS/OPEN ENDED TERMS	c. COSATI Field/Group

18. DISTRIBUTION STATEMENT RELEASE TO PUBLIC	19. SECURITY CLASS *(This Report)* UNCLASSIFIED	21. NO. OF PAGES 191
	20. SECURITY CLASS *(This page)* UNCLASSIFIED	22. PRICE

EPA Form 2220-1 (Rev. 4-77) PREVIOUS EDITION IS OBSOLETE

ABSTRACT

The ability to measure the quality of water in U.S. lakes, reservoirs and rivers to detect deterioration due to continued industrial growth and urban development has become increasingly important in the past decade. The lack of efficient cost-effective measurement techniques hampers measurement of the parameters that qualtitatively describe the aqueous environment. This study investigates the capability of the lidar polarimeter to measure the concentration of suspended solids in water for a variety of measurement conditions.

The lidar polarimeter is an in situ instrument that measures two orthogonally polarized components of laser energy backscattered from a scene. In this study the scene is sediment-laden water. Previous laboratory and field measurements have demonstrated the potential of the polarimeter to measure turbidity, transmittance, and suspended solids under field conditions.

Backscatter measurements were made from water as a function of concentration of sediment from three different soil-related particles to examine the effects of particle characteristics, water surface roughness and the presence of organic suspended solids on the like-polarized and cross-polarized backscattered lidar energy. The size, shape and color of the scattering particles were varied during the experiment.

Results confirmed that lidar polarimetry can be used to measure suspended solids concentrations in water. Backscattered energy is directly depended on particle concentrations for a wide range of soil colors and particle size. However, particle characteristics do have an effect on the backscattered energy at both higher and lower particle concentrations. Irregular particle shape affects sensitivity at very low concentrations. Size does not greatly affect the depolarization ratio. Color effects are particularly evident at higher particle concentrations, reaching a point where the backscattered energy does not increase for additional increases in the particle concentration. Small scale water surface roughness and the presence of a low concentration of organic (algal) suspended solids do not directly affect the backscattering process.

Further laboratory measurements and field experiments are needed to better determine particular particle effects.

TABLE OF CONTENTS

Abstract iii

List of Figures vii

INTRODUCTION 1
  In Situ Measurements 1
  Historical Review. 2
    Lidar Polarimeter Development at TAMU. 2
    Summary of Results 5
  Report Objectives. 5
  Scope of Report. 6

BACKGROUND 7
  Water Quality. 7
  Remote Sensing Measurements. 7
    Passive Techniques 8
    Active Techniques 9
  Turbidity. 11
  Suspended Solids 12
    In Situ Measurement. 12
    Sedimentation. 13
  Pollutant Transfer 13

EXPERIMENTS 16
  Dichromatic Lidar Polarimeter. 16
    Transceiver. 16
    Signal Processor 18
  Measurement Configuration. 18
  Concentration Measurements 18
    Sample Description 20
    Particle Size Distribution 24
    Measurement Procedure. 28
  Algae Measurements 28
  Surface Roughness Measurements 30
  Depth of Measurement 31

DATA REDUCTION 32
  Cross Section Calculation. 32
  White Target Calibration 33
    Optical Alignment. 33
    White Target Cross Section 33

TABLE OF CONTENTS (Cont'd)

RESULTS. 37
  Scattering Phenomena 37
  Discussion of Measurements 43
    Sediment Concentration 43
      Particle Shape 44
      Particle Color 49
      Extinction Depth of Measurement. 58
      Size Distribution. 62
    Algae Measurements 62
    Surface Roughness. 71
  Instrumental and Measurement Artifacts 76
    Clear Water Offsets. 76
    Effects of Tank Bottom. 81
    Particle Settling. 81

CONCLUSIONS AND RECOMMENDATIONS. 92
  Conclusions. 92
  Recommendations. 93
    Laboratory Measurements. 93
      Scattering Measurements. 94
      Scattering Model 95
      Measurement Procedure. 96
    Field Measurements 97
      Location 97
      Ground Truth Information 97
      Lidar Design Rationale 98

REFERENCES 99

APPENDIX A 102
APPENDIX B 132
APPENDIX C 138
APPENDIX D 150
APPENDIX E 155

LIST OF FIGURES

Figure Page

1 Dichromatic Lidar Polarimeter System 17
2 Measurement Tanks. 19
3 Micrographs of White Sand Particles. 21
4 Micrographs of White Silt/Clay Particles. 22
5 Micrographs of White Clay Particles. 23
6 Micrographs of Red Silt Particles. 25
7 Micrographs of Brown Silt Particles. 26
8 Particle Size Distributions for Each Sediment Type 27
9 Scattering from Sediment Laden Water 29
10 White Target and Transmitted Power Measurements. 36
11 Approximate Relative Size Distribution for Dow Plastic Pigment 722 (after Sheives [6]). 39
12 Photomicrograph of Dow Plastic Pigment 722 (after Sheives [6]) .39
13 Comparison of Depolarization Ratio as a Function of Field of View and Latex Particle Concentration (after Sheives [6]). . .40
14 Approximate Relative Size Distribution for Dupont TFE 30 (after Sheives [6]). 41
15 Photomicrograph of Dupont TFE 30 (after Sheives [6]) 41
16 Graph of Depolarization Ratio as a Function of Teflon Particle Concentration (after Sheives [6]). 42
17 Depolarization Ratio Versus Sediment Concentration for White Silt Measured at 632 nm. .45
18 Depolarization Ratio Versys Sediment Concentration for White Silt Measured at 442 nm. .46
19 Depolarization Ratio Versus Sediment Concentration for Red Silt Measured at 632 nm 47
20 Depolarization Ratio Versus Sediment Concentration for Red Silt Measured at 442 nm 48
21 Depolarization Ratio Versus Sediment Concentration for Brown Silt Measured at 632 nm 50
22 Depolarization Ratio Versus Sediment Concentration for Brown Silt Measured at 442 nm 51
23 Cross Section Versus Sediment Concentration for Red Silt Measured at 632 nm 54
24 Cross Section Versus Sediment Concentration for Red Silt Measured at 442 nm 55
25 Cross Section Versus Sediment Concentration for Brown Silt Measured at 632 nm 56
26 Cross Section Versus Sediment Concentration for Brown Silt Measured at 442 nm 57

LIST OF FIGURES (Continued)

Figure Page

27 Measurement Depth as a Function of White Silt Sediment Concentration. 59
28 Measurement Depth as a Function of Red Silt Sediment Concentration. 60
29 Measurement Depth as a Function of Brown Silt Sediment Concentration. 61
30 Depolarization Ratio Versus White Clay and Silt Concentration Measured at 632 nm 63
31 Depolarization Ratio Versus White Clay and Silt Concentration Measured at 442 nm 64
32 Cross Section Versus White Silt and Clay Concentration Measured at 632 nm. 65
33 Cross Section Versus White Silt and Clay Concentration Measured at 442 nm. 66
34 Depolarization Ratio Versus Algae and Sediment Concentration Measured at 632 nm 67
35 Depolarization Ratio Versus Algae and Sediment Concentration Measured at 442 nm 68
36 Cross Section Versus Algae and Sediment Concentration Measured at 632 nm. 69
37 Cross Section Versus Algae and Sediment Concentration Measured at 442 nm. 70
38 Depolarization Ratio Versus White Silt/Clay Sediment Concentration and Surface Roughness Measured at 632 nm 72
39 Depolarization Ratio Versus White Silt/Clay Sediment Concentration and Surface Roughness Measured at 442 nm 73
40 Cross Section Versus Sediment Concentration and Surface Roughness for White Silt/Clay Measured at 632 nm 74
41 Cross Section Versus Sediment Concentration and Surface Roughness for White Silt/Clay Measured at 442 nm 75
42 Cross Section Versus White Clay Sediment Concentration Measured at 632 nm. 77
43 Cross Section Versus White Clay Sediment Concentration Measured at 442 nm. 78
44 Cross Section Versus White Silt/Clay Sediment Concentration Measured at 632 nm 79
45 Cross Section Versus White Silt/Clay Sediment Concentration Measured at 442 nm 80
46 Depolarization Ratio Versus White Silt/Clay Sediment Concentration Measured at 632 nm 82
47 Depolarization Ratio Versus White Silt/Clay Sediment Concentration Measured at 442 nm 83
48 Cross Section Versus White Sand Sediment Concentration Measured at 632 nm. 85
49 Cross Section Versus White Sand Sediment Concentration Measured at 442 nm. 86
50 Cross Section Versus White Silt Sediment Concentration Measured at 632 nm. 87

LIST OF FIGURES (Continued)

Figure Page

51 Cross Section Versus White Silt Sediment Concentration Measured at 442 nm. 88
52 Cross Section Versus White Silt and Clay Sediment Concentration Measured at 632 nm 89
53 Cross Section Versus White Silt and Clay Sediment Concentration Measured at 442 nm 90

CHAPTER I

INTRODUCTION

The lakes, rivers and coastal regions of the United States make up a very complex, dynamic ecosystem. This aqueous environment can be described in quantitative terms by water quality parameters, which describe the physical, chemical and biological characteristics of the water environment. The gradual deterioration of the water quality in the United States has been caused by many factors including the continued growth and industrial development of the nation. Due to the concern of many environmentalists and the general public, government involvement in the study and control of water quality has increased in the past decade. The government agencies whose duties include water quality determination have often been hampered in the execution of this responsibility due to the lack of efficient measurement techniques. The ability to make water quality measurements in real time and at a reasonable cost would greatly aid in the study of the dynamic water environment.

The techniques currently used for water quality determination typically rely on manpower-intensive methods of direct sampling and laboratory analysis. For some types of analysis no other method is available or could provide better results. However, for continuous sampling or coverage of large areas, direct sampling can fail to give an accurate measure of the water quality in the field due to insufficient sampling to monitor the dynamics of the ecosystem and changes in the sample caused by the delay of the analysis. Other disadvantages include inconsistent sampling techniques by personnel in the field and the cost of maintaining and moving a large number of people in the area being sampled. The majority of the cost for a project of this nature is often the expense of personnel [1].

IN SITU MEASUREMENTS

In situ measurements have in certain cases helped alleviate some of these problems. By performing analysis at the sample site with portable or automated measurement equipment, the time delay between sampling and analysis can be greatly decreased or eliminated. These methods have proven effective for some applications where a limited number of water quality parameters are of interest. However, several disadvantages still affect the cost effectiveness of these measurements: the number of technically experienced personnel in the field is increased, and the cost of moving personnel and equipment and to cover large areas with in situ sensors is restrictive. Continued research and improvements in the areas of in situ sensors will help to lower the cost of the equipment, increase the ruggedness of the sensors for field applications and expand the number of parameters that can be measured.

To better develop this particular area of water quality measurements, the U.S. Environmental Protection Agency (EPA) cosponsored the Automated In Situ Water Quality Sensor Workshop in February of 1978 [1]. The EPA cosponsored this workshop with the National Oceanic and Atmospheric Administration (NOAA) and the Interagency Working Group on Satellite Data Collection Systems. The participants represented all of the federal agencies and organizations currently involved with in situ water quality sensors. The workshop established communication between the many agencies involved in this area. It was also emphasized that the actual water quality sensor was the least developed of the large number of systems needed to collect water quality data.

The responsiblities of the workshop included a review of the current applications of sensors in the research and development activities represented. Similarities and overlaps, as well as gaps, in the sensor requirements and development activities were examined with the possibility of cooperative efforts also being identified. The technological capabilities of the electrochemical, electrophysical, optical and automated wet chemical areas were reviewed to identify the measurement parameters that can currently be measured and the areas where research would be of best benefit. The need for automated in situ water quality sensors was emphasized by the wide range of purposes and requirements of the many agencies represented. The workshop recommendations were of particular benefit in pointing out 1) the benefit of cooperation between agencies, 2) the common problem areas and 3) the high potential technological areas. The development of the lidar polarimeter for automated measurement of sediment concentration was identified as a high potential, high technology area. This study is a direct result of the workshop recommendations to further pursue this particular area of automated, in situ water quality measurements.

HISTORICAL REVIEW

The lidar polarimeter is a remote sensing device that has high potential for use as an airborne or automated in situ water quality measurement tool [2]. The lidar polarimeter is a "laser radar" that has the capability of measuring two orthogonally polarized components of the energy backscattered from a target.

A linearly polarized laser illuminates a target, typically a volume of water. A receiver collects the energy scattered back toward the instrument and separates the return into two orthogonally polarized components. The like-polarized return is polarized in the same plane as the transmitted laser beam. The cross-polarized return is measured in a plane orthogonal to the transmitted polarization. The depolarization ratio is defined as the cross-polarized return divided by the like-polarized return. Several studies conducted at the Remote Sensing Center of Texas

A&M University (TAMU) have examined the potential of the lidar polarimeter in the measurement of water quality.

Lidar Polarimeter Development at TAMU

The depolarization of laser light was investigated in a study by Wilhelmi, Mayo and Rouse [3]. A lidar polarimeter using a 5 mw He-Ne (632 nm) laser was constructed. Measurements were made of the polarized return from laboratory simulations of turbid water using spherical Teflon particles as scatterers. The motivation for these measurements was to test the hypotheses that: 1) the depolarization of the incident laser energy was due to the particulate material in the water and 2) the amount of depolarization would indicate the relative concentration of scattering particles. The laboratory measurements supported both hypotheses and established the potential of measuring suspended solids, turbidity and transmissivity using a lidar polarimeter.

A subsequent investigation by Mayo, Wilhelmi and Rouse [4] using this same device examined finite beam effects in laboratory and daylight measurements of turbid water, again using Teflon particles as the scattering material. The results of this study indicated that a lidar polarimeter can measure true volume reflectance from a target with negligible interference from sunlight and sky reflectance. The depolarized backscattered component was found to be more sensitive than the like-polarized component to the concentration of both scattering and absorbing materials in the water.

In this study also it was determined that the depolarization ratio was less affected by surface waves than either the like- or cross-polarized returns and that the depolarization ratio is independent of transmitted power and other system constants. These two advantages indicated the depolarization ratio could prove more useful for water quality measurements than either the like- or cross-polarized returns alone.

A theoretical development by Wilhelmi [5] related the polarized and depolarized backscattered energy from both a rough surface and a smooth surface to single scatter surface and multiple scatter subsurface effects. Laboratory tests to verify the validity of this model included measurements from both cast dielectric targets with known surface roughness characteristics and laboratory simulations of turbid water (a diluted casein solution). The returns predicted by the model and the measured results had correlation coefficients greater than 0.90. This high correlation confirmed the multiple volume scattering mechanism assumed in the model development.

The model was further extended by Sheives [6] to include a single scattering from the subsurface. Sheives also modeled oil on water as a lossy dielectric over a turbid water background. Laboratory measurements confirmed that single scattering should not be ignored, except at very high concentrations of scattering particles. The scattering particles used in this experiment were polystyrene latex spheres and a Teflon resin dispersion. Both particles have well defined shape and size distribution characteristics.

Measurements of different types of oil floating on simulations of turbid water were also made [6]. The results of the oil film experiments confirmed the oil on water model, showed that the depolarization ratio was not significantly changed by a homogeneous oil film, and showed that the attentuation due to the oil was a function of oil type, film thickness and transmitted wavelength. Based on the last result, a technique using two wavelengths was recommended which could not only detect oil on water, but also indicate the type of oil and estimate the thickness of the film.

Sheives [6] also conducted field measurements from a bridge over the Brazos River and from a boat in the Houston Ship Channel and lower Brazos River. The validity of the proposed models was confirmed for conditions encountered in the field experiments. The like- and cross-polarized returns were found to vary directly with "turbidity" and suspended solids and inversely with transmittance. The field tests supported the use of the lidar polarimeter in measuring these water quality parameters.

In subsequent investigations, a dual wavelength lidar polarimeter was constructed by the Remote Sensing Center [7] using a He-Ne laser (632 nm) and a He-Cd laser (442 nm) to support a Coast Guard-funded effort to develop an oil spill detection device. Several system modifications improved the operation and data quality of this dichromatic system over the previous single wavelength lidar polarimeter. An interface to a minicomputer provided real time data reduction to further facilitate the acquisition of data. The blue wavelength was added to take advantage of the higher index of refraction of oils at this wavelength. The additional wavelength increase the sensitivity to turbidity levels and provided the potential for identifying oil type and measuring oil thickness.

An extensive measurement program was undertaken to evaluate system performance. Laboratory measurements of turbid water confirmed the model validity for the second wavelength and established the operational curve of the instrument for a wide range of scattering particle concentrations. The scattering particles used in these measurements were the same type polystyrene spheres and Teflon particles used in previous experiments. Field tests were then made to further evaluate the system performance in a field environment and verify the operational characteristics in field conditions. Additional laboratory measurements were then conducted to confirm the oil detection capability of the system over a wide range of oil types and thicknesses and background scattering concentrations. The system operated well under all conditions including worst-case sun angles.

The field measurements proved the lidar polarimeter to be a viable method of monitoring the water quality in harbors and inland waterways. The results of the laboratory tests proved that the shorter blue wavelength was more sensitive than the red wavelength to thin films of petroleum products and lower concentrations of the Teflon and polystyrene scattering particles. Later measurements of two natural water samples indicated that the blue wavelength was also more sensitive to lower concentrations of natural scattering particles [8]. These results indicated the helium-cadmium source to be a near ideal wavelength for the monitoring of "turbidity" and the detection of oil spills.

An Active Spill Detection System (ASDS) was designed and constructed based on the performance evaluation of the dichromatic system [9]. A single helium-cadmium laser was used in the ASDS as the transmitter (.442 nm wavelength). This system was designed to automatically monitor a bay or harbor area for oil spills, over an extended period of 6 months to a year with little maintenance. Scan capability was included to increase the monitoring area. The blue wavelength was used to give maximum sensitivity to thin oil films. However the environmental constraints required to properly house the delicate He-Cd laser greatly increased the complexity of the system. A micro-processor performed the necessary data reduction and system management for automatic spill detection which included control of the scan feature. Several problems were encountered during field tests of the system due primarily to subsystem failure and the lack of a hardened blue laser. However, the field tests confirmed the oil detection capability and the versatility of the microprocessor-based, algorithm implementation.

Summary of Results

The laboratory mesurement studies cited above have contributed greatly to an understanding of the backscattering phenomena at visible wavelengths. The significant results of these studies are summarized below.

Backscattered energy is a result of both single and multiple scattering by the particulate material in the water. The depolarized component of the return is due to only multiple scattering in the water volume.

Measurements have shown that the depolarization ratio (defined as the cross-polarized return divided by the like-polarized return) is less affected by surface waves than either of the individual terms. Any output power fluctuations do not affect the ratio since both cross and like terms are equally affected. These results indicate that the depolarization ratio is possibly the best measurement parameter for correlation with concentration of suspended scatterers in the water volume.

The blue wavelength of the helium-cadmium laser is excellent for scattering measurements. When compared to the red wavelength, the return from the blue laser is more sensitive to lower concentrations of scattering particles and to attenuation by thin oil films of the more transparent oil products. These characteristics make the blue wavelength excellent for both oil detection applications and scattering measurements. However, the convective cooling and delicate housing of this type of gas-discharge laser make it a less than optimum device for field applications. The environmental constraints of the blue laser make a hardened blue source necessary for field applications of this particular wavelength.

The field experiments have verified some of the results of the laboratory measurements for field conditions and proven the lidar polarimeter to be a viable method of making in situ water quality measurements.

REPORT OBJECTIVES

Most of the laboratory measurements described above have been made using Teflon particles and polystyrene spheres. These scatterers have a very uniform, "well behaved" shape and a narrow size distribution. The particles encountered in field measurements are more variable in shape and have a wider size distribution. The parent material and resulting color also cover a wide range.

Before a lidar system can be developed to measure suspended particles in water, several conditions and the magnitude of their effect on the lidar return must be examined closely. These conditions include the concentration and physical characteristics of the scattering particles, the surface roughness of the water, and the presence of organic suspended solids (algal). The purpose of this research is to investigate the effect of these conditions on lidar backscattering. Specifically, the objectives of this research are to: 1) measure the effects of the concentration of sediment particles on lidar backscatter measurements, 2) determine the effects of particle characteristics, water surface roughness and the presence of organic suspended material (algal) on the lidar returns, 3) make a comparison of the experimental results to expected theoretical results to verify and/or further develop an analytical model that can be used to predict the measurement capability of the sensor under a variety of sediment load conditions, and 4) provide a system design rationale for a lidar polarimeter to measure the concentration of sediment particles in water.

SCOPE OF REPORT

This study is concerned with the capability of a lidar polarimeter to measure the concentrations of suspended solids in water. A wide variety of techniques has been used to make similar water quality measurements using remote and in situ sensors. The first sections of Chapter II provide a background in these measurement techniques. The importance of suspended solids in sedimentation and pollutant transfer are discussed in Chapter II.

The lidar polarimeter system used in this study is described in Chapter III along with a discussion of the experimental design rationale and a description of the experiments. Chapter IV explains the analysis of the data which includes the reduction of the data to lidar cross section and the calibration of the returns using white target measurements. The results of the data analysis are discussed in Chapter V. The conclusions and recommendations are given in Chapter VI, as well as a discussion of a design rationale for a lidar polarimeter system to be used to measure the concentration of suspended solids in water.

CHAPTER II

BACKGROUND

WATER QUALITY

Water quality is the condition of the water in a lake, reservoir or waterway. This condition is usually associated with some use such as recreation, a source for drinking water or navigation. Water quality parameters are a quantitative description of the characteristics of the water. Typically, these parameters can be separated into physical, chemical, and biological groups. Physical water quality parameters include clarity, color, and the acoustic properties of the water. Biological parameters are related to the organisms in the water, such as the concentration of phytoplankton, chlorophyll or coliforms. Chemical water quality parameters include the concentration of pollutants or dissolved substances and the salinity of the water. Often the groups are dependent. For example, the color of water is affected by the concentration of different types of algae.

Physical water quality parameters are often the most convenient measurements to make using in situ or remote sensing methods. The dependence of the physical properties on other parameters allows these measurements to be used to estimate a wide range of useful water quality measurements.

REMOTE SENSING MEASUREMENTS

The field of remote sensing has shown considerable promise in the measurement of many water quality parameters. Remote sensing techniques are used to measure the characteristics of water at visible, infrared, or microwave frequencies. The spectral characteristics of reflected light or the scattering of microwave energy can be related directly or indirectly to many water quality parameters, including the concentration of phytoplankton, chlorophyll or suspended solids in the water, or the presence of a contaminant such as oil on water. These techniques are especially useful for measurements that are to be made over a large area. Few methods of measurements give the synoptic view available from remote sensing measurements. Some techniques, such as the airborne fluorosensor or remote lidar bathymeter allow a large number of point samples to be recorded rapidly [10].

Two disadvantages limit the usefulness of remote sensing measurements. First, some techniques require a large amount of post-processing which prevents real-time observations of some water quality parameters. Second, the indirect nature of some measurements permits only qualitative measurements to be made. Additional measurements are often necessary to provide the required information needed to increase the accuracy of the measurements.

Passive Techniques

Passive methods of remote sensing measure the backscattered solar energy from a scene. This type of remote sensing includes photography, and radiometric and spectroradiometric measurements.

Photography is the simplest method of remote sensing. The advantages of photography, which include large ground coverage, good spatial resolution, and the flexibility of being able to use different filters and types of film, make this method very versatile in measuring water quality.

One of the first applications of photography was the mapping of turbidity plumes caused by both industrial wastes and the natural influx of rivers into lakes and bays. One study of the San Francisco Bay using a UV filter and color film examined a turbidity plume for approximately a year [11]. Aerial observations from light aircraft recorded the extent and movement of sediment laden water discharged into the San Francisco Bay by the Sacramento San Joaquin River system. During some seasons, the suspended sediment pattern was visible only from the air. Thermal radiometer measurements for aircraft were also used to map isothermal regions in the bay. These temperature characteristics represented a more integrated record of the thermal plume caused by the influx of water. The aerial measurements enabled an effective determination of the seasonal changes in the flow rates of the water discharged into the bay and the circulation of the water in the estuary. Both factors are important when developing physical or chemical models of the estuary system and surrounding coastal waters.

Another type of passive remote sensing is the measurement of ocean color using spectroradiometer. The spectral response of energy from below the surface of the ocean is measured as a function of wavelength. The input energy into the ocean is both direct sunlight and sky reflectance. The transfer function of the ocean as a function of wavelength can then be computed from the input and output measurements. This technique determines the scattering and absorbing properties of the ocean due to the particulate and dissolved material in the water. A ratio of the transfer function at two particular wavelengths can be used as a measure of the chlorophyll concentration in the ocean. Curran [12] examined the transfer function models, the effects of atmospheric scattering and the accuracy of the spectroradiometric measurements required to assure meaningful measurements of ocean color from a satellite. Preliminary measurements from aircraft at two altitudes showed good correlation with the predicted values of ocean color.

Another theoretical study by Kattawar and Humphreys [13] determined the effect of chlorophyll on the ratio of upwelling to downwelling radiance and irradiance from an atmosphere-ocean system. A Monte Carlo simulation program computed the desired output parameters as a function of wavelength, altitude above the ocean, depth within the ocean, chlorophyll concentration, turbidity, and solar zenith angle. The program uses several cross section parameters which describe the scattering and absorption characteristics of both the atmosphere and ocean mediums for both Rayleigh and Mie particles, as well as absorption by ozone in the atmosphere. The effect of chlorophyll was included in the program by introducing the absorption of chlorophyll in the cross section parameters. The irradiance and radiance ratios can then be computed at any position in the system for a given set of conditions. Different heights or particular wavelength ratios can then be observed to determine the characteristic behavior of the system. This study concluded that: 1) the absorption characteristics should allow chlorophyll to be measured by both remote and in situ systems, though turbid water could mask lower concentrations of chlorophyll, 2) a three filter system at appropriate wavelengths could distinguish the chlorophyll when turbidity was due to other substances, and 3) an airborne system should be flown as close to the water surface as possible, to decrease the noise from reflected skylight.

Ritchie, Schiebe and McHenry [14] utilized a spectroradiometer to measure the incident and reflected solar radiation from six reserviors in northern Mississippi. These measurements were made from a height of 20 to 50 cm above the water surface from a boat. The concentration of suspended sediment was also measured from collected surface water samples. The sun angle was calculated for each set of measurements. Data equivalent to that recorded by LANDSAT as calculated by integrating the area under the reflected solar radiation spectra between the regions of 500 to 600 nm, 600 to 700 nm, 700 to 800 nm and 800 to 1100 nm. A linear least squares routine was used to determine the correlation coefficients between the spectral measurements and the concentration of suspended sediments. The best spectral region to determine the concentration of suspended solids from measurements of the reflected solar radiation was found to be 700 to 800 nm. Sun angles within 40° of solar noon were also found to improve the correlation coefficients. This study indicated that it should be possible to quantitatively determine suspended sediments in surface waters from remote platforms.

Merry [15] reported a study of Lake Powell, Utah, in 1975, which correlated airborne spectroradiometer measurements with surface water characteristics. Field measurements included percentage of light transmittance, surface temperature, pH, and Secchi disk depth. Water samples taken at four locations were analyzed to determine the composition and concentration of the suspended particulate material. The multispectral data for the airborne spectroradiometer were analyzed for the four water sampling locations. The comparison of the multispectral data and the water sample characteristics showed that: 1) as the percentage of light transmittance of the water samples decreased, the reflected radiance increased and, 2) as the suspended sediment concentrations (mg/l) increased, the reflected radiance increased in the 1-mg/l to 80-mg/l range. The reflected radiance measured at a wavelength of 0.58 μm was directly correlated to the suspended sediment concentration. From the results of this study, the airborne multispectral measurements were shown to relate valuable qualitative information on the surface turbididy of Lake Powell.

Active Techniques

Active methods of remote sensing transmit energy toward a target and measure the amount of energy that is reflected or scattered back toward a receiver. These types of techniques include laser flouorosensor, radar and lidar (laser radar) measurements.

The development of the laser greatly influenced the field of remote sensing. Several applications of the laser in the area of water quality measurements have proven the ability of these systems to make in situ and remote water quality measurements. These measurements include temperature and sea state determination, the detection of oil spills and the concentration of algae of suspended solids in water [10].

The property of fluorescence exhibited by chlorophyll-a has provided an effective method of measuring the concentration of phytoplankton in natural water. The laser made possible these types of measurements from airborne platforms. The EPA has been involved in airborne measurements using a fluorosensor system for several years [16]. This system uses a flashlamp pumped dye laser and a telescope receiver. The return signals are detected using a gated photomultiplier tube, digitized and recorded on a nine-track tape. The photomultiplier signal is also displayed on an oscilloscope to measure aircraft altitude. The system is mounted in a helicopter for convenient airborne measurements.

Field tests have been conducted with this system over Lake Mead, Nevada. Las Vegas Wash which flows in to Lake Mead, receives both treated and untreated sewage from Las Vegas, resulting in a reasonable variation in algae concentration for airborne measurements. Buoys mark the flight line as well as ground truth sample locations. Surface water samples taken in an area around each buoy were mixed to remove patchiness in the algae concentration. The concentration of chlorophyll-a in five different subsamples of each mixed surface water sample was determined using spectroscopic or fluorometric methods. The airborne fluorescence signals were corrected for slight variations in aircraft altitude and laser power level. Linear correlation coefficients between the normalized fluorosensor measurements and the mean chlorophyll-a concentration of the surface water samples ranged from 0.77 to 0.95 for five different flights.

A major factor that directly affects fluorosensor measurements is the volume of water that is illuminated by the laser. This volume varies due to scattering and absorption by suspended solids and high concentrations of algae in the water. One method of remotely connecting for variations in the volume of water illuminated by the laser is to measure the Raman emission concurrently with the fluorescence signal. The Raman emission is only a function of the water illuminated by the laser. As the volume decreases due to scattering, the Raman emission also decreases. The EPA system has been modified by the addition of another photomultiplier channel filtered at the proper wavelength to measure the Raman signal.

Preliminary measurements have shown that the fluorescence signal can be corrected for variation in sample volume by using the Raman returns.

Another fluorosensor system developed by NASA Langley [17] further utilizes the property that distinct color groups of algae exhibit different spectral response to the input energy which causes fluorescence. Particular input wavelengths can thus be chosen to maximize the fluorescence of a particular color group. A unique four-color dye laser is used to input energy at the required wavelengths. The fluorescence at 685 nm caused by each input wavelength is then measured. A matrix inversion technique then relates the fluorescence and corresponding concentration of chlorophyll-a associated with each different color group of algae. In situ and airborne measurements have been made with good correlation to ground truth data.

TURBIDITY

One of the water quality parameters that is often measured is turbidity. This parameter is an indication of the clarity of the water. Turbidity is related to the extinction length of light in water. Attempts to correlate turbidity measurements with the concentration of suspended solids have met with limited success.

Transmissometers, nephelometers, or a combination of the two, are used to measure turbidity. Transmissometers measure the attenuation of light through the water between a light source and a detector a particular distance apart. These instruments are usually submersed in the water to be measured and often give a profile of transmissivity as a function of depth. They are particularly sensitive to organic dyes that absorb light [18].

Nephelometers or scattering meters measure the amount of light that is scattered from the particulate material in water for one or more angles. Laboratory models of scattering meters measure the light scattered (usually at 90°) from a small sample or a flow of water through the instrument. Other instruments are submersible in the water to be measured. Different configurations of these meters measure the scattering for a wide range of angles. Some models measure only one angle which could be 45°, or a very small angle, less than 10°. Other meters measuring the scattering at a set of angles, for example 45°, 90°, and 180°. Still other models are adjustable, to be set depending on the conditions to be measured. The advantage of multiple angles or a variable angle is related to the size distribution of the particles to be measured [18].

Some instruments are a combination of both the transmissometer and nephelometer configurations. These meters, which are usually submersible, simultaneously measure both the scattering and attenuation of light by material in the water. This type of instrument can be used to correct the measurement of scattering for the absorption by the water or the effects of deposits on the detector and source windows [18].

A field study conducted by the USDA [19] determined the accuracy of a turbidimeter in measuring suspended sediment concentration. This turbidimeter using a photocell measures the amount of light which passes through a thin falling stream of water. A pumping-type sediment sampler provided water during a runoff event for both the turbidimeter and sediment samples. Besides normal flow measurements, samples were also measured as a function of particle size. Several different samples were fractionated by sedimentation and decantation (using Stokes Law) at six arbitrarily selected sizes. Each decanted fraction was measured with the turbidimeter. After the successive fractionation was completed, the samples were recombined and analyzed for size distribution, using pipette analysis.

The turbidimeter's accuracy in measuring suspended sediment concentration was not good. The inaccuracy was attributed to the lack of sensitivity to the larger sediment sizes. The results of this study indicate that turbidimeters are generally not suitable for determining the total sediment concentrations. However, the findings of the size measurements indicate that they may be useful where predominantly fine material is of interest.

A workshop on turbidity was sponsored by the National Oceanographic Instrumentation Center of the National Oceanographic and Atmospheric Administration (NOAA) in May of 1974 [20]. The findings of this workshop determined that the term turbidity was ambiguous. The measurement of turbidity was of a qualitative nature and could not be directly related to the concentration of the suspended solids without additional information concerning particle shape, size distribution, and index of refraction. Instrument to instrument comparisons of turbidity measurement were valid only when proper transfer functions and calibration procedures were used. Attempts to infer the concentration of suspended solids from turbidity measurements without considering the effects of particle shape, size distribution, and index of refraction were found to be misleading or incorrect.

SUSPENDED SOLIDS

The concentration of suspended solids is a water quality parameter that is of particular importance for several reasons, including the relocation of sediment by rivers and the dependence of pollution transfer on the suspended solids carried by rivers. Gravimetric methods of measuring the suspended solids in water are widely used. The amount of suspended particulates in water has several effects on the physical characteristics of water. The clarity of the water quickly decreases as the amount of particulates in the water increases, especially for very small particles. In municipal water sources this contaminant must be removed by filtering or settling before the water can be used. In natural bodies of water, the amount of sunlight that is available to aquatic plants is greatly reduced by suspended solids in the water. A high concentration of very fine particles increases the severity of these effects since settling takes longer, filtering requires finer filters that restrict flow, and sunlight is further reduced [21].

In Situ Measurement

Suspended solids are usually measured by gravimetric methods. The suspended solids are filtered out of a water sample and then dried. The sediment in a sample can also be flocculated to quickly settle the suspended material and then decanted to remove the excess water. The remaining sediment is then dried. In both cases the dried sample is carefully weighed. For a known volume of water, the concentration of suspended solids is then computed in milligrams per liter (mg/l).

Less direct methods of measuring suspended solids have been used with limited success. The optical attenuation and scattering methods previously described generally report the measurements in optical units such as Jackson Turbidity Units (JTU) or Nephelometer Turbidity Units (NTU). The transfer functions needed to convert these optical units into concentrations of suspended solids in mg/l are not available. The qualitative nature of these methods limits their usefulness in measuring the actual concentration of suspended solids.

Sedimentation

The concentration of sediment in rivers is important for several reasons. A high concentration of sediment in rivers can be used as a tracer for nonpoint sources of pollution such as some geological formations or large clear cut areas. Since soil erosion is one of the main sources of sediment in rivers, the study and control of soil erosion and surface runoff can be directly assisted by the measurement of sediment in rivers. Monitoring the sedimentation of reservoirs and navigational channels as well as the effects of dredging operations can also be assisted by the measurement of sediment, which is relocated by rivers.

Pollutant Transfer

The measurement of suspended solids is also an important means of determining the potential pollutant transfer capabilities of a river. Several studies have indicated that pollutant transfer downstream is dependent on the sediment content of the river as a transportation medium. The transport mechanism of hydrocarbons, trace metals and heavy metals, particularly mercury, have been examined. In each case, the transportation by different mechanisms were all associated directly with the suspended solids in the water [22]-[25].

Heavy metals are a serious pollution problem due to their tendency to accumulate. These pollutants are toxic to fish and accumulate not only in the aquatic food chain but also bottom sediments. Even for very low effluent concentrations, the elevated levels which can accumulate on suspended particles or in bottom sediment are a potential health hazard [22].

Cranston and Buckley [23] evaluated a method to analyze the total mercury in solution, suspended particulate material and bottom sediments for nonindustrial river and estuary system (LaHave River, Nova Scotia). Water samples, suspended solids filtered from water, and grab samples of bottom sediment were taken at several locations in the river and estuary. One sample was separated into four size ranges, three of which were less than 60 μm. The highest concentration of mercury in the bottom sediment was associated with the very fine clay fraction (less than 4 μm). More than 80% of the total concentration of mercury was associated with the two size ranges of particles less than 20 μm in size. The mercury content of each size range was found to increase linearly with the log of the mean specific surface area for the three size ranges less than 60 μm. This result confirmed the hypothesis that the absorption of mercury was related to the specific surface area of the particles.

The concentration of lead, mercury, zinc, copper, nickel, cobalt, iron, manganese, and chromium in the bottom sediment of the Ottawa and Rideau Rivers was examined by Oliver in 1971 [22]. A large number of samples was take at 2 mile intervals along particular stretches of both rivers. The purpose of the study was to locate heavy metal discharges into the river using the accumulation in the bottom sediment as a long term record of continued discharge. In the analysis of the samples, the average concentrationof heavy metals in the silt fractions (less than 62 μm) was found to be significantly higher than the average for the samples with particles from 500 μm to 2000 μm. To compare different locations, the specific area of the sample was taken into consideration to determine if a particular sample had an unusually high concentration of contaminants. A high correlation between surface area and metal concentration for all metals except mercury was explained by the larger surface area and associated increase in the adsorptive capacity of the finer fractions. Industrial wastes, municipal sewage and snow contaminated by automobile exhaust were mentioned as the sources of the pollutants.

A study to determine the mechanisms of transport for the trace metals, iron, nickel, copper, chromium, cobalt and manganese in the Yukon and Amazon Rivers was reported by Gibbs in 1973 [24]. The mechanisms examined were: 1) in solution, 2) by adsorption, 3) in solid organic material, 4) as metallic coatings, and 5) in detrital crystalline material. The results of this study showed that 70% to 80% of the time these trace metals were transported by a combination of metallic coatings and incorporation in the crystalline structure of the particles. Only chromium and manganese had significant proportions transported by solution. Ninety-five percent (95%) of each of the other metals was transported by the mechanisms associated with the suspended solids in the river.

The effluents of a municipal wastewater secondary treatment plant on the Providence River were sampled over a one year period by Van Vleet and Quinn [25]. Surface water and bottom sediment were also sampled once during the same year at four locations along the river. Samples were analyzed for the presence of hydrocarbons in solution or for those associated with suspended solids. The suspended solids were further separated into the hydrocarbons associated with the organic materials, humic and fulvic acid and lastly the residual hydrocarbons. The test showed that approximately 90% of the hydrocarbons in the outflow were associated with the suspended solids and subject to rapid deposition in the bottom sediments after entering the river. This rapid deposition was also evident from the surface water and bottom sediment samples taken close to the outfall and downriver. This study showed that sewage from wastewater treatment plants is a major contributor to the oil pollution in this nation, and that this oil is transported largely by suspended solids from the original entry location into the river.

All of these studies have shown that suspended solids in rivers are the major transportation mechanism for trace metals, heavy metals and hydrocarbons. In the case of the heavy metals, the amount of contaminants in the sample was dependent on the specific surface area of the suspended material. The trace metals were shown to be transported in metallic coatings and also incorporated into the crystalline structure of the suspended materials. As mentioned in both of these studies, the composition and size of the particles are significant characteristics that affect the transportation of these pollutants. The larger surface area of the smaller size particles increases the potential amount of contaminant that can be transported, whether by absorption or coating.

Due to the greater surface area and resulting increase in pollutant transportation ability, the small suspended particles (less than 20 μm) are very important in the study of pollutant transfer. Since particles of this size settle very slowly, very little turbulence is required to maintain the particles in suspension. As a result, the likelihood that the particles are close to the surface is very high. Actually, the clay-sized particles are more or less evenly distributed in the flow of most natural waters [26]. A sensor, such as a lidar polarimeter, can thus measure the concentration of these supended solids in the entire water column from surface measurements. Valuable information can be collected in this manner on the pollutant transfer potential of a river or stream.

CHAPTER III

EXPERIMENTS

Several experiments were necessary to examine the effects of different measurement conditions on the lidar return from sediment laden water. The conditions that were examined were the concentration, size distribution, and color of the sediment particles, as well as surface roughness and the presence of organic suspended material. The depth of water that contributed to the backscattering was also determined for most of the above conditions. The laboratory measurements were designed to isolate the different conditions and determine their effect on the lidar return. The measurement configuration was also designed to simulate realistic measurement conditions as closely as possible. This section describes these experiments.

DICHROMATIC LIDAR POLARIMETER

The instrument in this investigation is a dual wavelength, dual polarized laser backscatter system [7] also called a dichromatic lidar polarimeter (Figure 1). Two laser beams are modulated and transmitted toward a target. A receiver collects the backscattered energy, separates the polarization components for both wavelengths and detects their magnitudes. A signal processor demodulates and scales the signals, converts the data to a digital representation, and combines the data with identification information to be serially transmitted to a mini- or micro-computer [27].

Transceiver

The two lasers used in this system are a 5 mw, helium-neon laser at 632 nm (red) and a 15 mw, helium-cadmium laser at 442 nm (blue). Due to long term aging effects, the transmitted powers were approximately 4.25 mw for the red laser and 1.5 mw for the blue laser. Both of these lasers are linearly polarized with vertical polarization being transmitted. Tuning fork choppers modulate the red laser at 690 Hz and the blue laser at 870 Hz to permit signal separation after detection, as well as synchronous demodulation. Two mirrors shift the blue output to allow near coaxial transmissions of the two laser beams. The mirror mounts are also adjustable for positioning the blue laser for proper optical alignment of the system.

The receiver is built around a threaded extension tube which allows

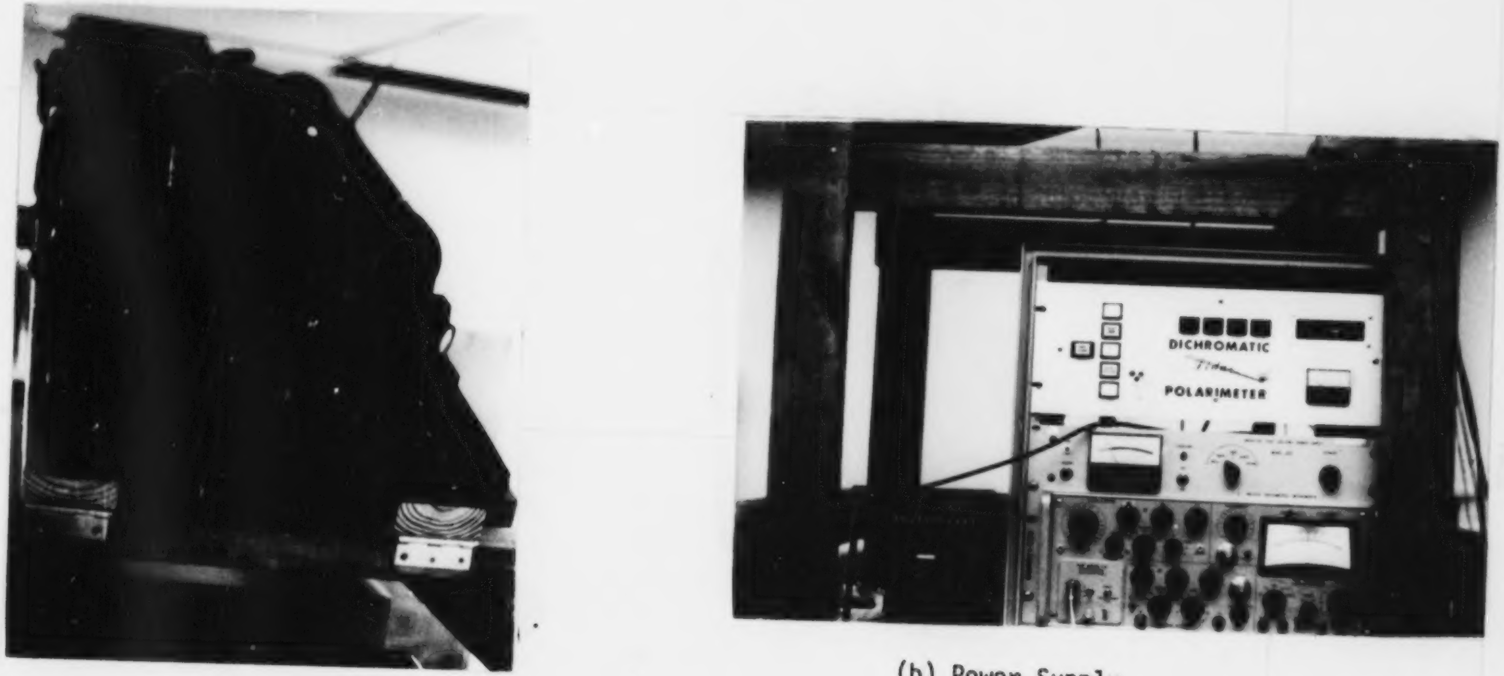
DICHROMATIC
POLARIMETER

(a) Optical Head

(b) Power Supply

Figure 1: Dichromatic lidar polarization system

precision mounting of the optical components. A 250 mm telephoto lens collects the energy backscattered toward the receiver. A pinhole mount directly behind the telephoto lens permits the field of view of the receiver to be decreased if desired. A small recollimating lens directs the energy from the telephoto lens through 1-nm laser line filters to remove background interference. A polarization splitting cube (calcite crystal) separates the energy into cross- and like-polarization components. Photomultiplier tubes (PMTs) detect these returns for processing.

Signal Processor

The signals from the two photomultiplier tubes are preamplified and then multiplexed together. Two electronic bandpass filters centered at the chopper frequencies separate the red and blue returns. The signals corresponding to each wavelength are demodulated individually to separate the vertical and horizontal polarizations. A reference signal from the chopper driver is used to detect the peak of the returns. A synchronous sample and hold circuit converts the signal to a DC voltage proportional to the return energy. The two channels (red and blue) are then multiplexed back together and converted to a digital representation. The signal for each polarization/color combination is then time averaged or integrated for sixteen sample periods. The data is then combined with identification information, formatted for a standard EIA interface and serially transmitted to a mini- or micro-computer for further processing. A controller produced the timing signals for the proper operation of the multiplexors, digital integrator and formatter circuits. The total integration time of the signal processor is 23 milliseconds for the red channel and 15 milliseconds for the blue channel.

MEASUREMENT CONFIGURATION

Most of the measurements described in this section were made using a large fiberglass tank, Figure 2a. The dimensions of the tank (120 cm x 106 cm x 60 cm, 700 liters) were as large as available space would permit. The large size of the tank allowed extinction lengths of five feet (1/5 meters) to be measured for very low concentrations of scattering particles. The inside of the tank was painted with grey epoxy paint to prevent any contamination of the water by fiberglass particles. The inside, bottom, back, and sides of the tank were given a second coat of black epoxy paint to decrease any reflections inside the tank, Figure 2b. Black fur absorbers were used to decrease the reflections of the unscattered laser beams at the bottom of the tank and the water surface reflected beams behind and above the tank. The range of the measurements were 3.8 m at an incident angle of 72° from nadir. The high incident angle was necessary due to the large tank and the area available for the measurements.

Two sets of measurements (the high concentration of the red and brown particles) were made in a 160 liter settling tank. The range for these measurements was 4.1 m at an incidence angle of 72°. For both of these

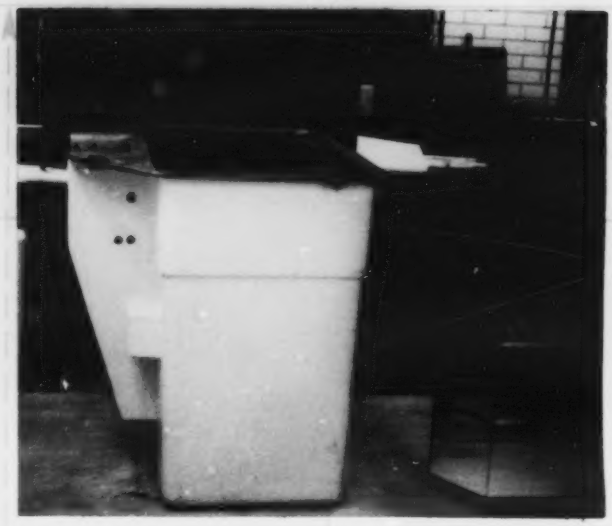

(a) Measurement and settling tanks

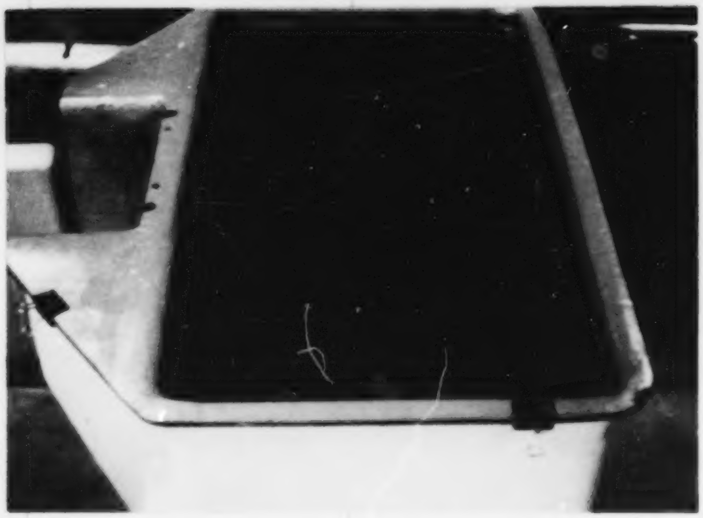

(b) Inside of Measurement tank painted with epoxy paint

Figure 2. Measurement tanks

tanks a circulation pump was used to keep the particles in suspension throughout the measurements.

CONCENTRATION MEASUREMENTS

To determine the different effects of particle characteristics on the backscattered return, several parameters were varied. These included: 1) varying the concentration of the suspended particles over a very wide range, 2) changing the particle size distribution, and 3) using different types of sediment. As mentioned earlier, the experiments were designed to isolate the separate effects as much as possible.

Sample Description

To examine the effects of different types of particles, three different soil-related particles were used as scatterers in this experiment. These three soil types were a white ceramic clay from South Texas, a red clayey soil from North Central Texas, and a brown clayey soil from the Brazos River flood plain. Many of the previous backscatter experiments had used polystyrene or Teflon particles for scattering measurements. These soil particles were chosen to better simulate actual sediment particles encountered in field measurements.

The definition of clay in the above description is with respect to the actual composition of the particles, i.e., mineral silicates of the smectite and chlorite groups. The word clay will also be used in conjuncion with "sand" and "silt" to describe the size of the particles. All of the particles are actually of a clay composition, with sand, silt, and clay size ranges.

The white clay sample was a commercially available ceramic clay (bentonite) consisting largely of smectite. The size of these particles ranged from approximately 75 μm down to less than 1 μm. To determine the effect of different particle sizes, this particular soil type was separated into three different size ranges. The different settling rates for particles of different sizes were used to separate the particles into the different size ranges. The size ranges were sand (75 to 30 μm), silt (30 to 5 μm), and clay (5 to 1 μm). These ranges correspond closely to the very fine sand (100 to 50 μm), silt (50 to 2 μm), and clay (less than 2 μm) size ranges used by the USDA. The slight differences were due to the available sample and a slightly more restricted size range needed for the measurements.

Micrographs of the different white particles are shown in Figures 3, 4 and 5. The irregular shape of the particles for all three sizes can be seen in these micrographs. The extremely small particles which were not completely removed from these samples are also shown in these micrographs. These micrographs of the different soil samples were made using a scanning electron microscope at the Electron Microscopy Center of Texas A&M University. The size of the particles in the micrographs was chosen to be as representative of the samples as possible.

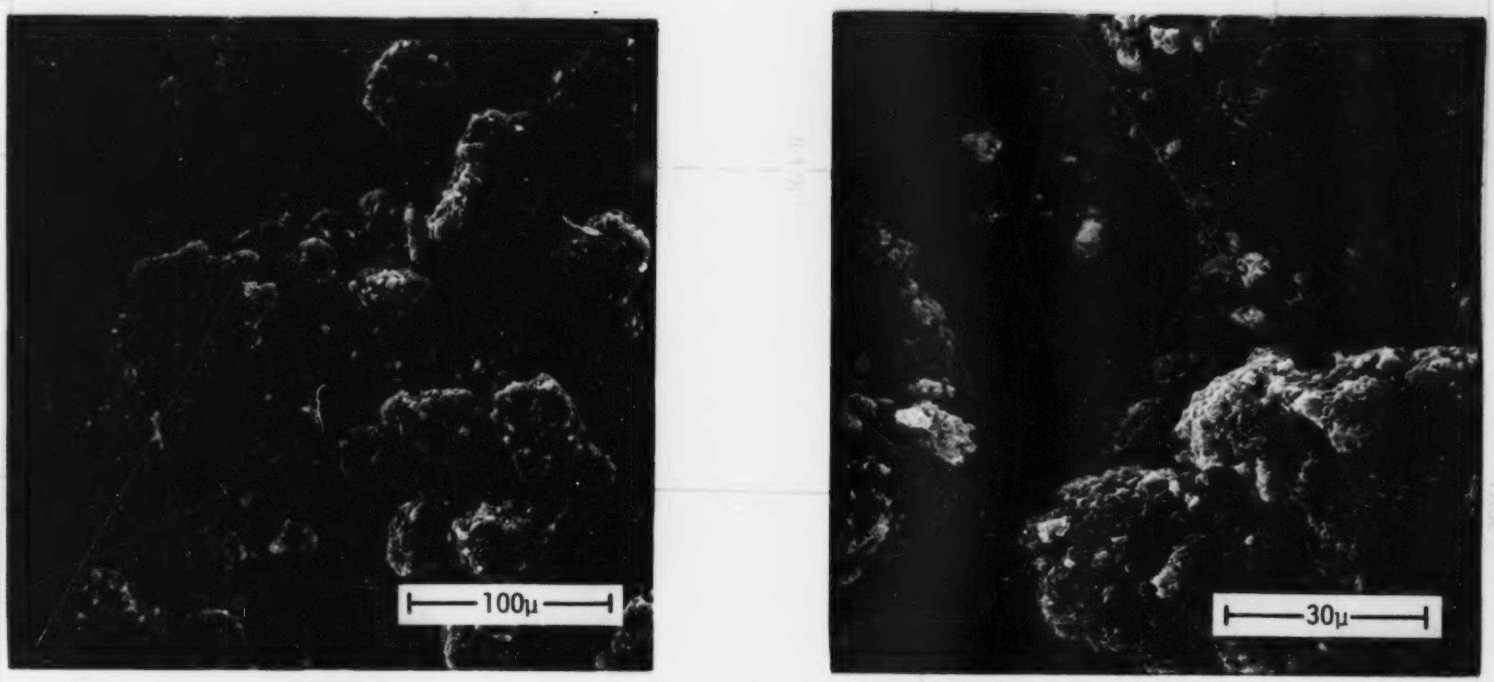

(a) 300x

(b) 1000x

Figure 3. Micrographs of White Sand Size Particles

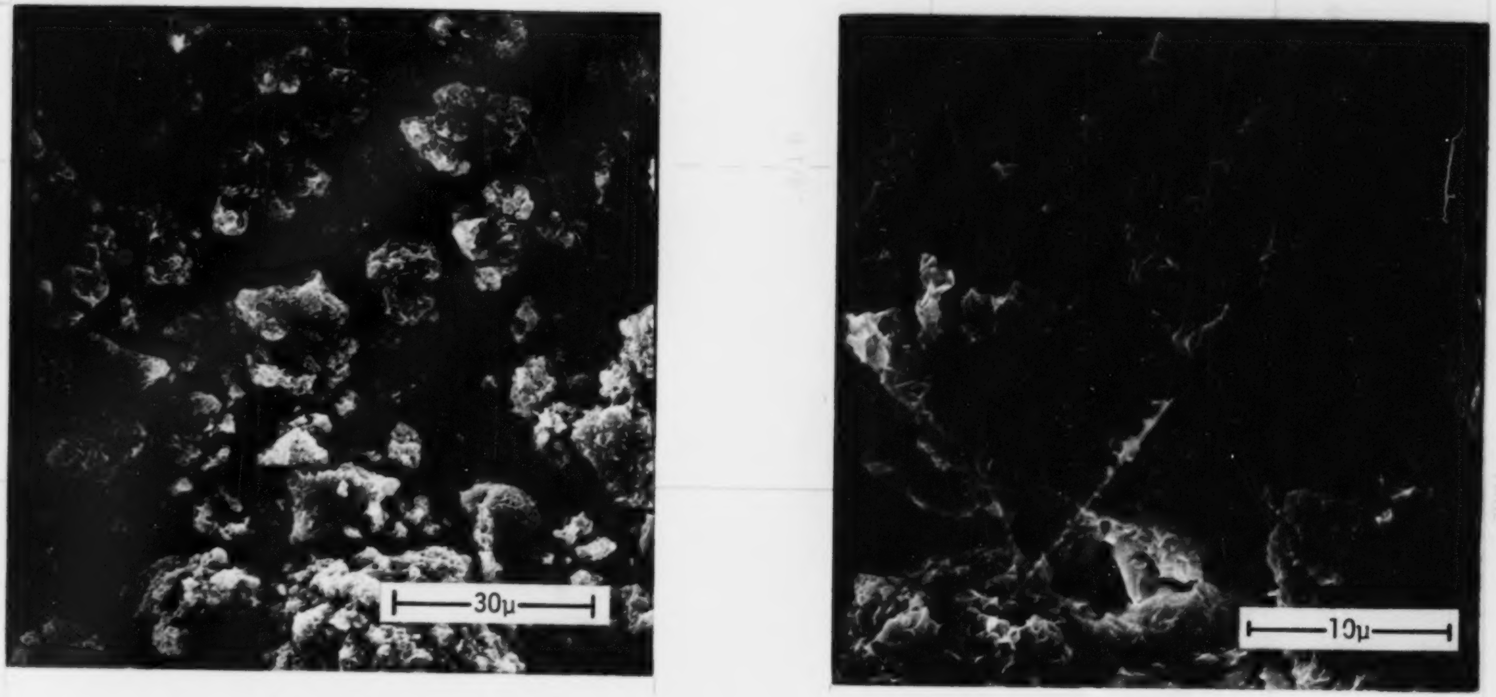

(a) 1000x

(b) 3000x

Figure 4: Micrographs of white silt clay size particles

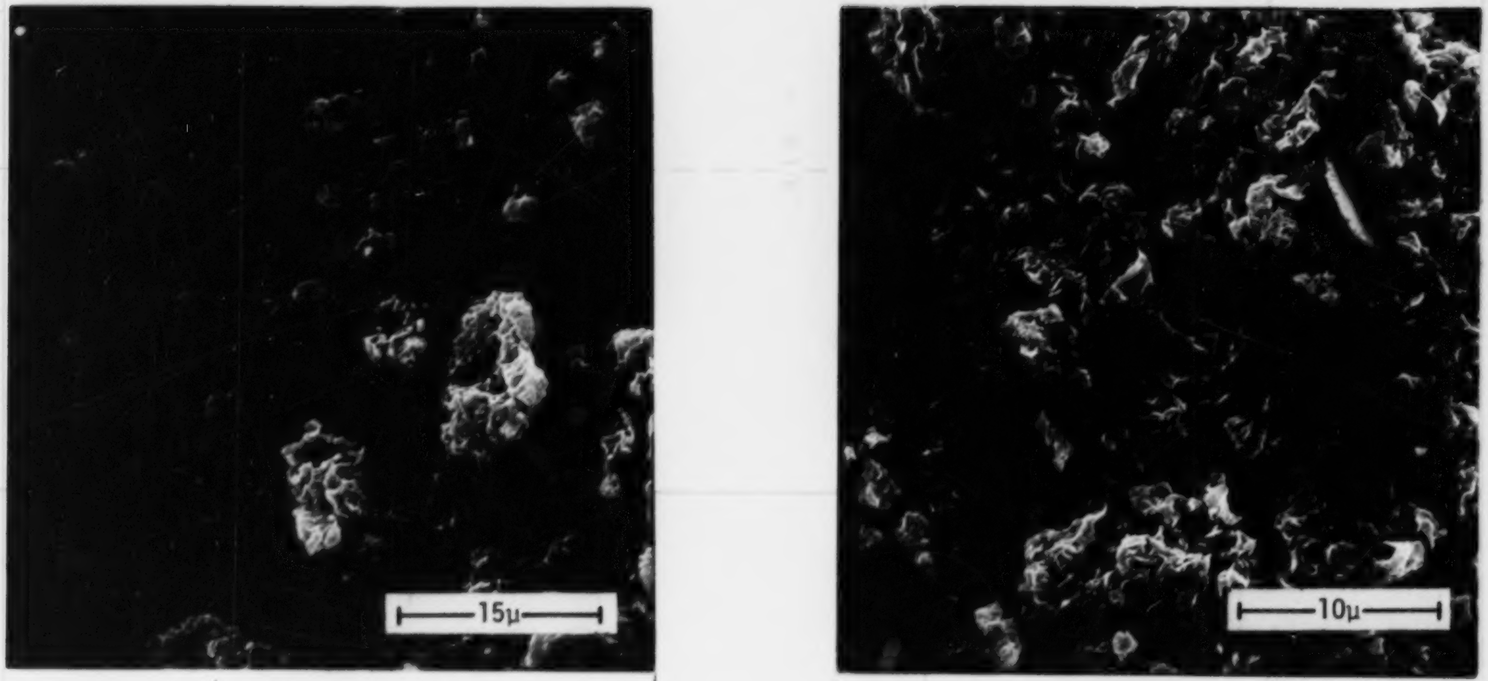

(a) 2000x

(b) 3000x

Figure 5. Micrographs of white clay particles

The red particles used in this experiment were from a red clayey sand obtained in the northern Central Texas area. The size distribution of this sample was restricted to approximately the same distribution as the silt size range of the white sample. The micrographs of this sample are shown in Figure 6. The larger cubic crystals in the micrographs are calcite crystals. The large irregular particles are quartz crystals. A soil survey map of the area where this soil sample was collected indicated that the much smaller clay fraction is a wide mix of kaolinite, smectite, mica, chlorite, and vermiculite. These smaller particles can be seen in the more highly magnified micrograph, Figure 6b. The very sharp edges of the calcite crystals indicate a lack of erosion for these particles. The red color of the sample is coated on the particles and indicates a high degree of oxidation in the soil [28].

The brown soil used in this experiment, shown in the micrographs of Figure 7, was Miller clay from the Brazos River flood plain. The larger particles of this sample are made of quartz, feldspar and calcite. The smaller sized particles are largely smectite and kaolinite. The eroded edges of the few calcite crystals in the micrographs indicate that this particle closely simulates actual sediment particles [28].

Particle Size Distribution

The size distributions of all the samples were determined using pipette analysis. This analysis is based on the differential settling times for particles of different sizes in a column of water [29]. The sediment sample is first filtered and mixed with water in a graduated cylinder. After waiting a specified time based on the particles size and density, a pipetter is used to remove a measured volume of water at a particular depth. Since all particles of a larger size have settled past the point that is sampled, the pipette contains only particles smaller than the particular size for that sample. A sequence of such samples is taken to give the density of the water column as a function of time. Each pipette sample is evaporated to dryness and very accurately weighed. The difference in consecutive weights represents the weight for particles of a particular size. These series of weights can then be related to a weight distribution of the original sediment sample as a function of particle size. The size distributions for the samples are shown in Figure 8.

A similar settling technique was used to separate the size ranges for the sand, silt, and clay size distributions described previously. For all of the white, red, and brown samples, a large amount of soil was mixed with water in a 160 liter settling tank, and allowed to soak over night. The sediment was then mixed again and allowed to settle for a particular period based on the size range and water depth. The unsettled particles were then siphoned off and, depending on the size range, discarded or saved for further settling. By repeating this procedure and using different settling times, any unwanted particle sizes could be removed from the different samples.

The smaller particles were particularly difficult to remove from the white samples. Even after repeated settling and removal of the smaller

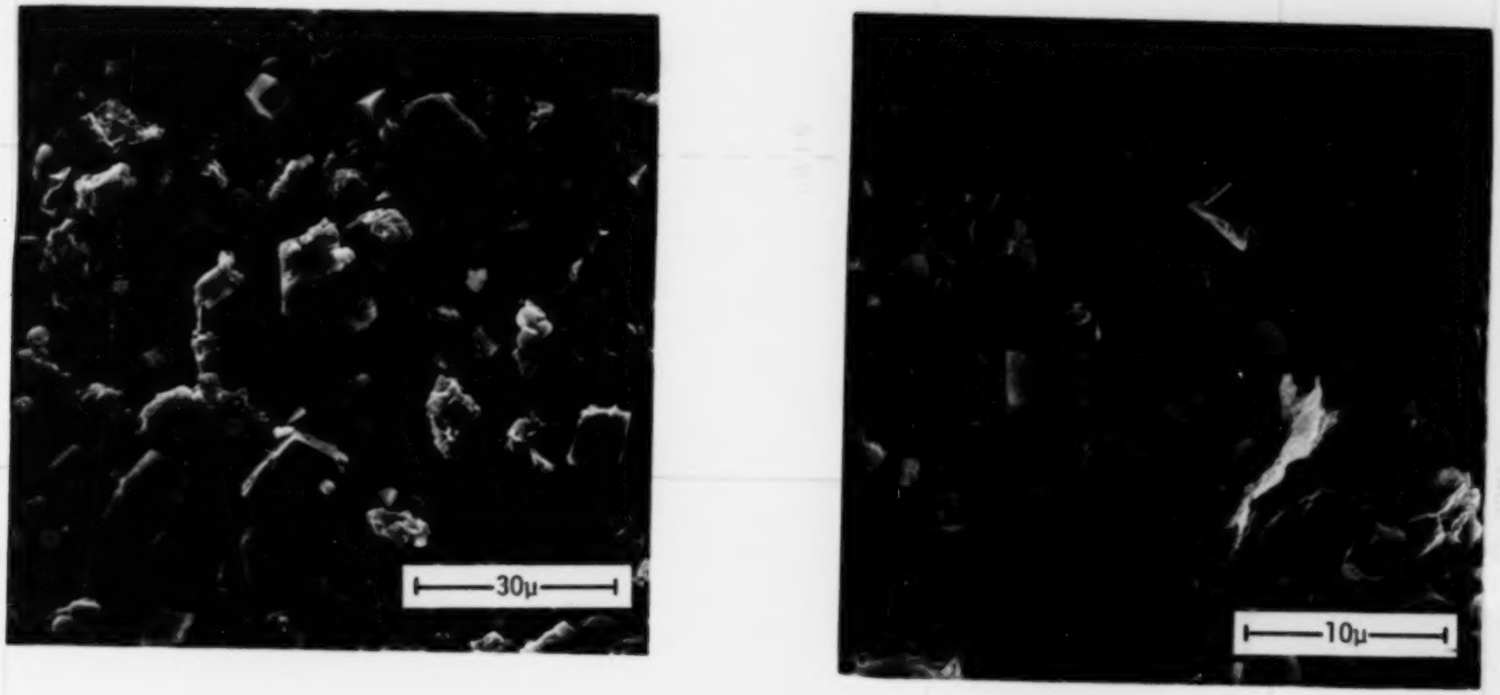

Figure 6. Micrographs of red silt particles

Figure 7. Micrographs of brown silt particles

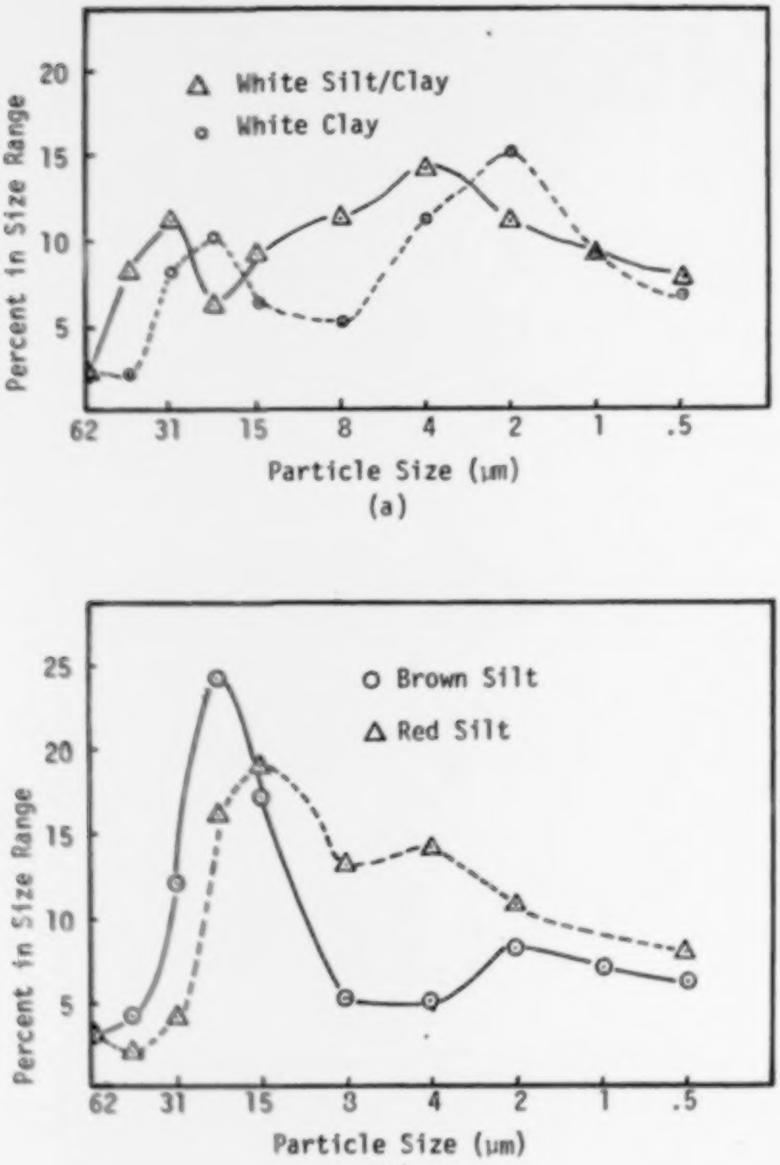

(a)

(b)

Figure 8. Particle Size Distributions for Each Sediment Type

particles, some of the smaller clay-sized particles persisted. When the size distribution of the white silt sample was analyzed, the distribution was found to be skewed considerably toward the smaller clay distribution, Figure 8a. This sample will be referred to as the white silt/clay-sized sample. Another white silt sample was prepared. The smaller particles were more completely removed by repeated settling of this sample. Though no pipette analysis of the sample was performed, the size distribution was estimated by the settling rate of a sample of this silt size range. The median of this sample was approximately 20 μm. Ninety percent of the sample was larger than 6 μm. From the settling of this sample, the size distribution appeared to be very close to the desired size range for the silt classification 30 to 5 μ), Figure 8b. This sample will be referred to as the white silt sample. Though no micrographs were taken of this sample, the irregular shape of all three of the other white samples indicate a similar shape for this sample.

Pipette analysis could not be used to determine in detail the size range distribution of the white sand-sized sample. However, 51 percent of the sample was larger than 64 μm. A pipette analysis of the smaller particles indicated that most of the small particles were less than .5 μm in size (28%). The remainder of the sample was between 32 μm and 1 μm in size.

Measurement Procedure

Each of these different soil samples was used as scattering particles in the backscatter measurements (Figure 9a). These measurements were made as a function of sediment concentration. Due to the size separation process. the soil samples were in the form of a concentrated suspension. Measured amounts of this slurry were poured into the measurement tank (Figure 9b) to vary the concentration of sediment from a very low level to a level high enough to "saturate" the scattering process. The concentration of the suspended particles was computed from the volumes of the added sample and the measurement tank along with the concentration of the slurry. The measurement sequence included measuring the backscattering from a white calibration target. This measurement allowed the optical alignment of the system to be checked and served as a power measurement to normalize the sediment return. Data were taken for 55 seconds and averaged to give the indicated measurements. The data from these measurements are tabulated in Appendix A.

ALGAE MEASUREMENTS

A simple algal specie was used as a scattering particle to determine the effect of organic suspended particles on the backscattering measurements. Measurements were also made from a mixture of the algae and sediment particles over a wide range of sediment concentration.

The algae used in this experiment was a green flagellated specie, Chlamycomonas. The cell size of this algae is approximately 30 μm. Preliminary measurements showed that a high concentration of the algae would

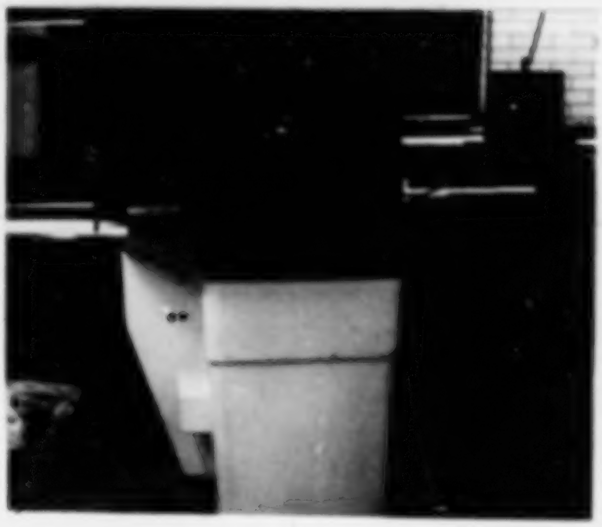

(a) Test tank with high sediment concentration

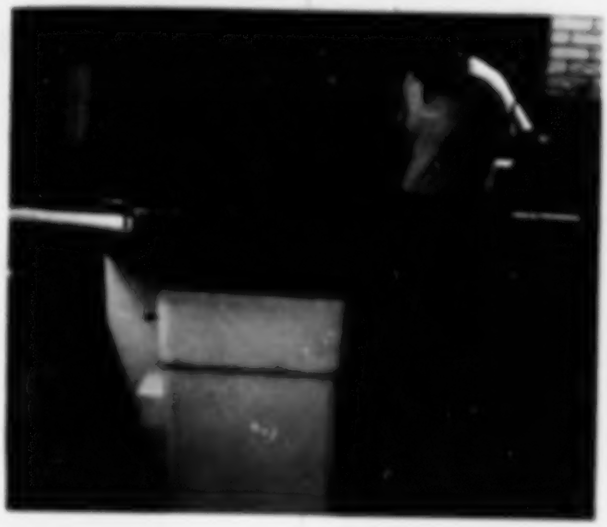

(b) Increasing the sediment concentration

Figure 9. Scattering from sediment-laden water.

be needed to make measurements in the large measurement tank. Two cultures were grown in a 10 liter carboys for the experiment. The cultures were allowed to grow to a bloom condition of approximately 2.0×10^5 cells, liter.

Backscatter measurements were first made from only the algae. The concentration of the algae ranged from 1.44×10^3 cells/liter to a maximum concentration of 5.76×10^3 cells/liter. When the maximum concentration of algae had been reached, sediment was then added for further measurements.

The sediment used in this experiment was the second white silt particle described previously. The concentration of sediment ranged from 21.6 mg/liter to 540 mg/liter. These results are tabulated in Appendix B.

SURFACE ROUGHNESS MEASUREMENTS

Measurements of backscattering from sediment laden water were also made for different levels of water surface roughness. A small fan was used to disturb the surface of the water close to the entry point of the lasers for three different wave heights. Measurements were made for the red and brown silt samples, as well as the white silt/clay fraction. The depth of water that contributed to the lidar backscattering was also determined for several different concentration and surface roughness conditions.

Backscatter measurements were made for three surface roughness levels using the three silt sediment samples as scattering particles. For each particle type, the concentration was varied similar to the previous measurements, but at wider intervals. At each concentration level, backscatter measurements were made for all three levels of surface roughness.

The reflection of the lasers from the water surface could be seen on the black absorbing material behind the measurement tank. When the fan was used to disturb the water surface, the pattern of the reflected laser beams on the absorbing material could be used as an indication of the level and pattern characteristics of the surface waves. By repeating the reflected pattern, the level and pattern of the surface waves could be repeated between the different sediment types. A reflected pattern was generated which indicated that no longitudinal or traverse wave structure was present. The pattern was roughly a circle with very little symmetry, indicating a "random" surface function was being generated.

The characteristics of the surface waves are difficult to quantify and as a result these descriptions are somewhat subjective in nature. The circulation pump used to keep the particles in suspension produced some ripples on the surface. At the entry point of the lasers, these ripples were insignificant, causing no deflection of the reflected laser beams. Estimations of the surface wave characteristics caused by the fan were difficult to measure because of their extremely small size. The calm surface roughness was a wave height of approximately 1 mm, with a period of 10 cm. The laser deflection indicated a change in reflected angle of only 3°. The medium surface roughness had an approximate wave height of 2 wave conditions. Consequently, the lasers were reflected completely out of the water for short periods during the measurements. The high incident angle and small surface area of the tank prevented these surface wave characteristics from being more representative of actual field measurement conditions.

The results of the experiment are tabulated in Appendix C.

DEPTH OF MEASUREMENT

The depth of water that contributed to the backscattering was also determined during the surface roughness experiment. This measurement was made for the same set of conditions as the surface roughness mesurements (i.e., each concentration of sediment for all three silt fractions at each surface roughness level). To make these measurements, a black absorber was moved up the laser path until a decrease was discernible in the return from the tank. With one person watching the system output, and another moving the absorber, the measurement was repeated several times to give an accurate indication of the greatest depth of water that contributed to the measured backscattering. The depths given are along the laser path in the water. Appendix C contains the laser measurement depths and Secchi depths for these measurements.

CHAPTER IV

DATA REDUCTION

The backscatter measurements were reduced to lidar cross section. The lidar cross section is a target parameter which relates the incident and backscattered power density levels at the target. Reduction of the data measurements to a lidar cross section format removes characteristics of the measurement system and permits meaningful interpretation of the measurement in terms of target phenomena.

To calculate the cross section, the system gain and optical efficiencies are used to reduce the raw measurements to actual backscattered power measurements. For a known transmitted power, the target power densities an cross section can then be calculated. A white calibration target was used as the reference cross section for these measurements to measure the transmitted power.

CROSS SECTION CALCULATION

One form of the lidar cross section equation (assuming no path loss) [30] is given by:

$$\sigma_{ij} = 4\pi R^2 \frac{P_R/A_R}{P_T/A_T} \qquad (1)$$

where

R = Range to target
P_R = Received power
P_T = Power transmitted
A_A = Area of receiver
A_T = Area illuminated at target.

The i and j relate to the transmitted and received polarization, respectively. The range and areas are easily measured or calculated from system characteristics and the measurement configuration. The received power is calculated from the measurements by including system gains and optical efficiencies. Specifically, the received power is given by:

$$P_R = \frac{V}{S} G_1 \qquad (2)$$

where

G_1- A gain constant of the system which depends on the optical efficiencies of the filters and photomultiplier tubes at the laser wavelengths and the preamplifier impedance
V - Preamplifier output
S - Photomultiplier sensitivity

The system gain, G_1, and the photomultiplier sensitivity, S, are explained in Appendix D. The preamplifier output is scaled by the system electronics and converted to a digital word to be sent to the computer for further processing. A maximum of 10 millivolts at the output of the preamplifier is converted to an integer of 4095 for use by the computer. The conversion constant for the digitization process is 2.44×10^{-6} volts/bit, e.g.,

$$V = \text{Digital word} \times 2.44 \times 10^{-6} \text{ volts/bit} \qquad (3)$$

The photomultipler tube sensitivity is related to the PMT supply voltage (V_{VMT}) by

$$S - \exp(8.15 \ln V_{PMT} - 57.1) \text{ amps/lumen.} \qquad (4)$$

The constants 8.15 and 57.1 were determined from measurements of a constant backscatter at different PMT sensitivities and from the PMT sensitivity specifications for these particular photomultiplier tubes (Appendix D). The same sensitivity calculations were used for both photomultiplier tubes.

The remaining term, the transmitted power (P_T), was initially measured using a Jodon optical power meter. Subsequent transmitted power fluctuations were measured using a white target as described below.

WHITE TARGET CALIBRATION

A white calibration target was used to optically align the lidar system and to monitor the transmitted power for use in equation (1). This white target is a sheet of opaque plexiglass that is white in color. The scattering characteristics of the white plexiglass completely depolarize the incident laser beams. The constant scattering cross section of the white target also permitted its use as a known cross-section calibration target.

Optical Alignment

The lidar system must be properly aligned to detect the backscattered energy from a target. The receiver alignment is important to the proper transmission of the backscattered energy through the filters and polarization splitting cube in order to be detected by the PMTs. The scattering from the white target is used as a reference return which has equal like- and cross-polarized components. With the red laser on the white target at the proper measurement range, the receiver view angle is scanned in azimuth (without moving the red laser position) until both the red horizontal and vertical signals are equal. The two mirrors which shift the blue laser out put are then used to properly position the blue beam at the target for equal horizontal and vertical returns. When the alignment is completed, the depolarization ratio is unity for both the red and blue wavelengths. This system must be realigned whenever the measurement range is changed.

White Target Cross Section

The white target was also used as a calibration target to correct the sediment laden water measurements for laser power fluctuations (Figure 10a). The power meter used for the white target calibration was a Jodon optical power meter (Figure 10b). During one series of tests, laser power measurements were made concurrently with backscatter measurements from the white target. The cross section of the white plexiglass was computed for each backscatter measurement. These cross sections were then averaged to give a more accurate measurement of the white target cross section.

During the experimental measurement sequence described in Chapter III, a white target measurement was made concurrently with each sediment measure ment. Since the cross section of the white target was known, the cross section of the sediment in water could be computed without directly measuring the power of the lasers. The cross sections of the white target and sediment laden water are given by:

$$\sigma_{ij}^{WT} = 4\pi R^2 \frac{P_R^{WT}/A_R}{P_T/A_T} \qquad (5)$$

$$\sigma_{ij}^{S} = 4\pi R^2 \frac{P_R^{S}/A_R}{P_T/A_T} \qquad (6)$$

where the supercripts WT refer to white target cross section and S refers to water/sediment cross sections. For a constant measurement configuration the range and respective areas also remain constant. Assuming the transmitted power also remains constant between the water and white target measurement,the white target cross section can be solved for transmitted power and substituted into the water/sediment cross section equation, which yields:

$$\sigma_{ij}^{S} = \frac{P_R^{S}}{P_R^{WT}}\sigma_{ij}^{WT} \tag{7}$$

Since the system gain constants, defined previously for P_R are also constant, the above equation reduces to:

$$\sigma_{ij} = \frac{S^{WT}}{S^{S}}\,\frac{DW^{S}}{DW^{WT}}\sigma_{ij}^{WT} \tag{8}$$

S, the sensitivity of the photomultipler tubes, was different for the white target and sediment measurements. In final form, the cross section for the sediment-laden water is given by:

$$\sigma_{ij}^{S} = \exp[8.15(\ln V_{PMT}^{WT} - \mathrm{in} V_{PMT}^{S})]\,\frac{DW^{S}}{DW^{WT}}\cdot\sigma_{ij}^{WT} \tag{9}$$

As shown by this equation, the cross section of the sediment-laden water was computed by 1) normalizing the sediment return by the white target return, 2) correcting for PMT sensitivity, and 3) multiplying by the white target cross section. Since the return from the white target for both the horizontal and vertical returns were used, this procedure also corrected for any system misalignment. Due to the averaging of the white target cross section, this method also provided a more accurate and more convenient measurement of laser power than that using the optical power meter during the sediment measurements.

It should be noted that this procedure was required to measure the transmitted power for the cross section calculations. A power monitor could be used to normalize the returns for field measurements. Power measurements are not necessary for measuring the depolarization ratio since both returns are equally affected by laser power fluctuations.

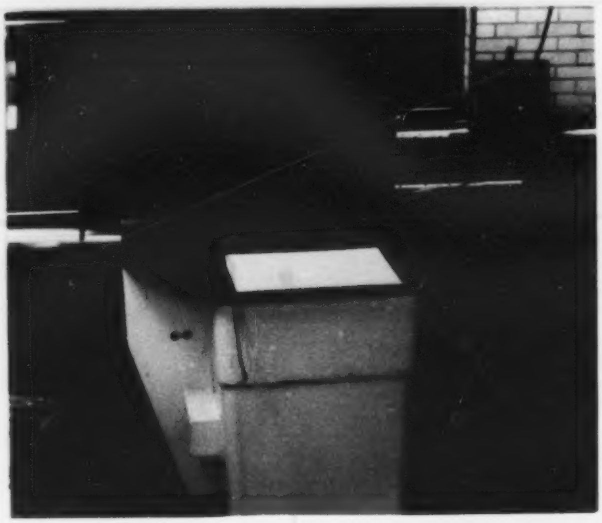

(a) White calibration target

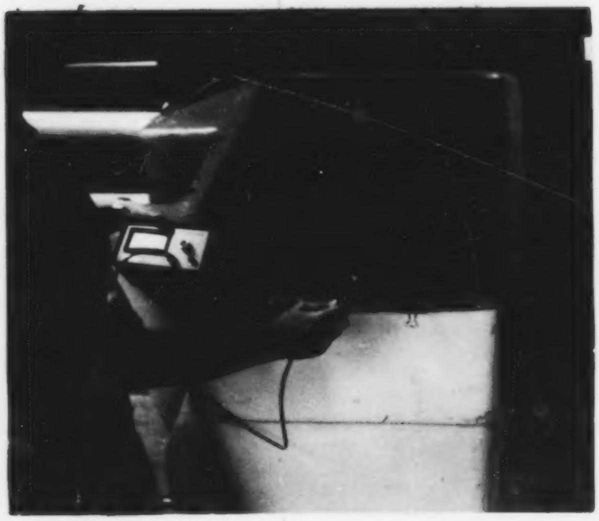

(b) Laser power measurement

Figure 10. White target and transmitted power measurements

CHAPTER V

RESULTS

The objective of this research was to examine the capability of a lidar polarimeter to measure the concentration of suspended solids in water under different measurement conditions. Chapter III describes the experiments which were performed to determine the effect on the lidar backscattering caused by sediment concentration, shape, color, and size distributions. The effects of water surface roughness and organic suspended solids (living algal) were examined and the depth of the scattering volume which contributed to the backscattered energy was also determined. Chapter IV explains the data analysis methods used to reduce the data to permit meaningful comparison of the different conditions. This chapter is a discussion of the measurement results and some of the problems encountered in the experiments. To better explain these results, it is advantageous to discuss the scattering characteristics shown in previous experiments. The additional effects caused by the scattering from sediment particles can then be better understood.

SCATTERING PHENOMENA

Previous experiments by Sheives [6] have compared backscatter measurements with returns predicted by a mathematical description of the scattering process. The model includes contributions from both single and multiple scattering processes. The excellent correlation between the predicted and measured returns (correlation coefficients of 0.95) have verified the validity of the model and the associated hypothesis that both single and multiple scattering must be considered when predicting the return from different concentration levels of scattering particles.

Multiple scattering occurs when the incident energy strikes more than one particle before being scattered back toward the receiver. This becomes significant when the concentration of scattering particles has reached a high enough concentration to scatter the incident energy out of the laser path and into the water volume around the incident beam. Multiple scattering depolarizes the incident energy due to the scattering caused by more than one reflection from the scattering particles. As a result of this lack of polarization, multiple scattering contributes equally to both the like- and cross-polarized backscattered returns detected by the lidar system.

Single scattering is the backscattered energy reflected from a single interaction between the incident radiation and the scattering particles. Single scattering occurs in the water volume only along the laser path.

This type of scattering from spherical particles does not depolarize the backscattered energy. Thus, single scattering contributes to only the like-polarized return. However, single scattering from non-spherical particles can result in a slight amount of depolarization due to the particle shape. The cross-polarized return due to this depolarization is therefore proportional (by a small fraction) to the like-polarized return caused by the single scattering.

The like- and cross-polarized components of the backscattered energy in terms of the two major scattering processes are given by

$$P_{VV} = P^{M}_{VV} + P^{S}_{VV}$$

$$P_{VH} = P^{M}_{VH} \tag{10}$$

The first subscript indicates the polarization of the transmitted energy (in this case, vertical). The second subscript denotes the receiver polarization (vertical or horizontal). The superscripts indicate the contribution to the return by single or multiple scattering. The like-polarized return is a combination of backscattered energy from multiple and single scattering. The depolarization ratio is then given by

$$\frac{P_{VH}}{P_{VV}} = \frac{(P^{M}_{VH})}{(P^{M}_{VV}) + (P^{S}_{VV})} \tag{11}$$

The results of backscatter measurements from turbid water made by Sheives [6] are an excellent example of the backscattering process as a function of particle concentration. The scattering particles used in this experiment were latex particles. Figure 11 shows the size distribution of these particles and Figure 12 shows their individual shape. The levels of particle concentration at which single and multiple scattering contribute to the returns are evident in the graph of the depolarization ratio shown in Figure 13. At the low concentration levels where only single scatter is present, the depolarization ratio remains constant at very close to zero. At higher concentrations, multiple scattering begins to increase the cross-polarized return and the depolarization ratio increases rapidly.

Backscatter measurements were also made from turbid water using Teflon resin as the scattering particles. The size distribution of these particles is shown in Figure 14 and their shapes are indicated in Figure 15. The plot of the depolarization ratio as a function of particle concentration is shown in Figure 16. At low concentrations of scattering particles, the depolarization ratio remains constant at a value of approximately 0.1. The higher ratio at the low concentration levels for this particle compared to the previous sample type is a result of the difference in shape of the two particles. The micrographs for the two particles (Figures 12 and 15) show the greater sphericity of the latex particle than that of the Teflon particle. The non-spherical Teflon particle slightly depolarizes the incident radiation. Since this depolarizaiton is proportional to the single scattering, and only single scattering is present at low particle

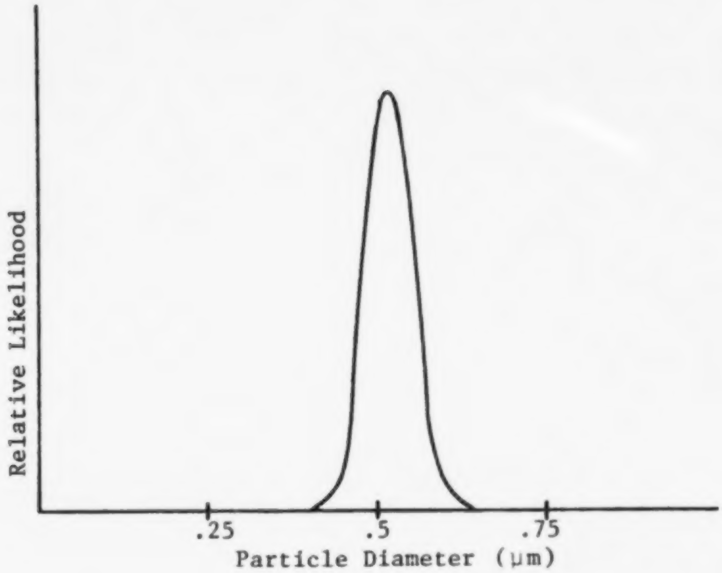

Figure 11. Approximate Relative Size Distribution for Dow Plastic Pigment 722 (after Sheives [6])

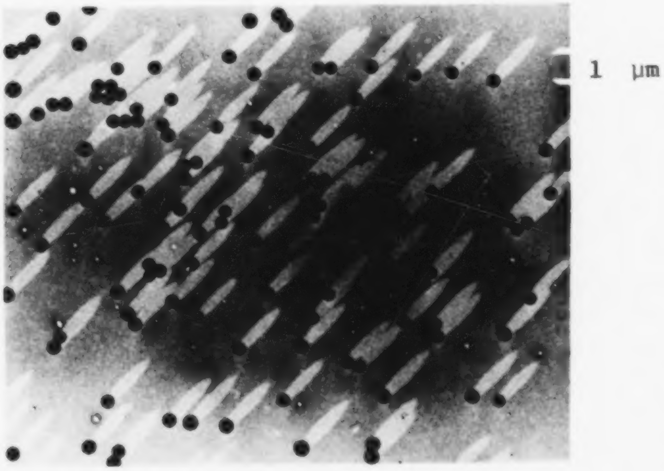

Figure 12. Photomicrograph of Dow Plastic Pigment 722 (after Sheives [6])

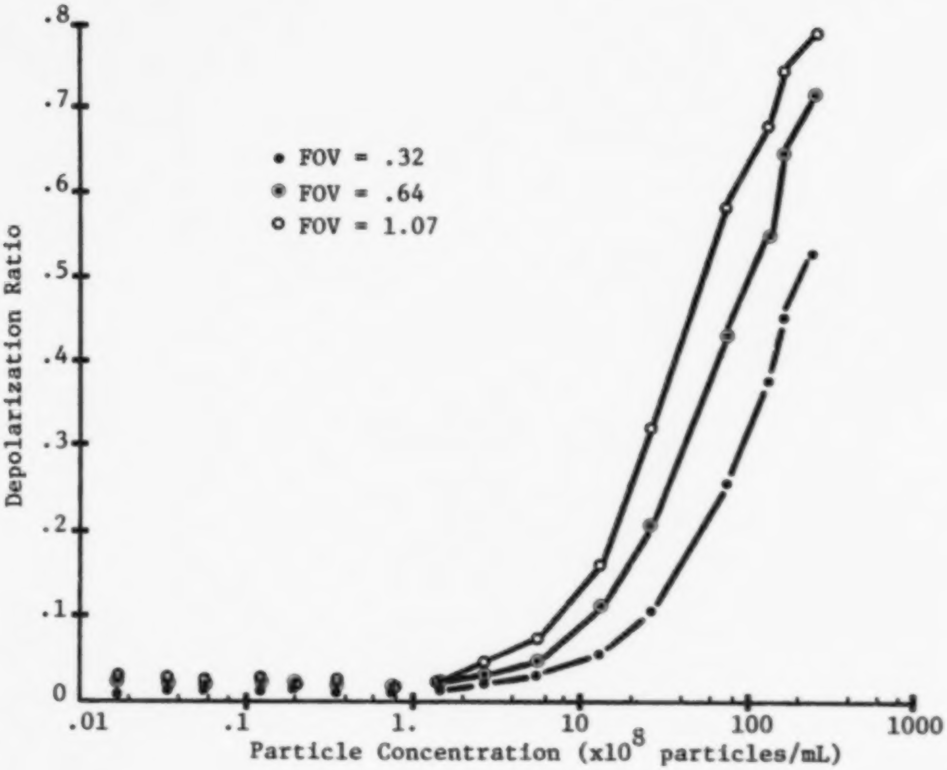

Figure 13. Comparison of Depolarization Ratios as a Function of Field of View and Latex Particle Concentration (after Sheives [6])

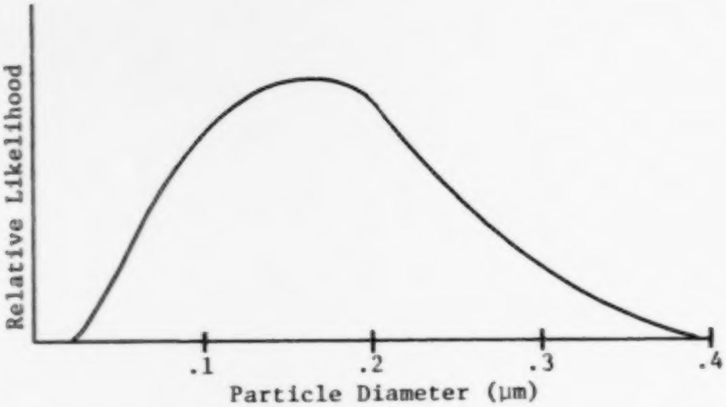

Figure 14. Approximate relative size distribution for Dupont TFE 30 (after Sheives [6]).

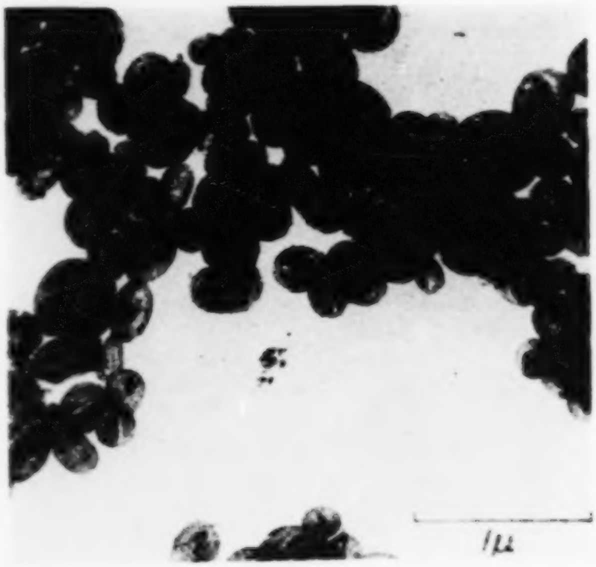

Figure 15. Photomicrograph of Dupont TFE 30 (after Sheives [6]).

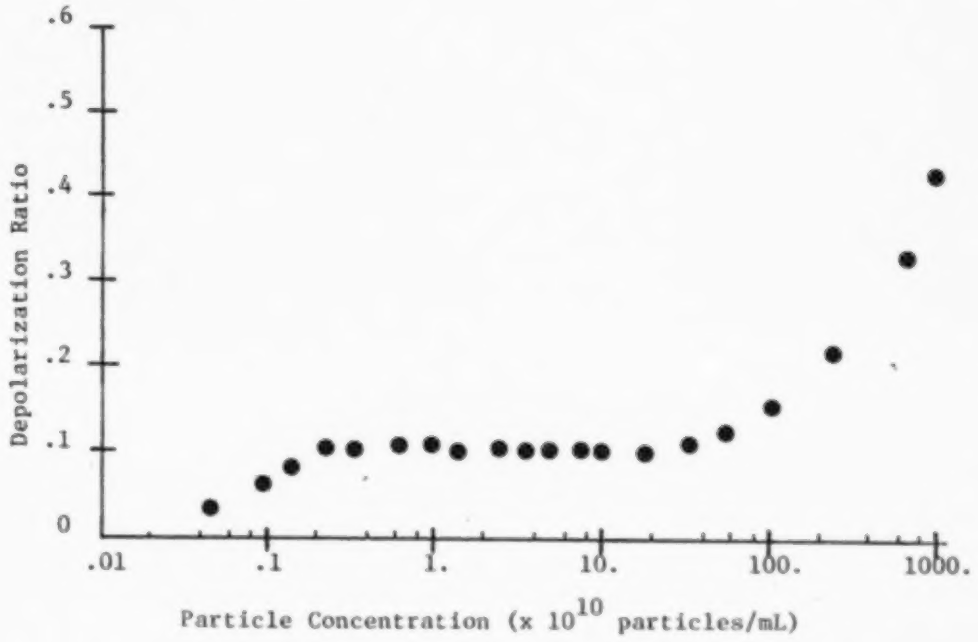

Figure 16. Graph of Depolarization Ratio as a Function of Teflon Particle Concentration (after Sheives [6])

concentrations, the depolarization ratio remains constant.

The results of the model correlations and the experiments by Sheives have determined several characteristics of the scattering process. Multiple scattering, which dominates the scattering at high concentrations, contributes to both the cross- and like-polarized components of the backscattered energy. Single scattering, which cannot be ignored at low concentrations of scattering particles, contributes to only the like-polarized return for scattering from spherical particles. For single scattering from non-spherical particles, the incident energy is depolarized by the particle shape.

The measurements made by Sheives [6] represent excellent examples of scattering from "well-behaved" particles. The regions where single and multiple scattering occur are clearly defined. The concentration level at which multiple scattering begins is also very evident. For the irregular sediment particles used in the present study, these concentration levels are not as easily determined. However, the results of the experiments using the latex and Teflon particles are a useful guide in estimating the concentration levels at which single and multiple scattering occur for the backscattering from sediment particles of the type used in the present study.

DISCUSSION OF MEASUREMENTS

The many experiments in this study were designed to isolate different measurement parameters and to determine their effects on the capability of a lidar polarimeter to measure the concentration of suspended solids. To accomplish this, the lidar returns were recorded as a function of concentration for a wide range of measurement conditions and particle types. The results of these experiments are discussed in this section.

Sediment Concentration

Many different measurement conditions were examined for a wide range of sediment concentrations. A direct dependence of the backscattered returns on sediment concentration was evident for all of the different particle types of approximately the same size range, and for different size ranges of the same particle type.

The depolarization ratio graphs for the white silt sized sample shown in Figures 17 and 18 are representative of the many measurement results. The direct dependence of the depolarization ratio on the sediment concentration shown in these graphs represents an excellent statistical correlation between the two variables.

As evident from Sheives [6] work, the concentration region where single scattering dominates the returns is characterized by a constant depolarization ratio at low concentrations of scattering particles. When multiple scattering begins, the depolarization ratio begins to increase rapidly.Similar characteristics are evident in the depolarization ratio graphs for the white silt particles. Though the depolarization ratio is not constant at low concentration levels, the rate at which the depolarization ratio increases is larger for the higher concentration levels. This more rapid increase in the depolarization ratio indicates that multiple scattering begins to occur at approximately 20 mg/l. The fact that the depolarization ratio does change for an increase in the concentration at concentration levels where only single scattering should be present, indicates that the particle shape has caused additional contributions to the scattering process besides single scatter. However, since the depolarization ratio is still less than 0.1, the depolarized component of the backscattered energy is less than 10% of the polarized return.

The color and shape of the sediment particle influenced the dependency of the lidar backscattering on particle concentration. The effects of reflectivity and absorbance of the particles were particularly evident at the high concentration levels. The effects caused by the shape of the particles were most noticeable at very low concentration levels. These different scattering characteristics and the concentration levels at which they affect the backscattered returns are discussed in the following sections.

Particle Shape

The effects of the particle shape on the lidar returns are most evident at the low particle concentrations, where single scattering is the predominant scattering process. Since single scatter from spherical particles at these concentration levels does not depolarize the backscattering, any depolarization that is present must be a result of the different effects of the particle shape. Some depolarization, due to the shape of the particle, causes a depolarized return that is proportional to the like-polarized return of the single scattering. However, since the depolarization ratio does change for an increase in particle concentration, some contribution from the additional scattering process is present, which increases the depolarized return more rapidly than the single scattering return. This effect causes the depolarization ratio to increase as the particle concentration increases for concentration levels below 50 mg/l. These effects are most apparent in the returns from the irregular shaped brown and red silt samples.

The depolarization ratio plots for red silt particles are shown in Figures 19 and 20. It should be noted that there are two sets of data shown in these figures. The set indicated by crosses was acquired late in the experiment in a small test tank in order to achieve very high concentrations. The difference in the two measurement sets is believed to be in the concentration estimate and not the lidar measurement. This is discussed later.

Figures 19 and 20 show slight increases in the rate at which the ratio increases above a concentration level of approximately 50 mg/l, which indicates significant multiple scattering above this level. The fact that the depolarization ratio does increase below this region indicates that multiple scattering is present at low concentrations also. The high depolarization ratios for the red silt partics at levels of concentration below 10b mg/l show that significant depolarization is present even when single scattering is the dominant scattering process.

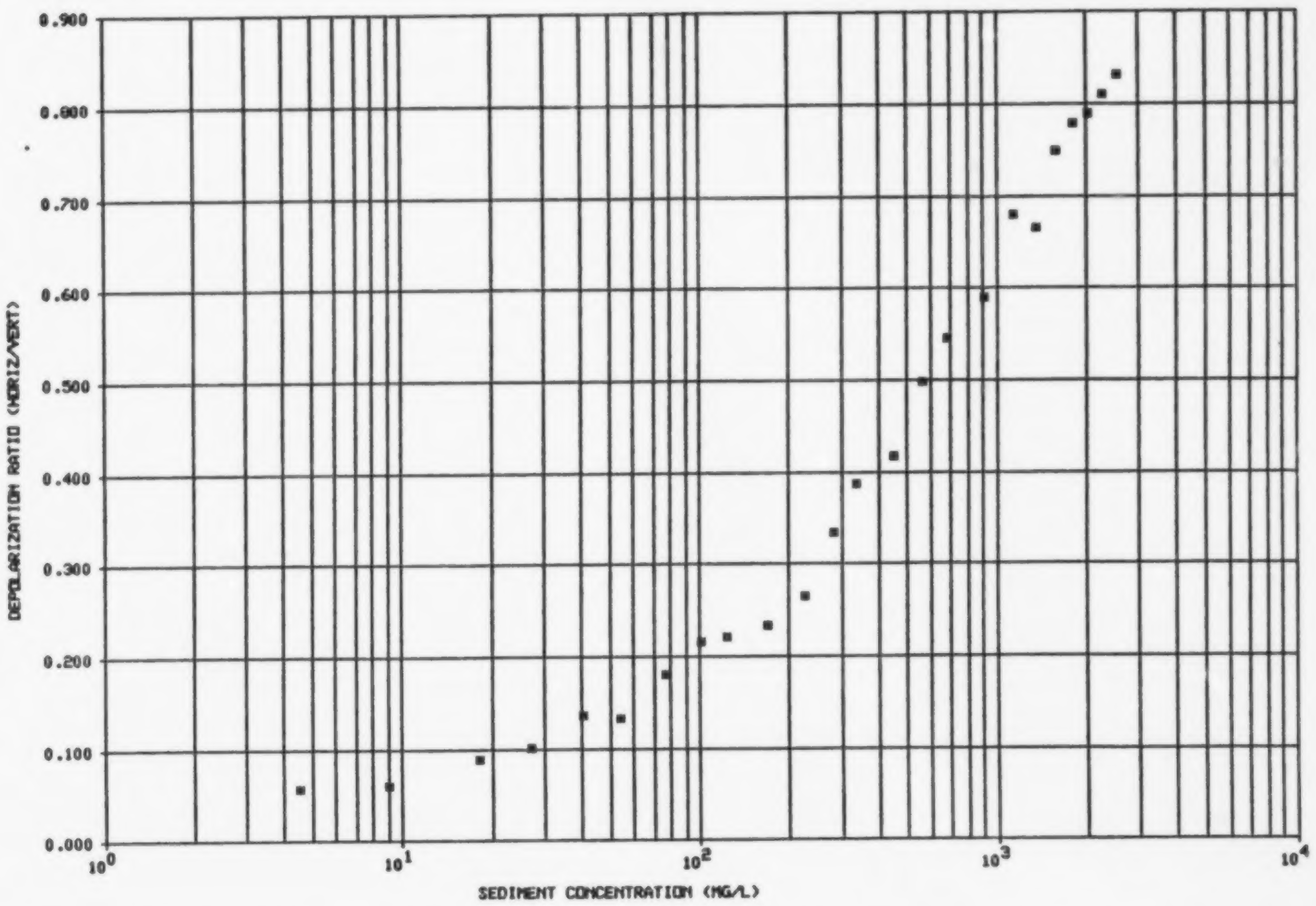

Figure 17. Depolarization Ratio Versus Sediment Concentration for White Silt Measured at 632 nm

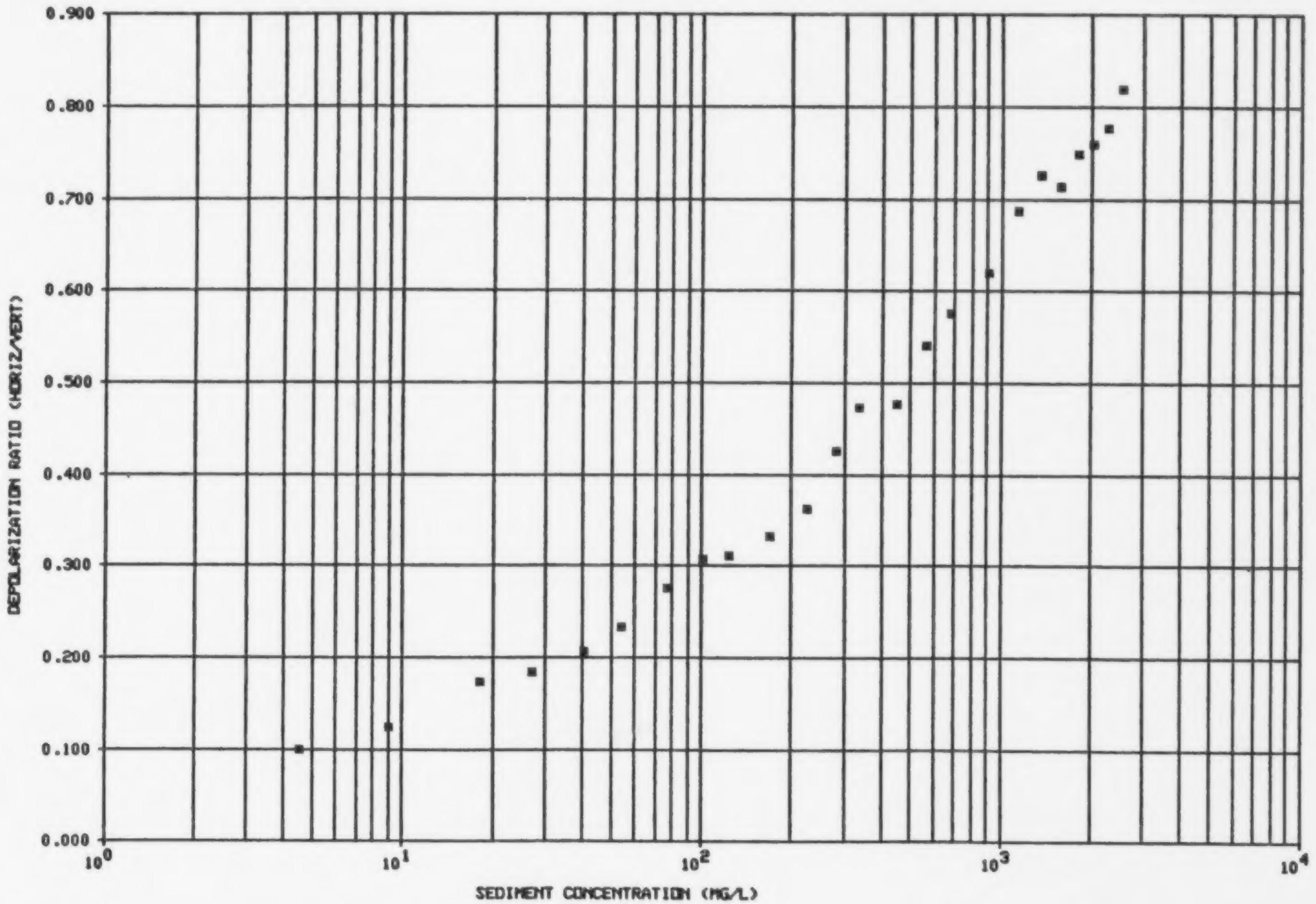

Figure 18. Depolarization Ratio Versus Sediment Concentration for White Silt Measured at 442 nm

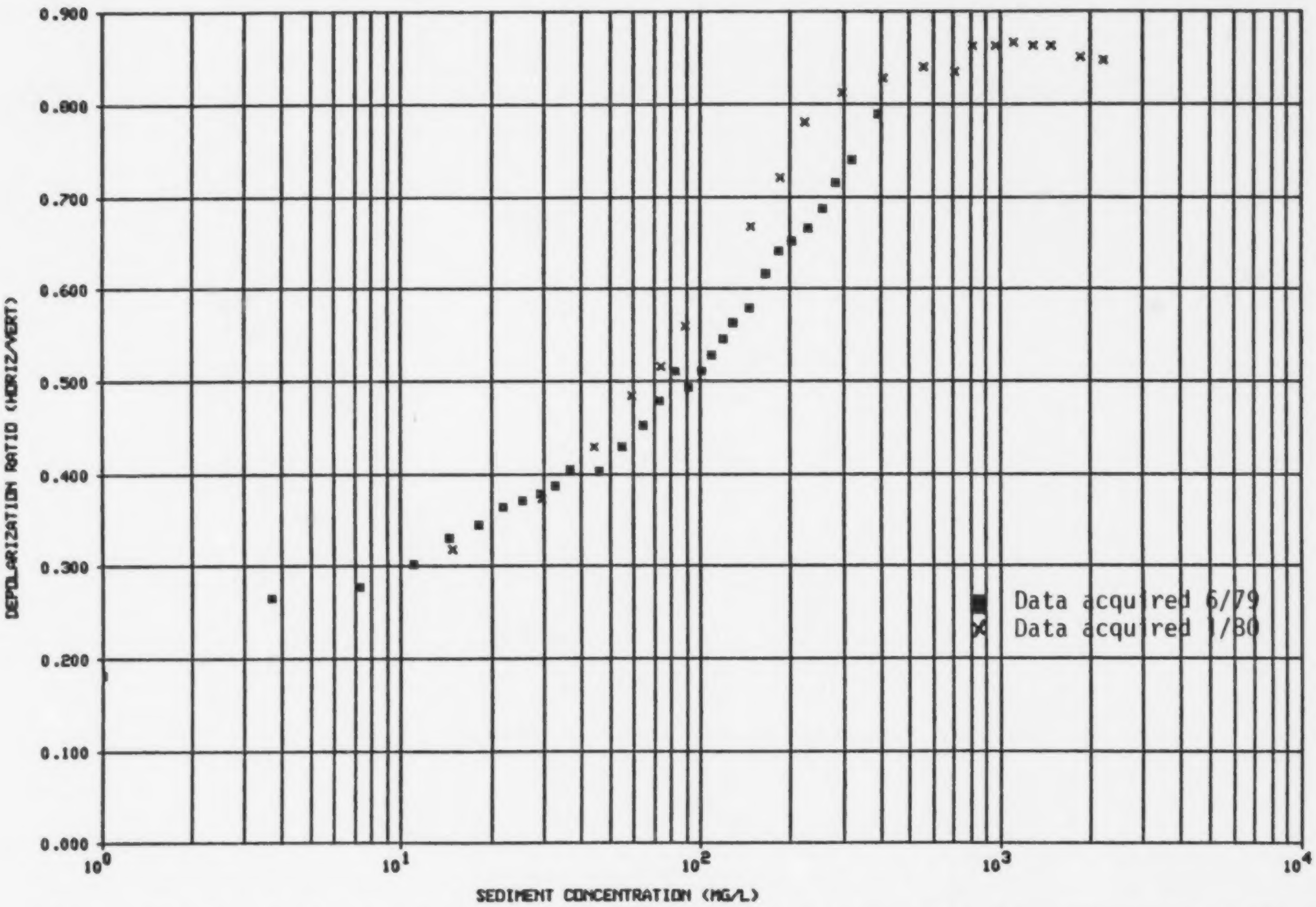

Figure 19. Depolarization Ratio Versus Sediment Concentration for Red Silt Measured at 632 nm

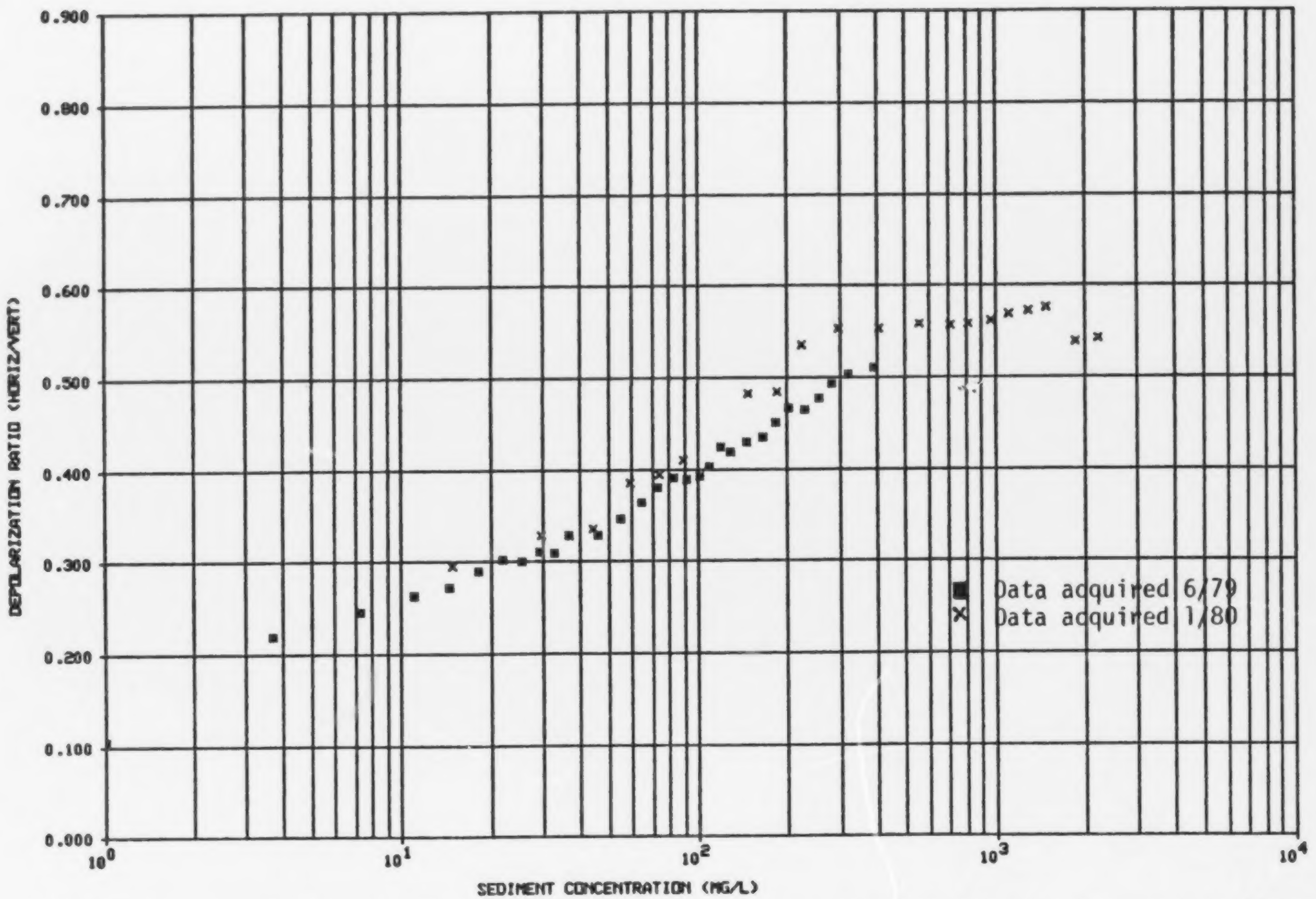

Figure 20. Depolarization Ratio Versus Sediment Concentration for Red Silt Measured at 442 nm

The micrographs of the white sand, silt and clay particles in Figures 3, 4 and 5 show the common irregular shape characteristic of the white particles. The depolarization ratio curves for the white silt sample shown previously in Figure 17 and 18 exhibit a depolarization ratio of less than 0.1 for concentration levels less than 10 mg/l. The depolarization ratio at for both red silt particles have depolarization ratio values well above 0.2 for the same very low concentration levels. The very angular shape of the red silt particles shown in the micrographs in Figure 6 causes much higher depolarization of the incident radiation at the low concentrations.

Since the depolarization ratio is not constant at very low levels of particle concentration, it appears that some multiple scattering is present even at these low concentration levels. The higher rate of increase for the more angular red and brown silt particles indicates the shape of the particle is a factor in this effect. Due to the depolarization caused by the irregular shape of the particles, the incident energy is reflected out of the laser path and into the surrounding water volume for very low concentration levels. As a result of this depolarization, multiple scattering, to a small extent, begins at a low particle concentration.

Particle Color

The color of the scattering particles affects the backscattered returns due to the different reflectivity and absorbance of the particles for the different wavelengths. These effects can be seen in the greater efficiency of the multiple scattering for particles with high reflectivity and the different values at which the depolarization ratio saturates due to the absorbance and scattering efficiencies of the particles at the different wavelengths.

The reflectivity of the particle determines the proportion of energy that is reflected from the particle. A high reflectivity causes more energy to be reflected from each interaction with the particles. A high reflectivity therefore greatly influences the scattering at high concentration levels where multiple scattering is predominant. For high concentration levels, this increase in the scattered energy causes additional multiple scattering and the multiple scattering depolarizes the incident energy, the efficiency of the depolarization process is increased by the reflectivity of the particles.

The depolarization ratio can be used to show this increased efficiency of the multiple scattering. Since the depolarization ratio is the result of dividing the cross-polarized return by the like-polarized return (equation 11), a simple increase in reflectivity would increase both terms equally and the effect would be cancelled. An increase in the efficiency of the multiple scattering would increase the contributions of this process to the depolarization ratio (P_{VV}^{M} and $P_{/VH}^{M}$) at levels where multiple scattering is present.

The effect of the increased efficiency of the multiple scattering due to a high reflectivity can be seen in the depolarization ratio graphs for the brown silt sample shown in Figures 21 and 22. By comparing these results at

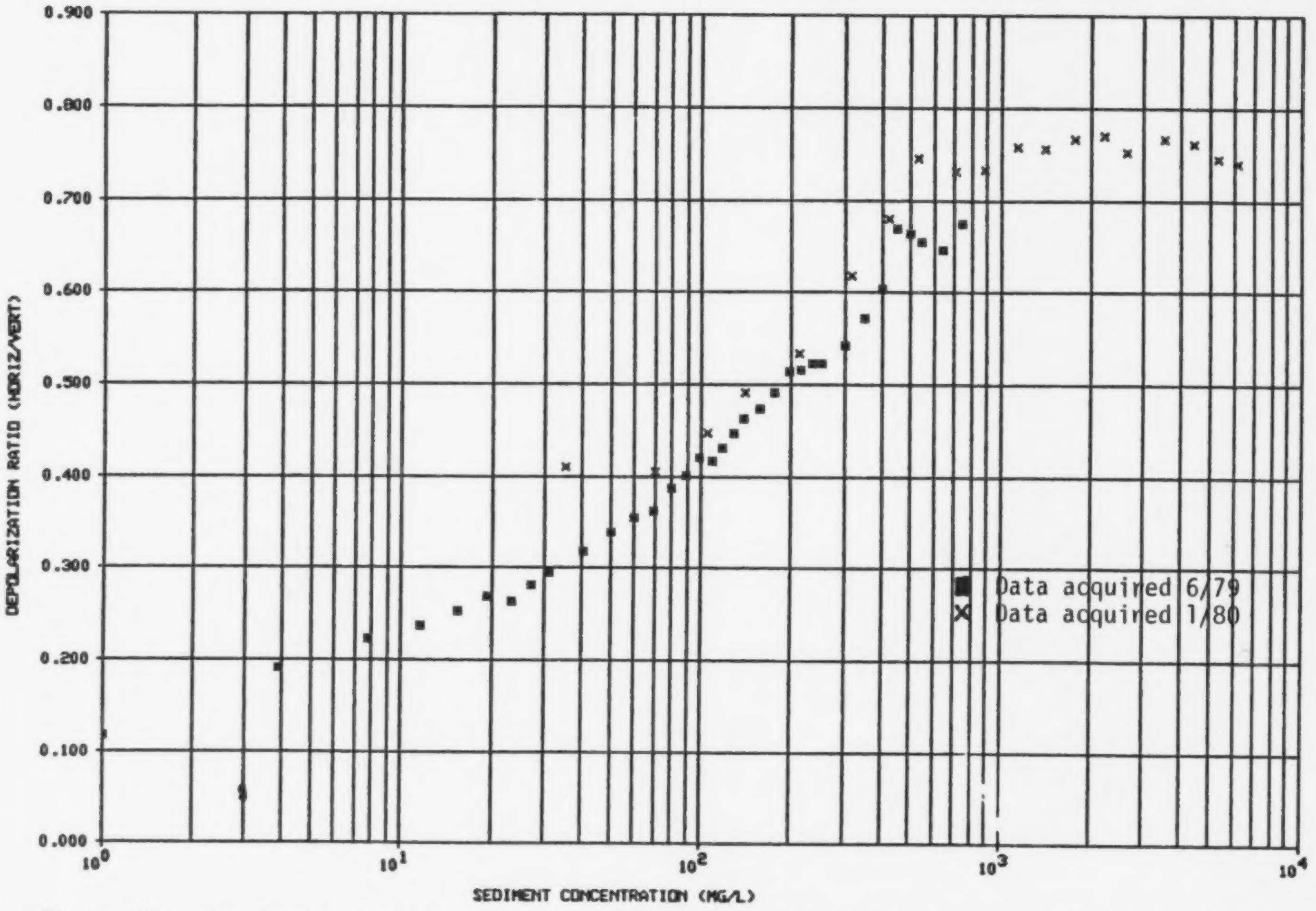

Figure 21. Depolarization Ratio Versus Sediment Concentration for Brown Silt Measured at 632 nm

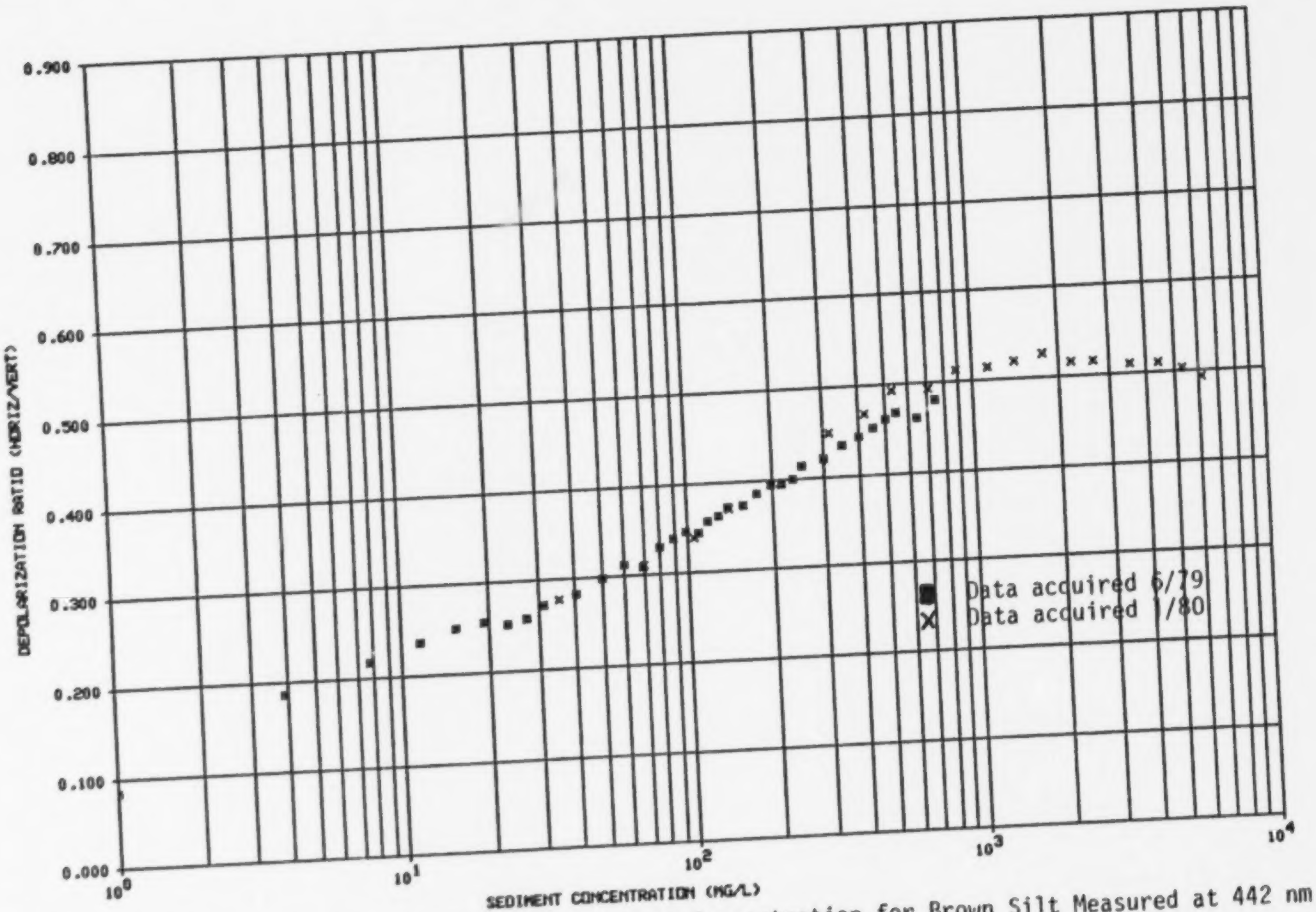

Figure 22. Depolarization Ratio Versus Sediment Concentration for Brown Silt Measured at 442 nm

the two different wavelengths the effects of the great reflectivity are easily observed. At the low levels of concentration where multiple scattering does not contribute greatly to the returns, the rate at which the depolarization ratio increases is very similar. However, when multiple scattering begins, the rate at which the depolarization ratio increases for the red laser is considerably more rapid than that for the blue laser. The higher reflectivity of the brown silt particles at the red wavelength has increased the efficiency of the multiple scattering process. As a result, the depolarization of the incident radiation is also greatly increased. The depolarization ratio plots for the red silt particles shown in Figures 19 and 20 also exhibit this characteristic.

To further examine this topic, measurements were made to determine the difference in reflectivity for the different particle colors at the wavelengths of the two lasers. Using the dichromatic lidar system, backscatter measurements were made from dry samples of the soil particles (Appendix E). The results of these measurements, shown in Table 1, are the measured return from the dry sediment sample dividied by the corresponding return from the white target. These values indicate that the red and brown silt particles are more efficient scatterers at the red wavelength than the blue wavelength. These measurements also show that the reflectivity of the red silt particles at the red wavelength is higher than the reflectivity of the brown sample at the same wavelength. The reflectivity of the white particles is approximately equal at the two wavelengths and considerably greater than the reflectivity of the red and brown particles.

The high reflectivity of the white silt particles can also be seen in the curves of the depolarization ratios for this particle type shown in Figures 17 and 18. Since the reflectivities for this particle at the two wavelengths are approximately equal, the depolarization ratios increase at roughly the same rate for the higher concentrations where multiple scattering is present. At the blue wavelength, the higher reflectivity of the white silt particles over the brown or red particles is evident by the much more rapid increase in the depolarization ratio for the white silt particles.

Another interesting effect can be observed in the depolarization ratio curves for the red and brown particle types shown in Figures 19-22. At approximately 800 mg/l the depolarization ratio does not continue to increase for an increase in the particle concentration. Not only does the depolarization ratio roll off, but the cross section measurements for these two particles shown in Figures 23, 24, 25, and 26 show that no additional energy is backscattered from the water beyond the saturation point. The value of the depolarization ratio at which the scattering from the different particles saturates for the particular wavelengths indicates that the absorbance of the particles contributes to this effect. At some level of scattering, the absorbance and scattering efficiencies of the particles prevent any further increase in the backscattered returns for an increase in the particle concentration. When this condition is reached, a higher concentration of particles causes more scattering but also more absorption. The higher absorption cancels the additional scattering, causing no change in the backscattered energy.

TABLE 1. Soil Reflectance Test Results

Sediment (Silt)	Wavelength	Polarization	20° Incidence		40° Incidence	
			Reflectance	Ratio	Reflectance	Ratio
Red	Red	Vert	0.722		0.943	
		Hor	0.538	0.745	0.644	0.687
	Blue	Vert	0.419		0.456	
		Hor	0.217	0.518	0.247	0.541
Brown	Red	Vert	0.594		0.898	
		Hor	0.509	0.857	0.571	0.636
	Blue	Vert	0.296		0.508	
		Hor	0.235	0.792	0.289	0.540
White	Red	Vert	1.106		1.230	
		Hor	1.179	1.066	1.206	0.980
	Blue	Vert	1.089		1.261	
		Hor	1.091	1.000	1.078	0.855

$$\text{Reflectance} = \frac{\text{Soil Return}}{\text{White Target Return}}$$

$$\text{Ratio} = \frac{\text{Hor Soil Refelctance}}{\text{Vert Soil Reflectance}}$$

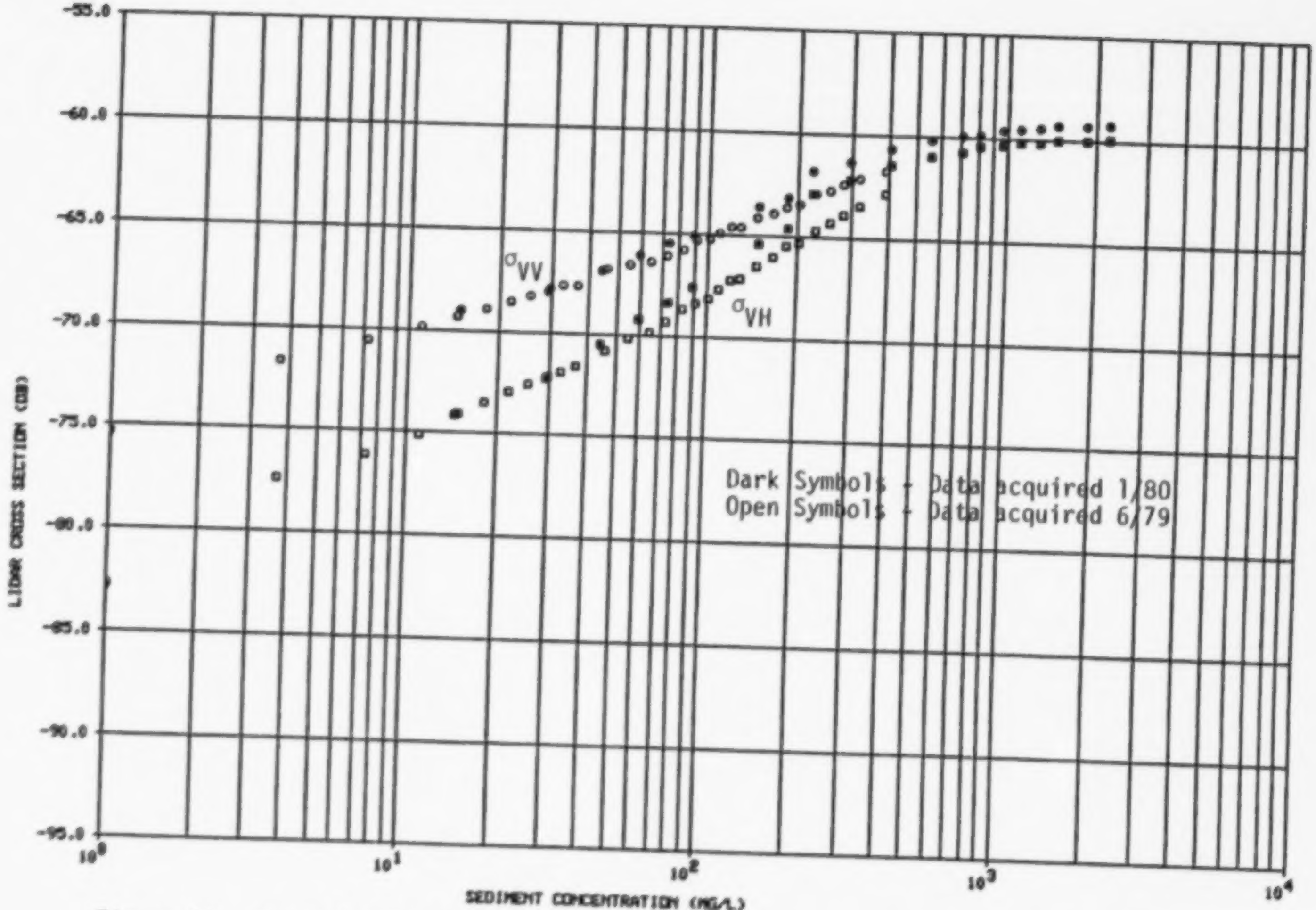

Figure 23. Cross Section Versus Sediment Concentration for Red Silt Measured at 632 nm

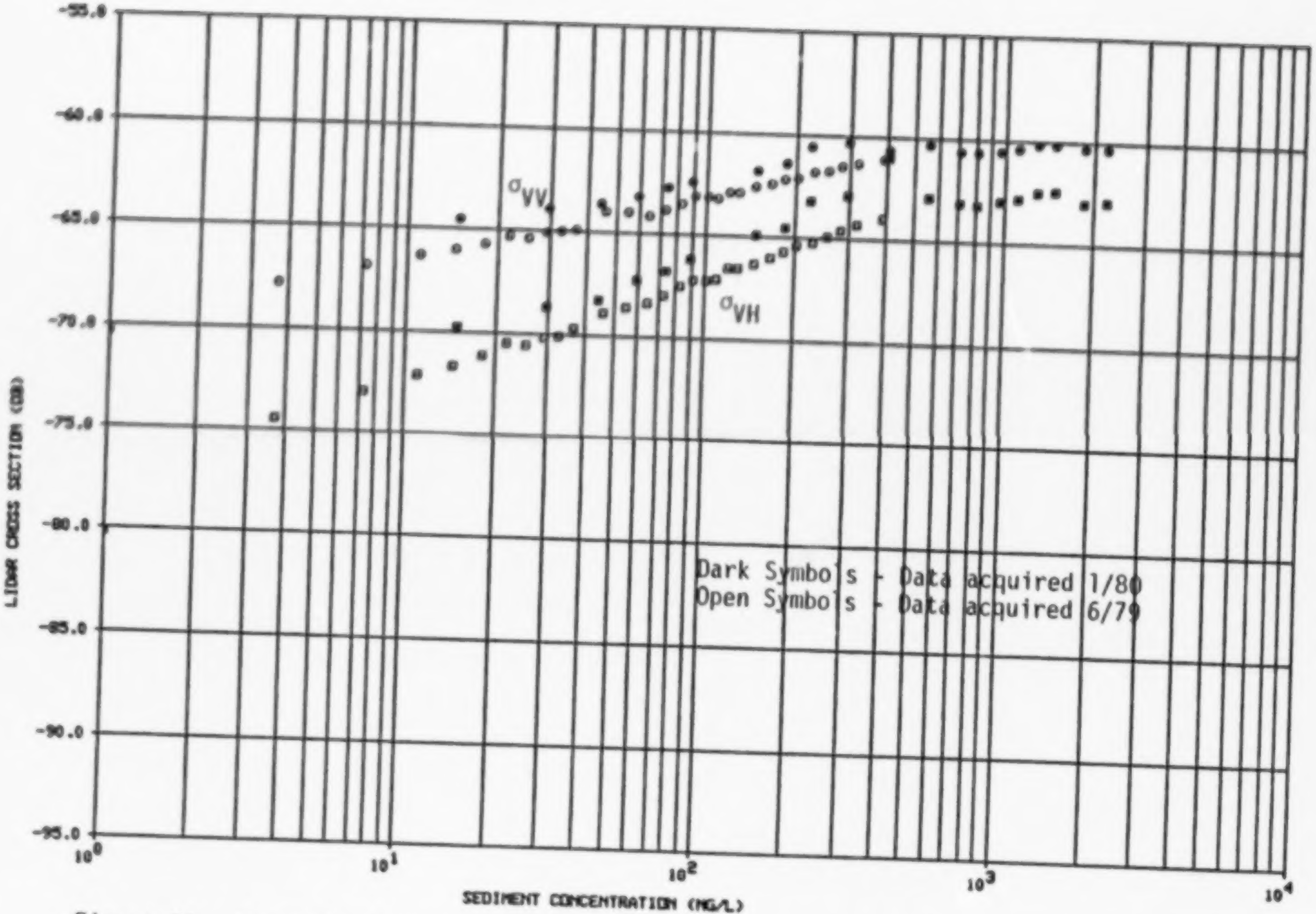

Figure 24. Cross Section Versus Sediment Concentration for Red Silt Measured 442 nm

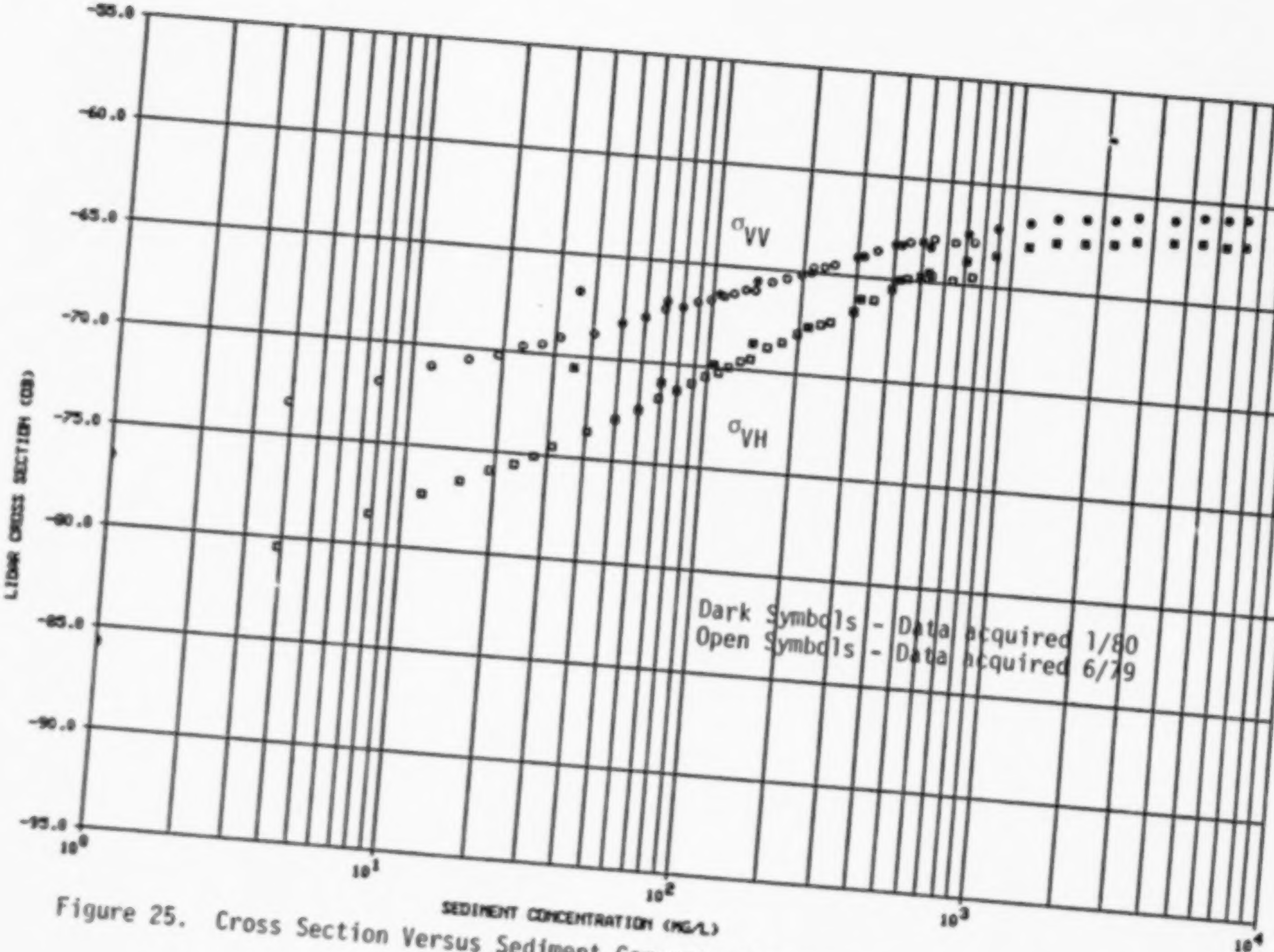

Figure 25. Cross Section Versus Sediment Concentration for Brown Silt Measured at 632 nm

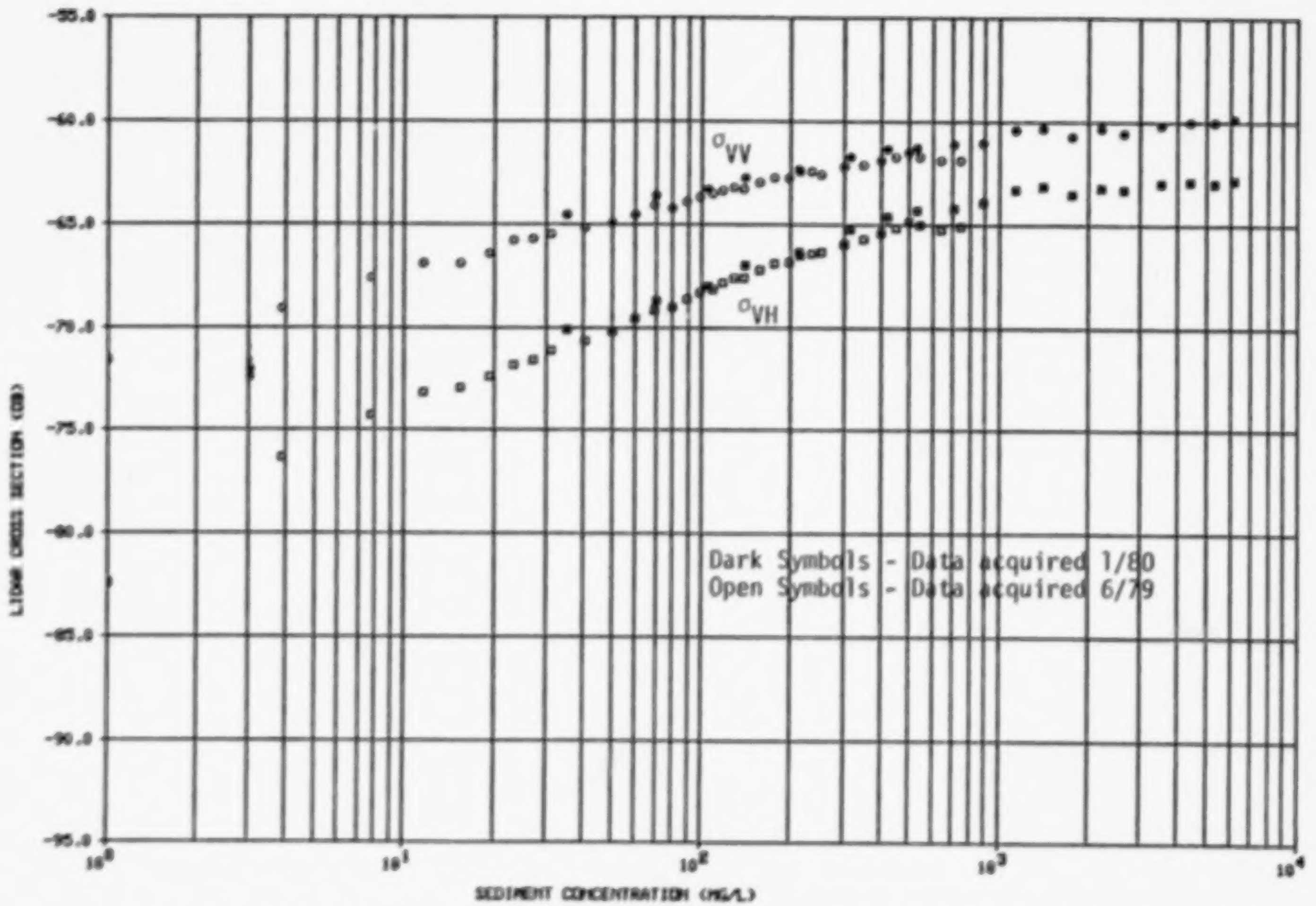

Figure 26. Cross Section Versus Sediment Concentration for Brown Silt Measured at 442 nm

The depolarization ratio at which the scattering saturates is determined partly by the absorbance of the particle at the measured wavelength. (For these very high concentrations of scattering particles where multiple scattering is present, the depolarization ratio is directly related to the relative amount of multiple scattering.) The high absorbance of both the red and brown silt particles at the blue wavelength is indicated by the low value of the depolarization ratio in which the scattering process saturates. The low absorbance at the red wavelength permits a higher depolarization ratio at the saturation point for both the brown and red particles.

The depolarization ratio curve for the white silt particles shows that the scattering from the sample does not reach a saturation point, even though the concentration of scattering particles has exceeded the saturation level for the red and brown particles. Due to the very low absorbance and the high scattering efficiency of this particle, a much higher particle concentration is required to saturate the scattering process at both the red and blue wavelengths.

Extinction Depth of Measurement

The results of the extinction depth measurement experiments shown in Figures 27, 28, and 29 confirm the relative absorbance indicated by the value of the depolarization ratio at which the scattering process saturates for the red and brown silt samples. If the measurement of the depth of water that contributes to the backscattered return is governed by a two-way extinction process, then the relation between the absorbance and the measurement depth become clear.

Several characteristics in the results of the depth of measurement experiment correspond to the relative absorbance of the different particles indicated by the saturation points described previously. The depth of water that contributed to the backscattering from the white silt particles was approximately equal for both the blue and red wavelengths, and considerably deeper than the measurement depth for the brown and red silt particles. The measurement depth for the red laser was consistently larger than that for the blue laser for scattering from both brown and red silt particles. Also for the red silt sample, the measurement depth for the blue laser was considerably less than that for the red laser.

These results are a good indication of the relative absorbance of the different particles at both of the measurement wavelengths. For the white silt particles, the absorbance at both wavelengths is approximately equal and considerably less than the absorbance levels for the brown and red silt particles. For the brown silt sample, the absorbance at the blue wavelength is greater than the absorbance at the red wavelength. The absorbance at the blue wavelength for the red silt sample is considerably greater than the absorbance at the blue wavelength.

The relative values of these absorbance levels correspond to the relative values of depolarization ratios at the saturation point for the different colors of particles. The white silt sample has approximately

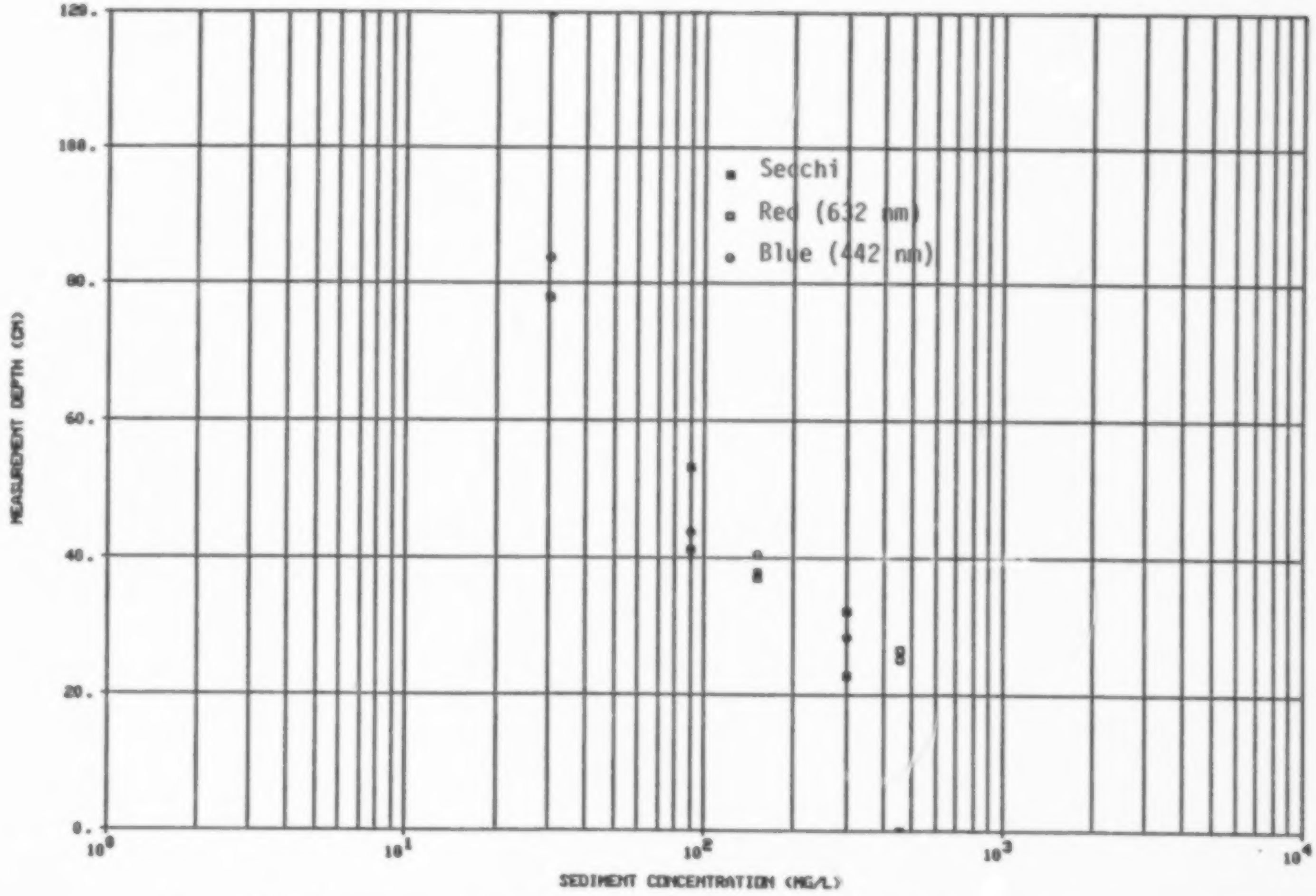

Figure 27. Measurement Depth as a Function of White Silt Sediment Concentration

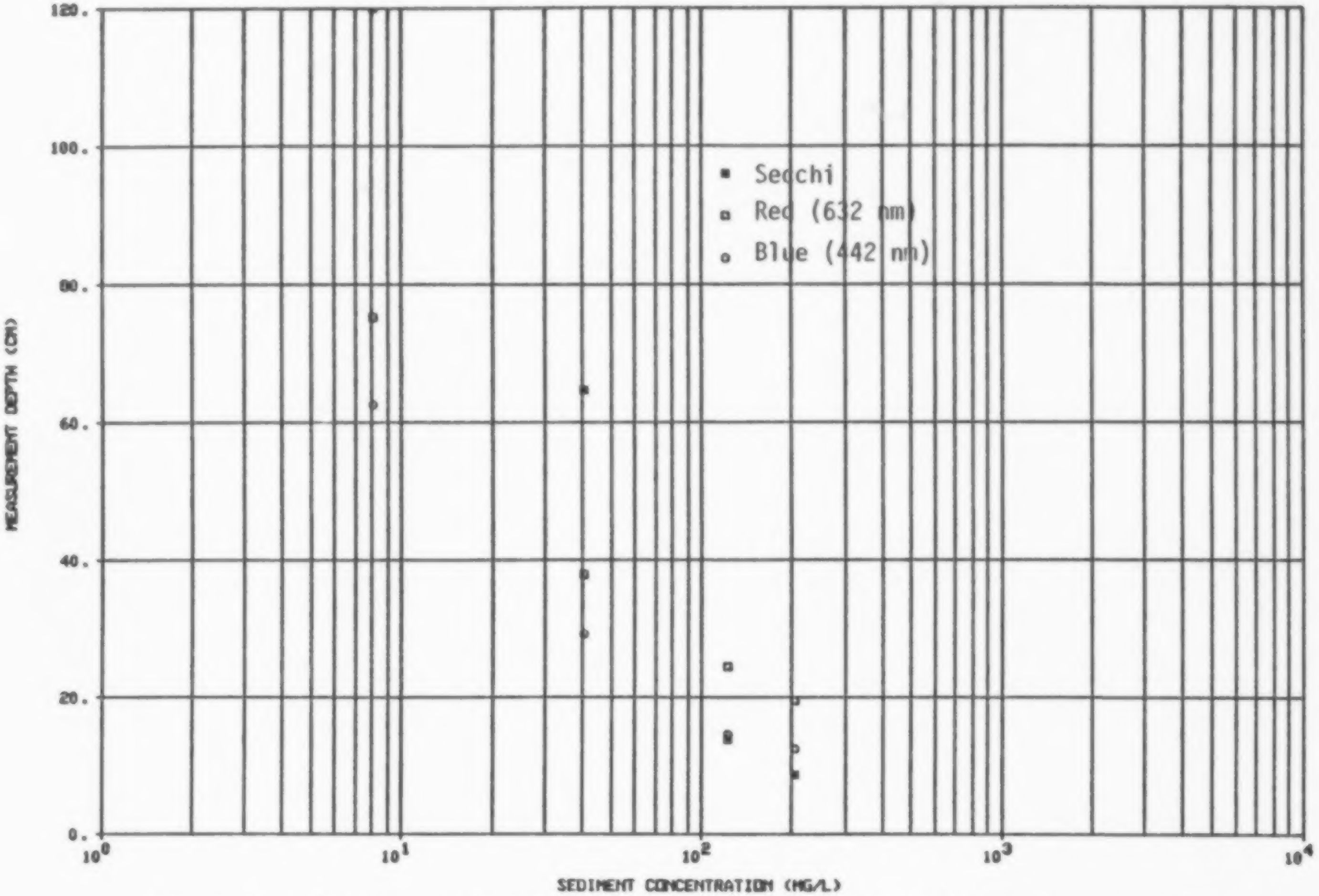

Figure 28. Measurement Depth as a Function of Red Silt Sediment Concentration

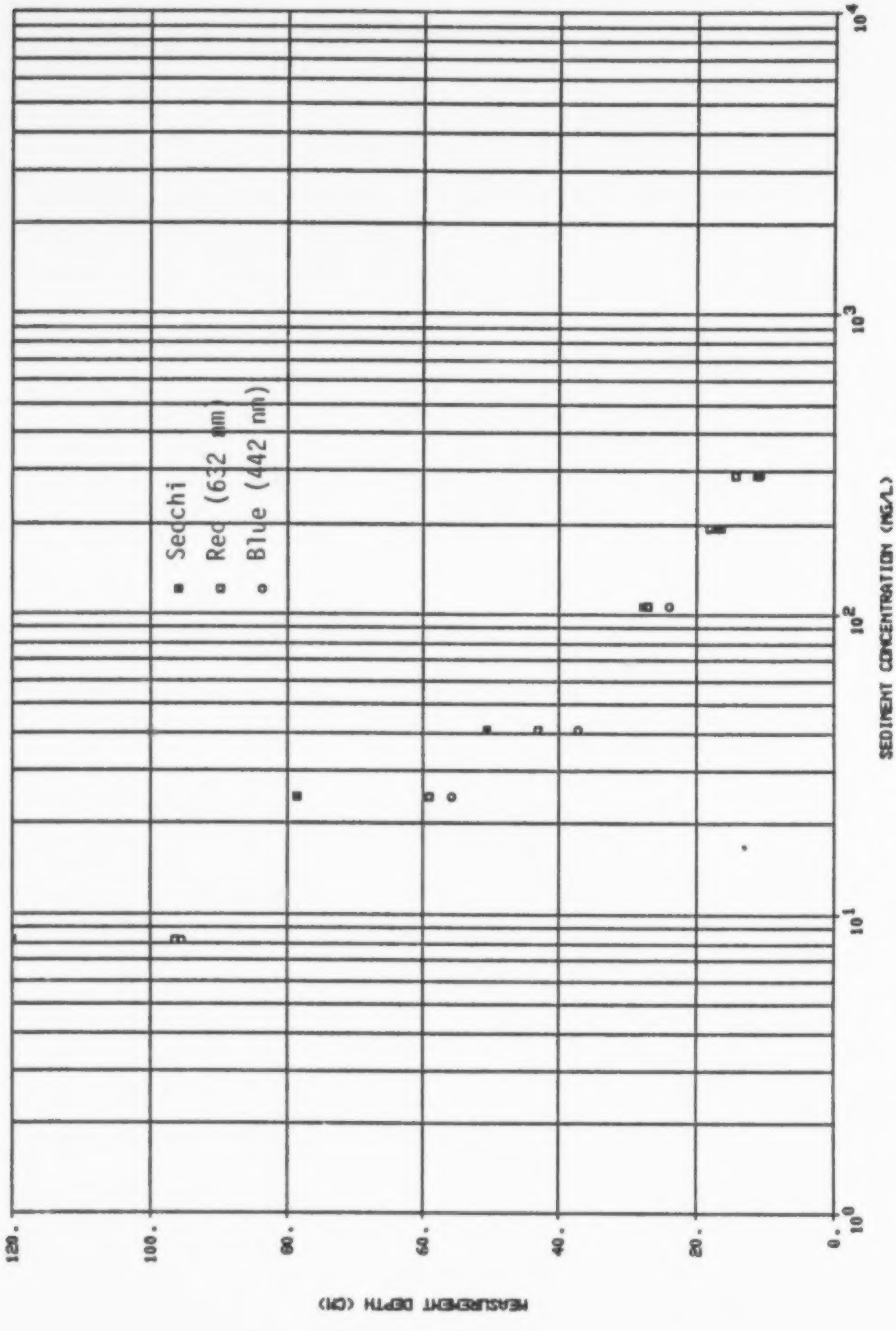

Figure 29. Measurement Depth as a Function of Brown Silt Sediment Concentration

equal response for the red and blue wavelengths and did not saturate at concentration levels well above the saturation level for the brown and red silt samples. The depolarization ratio at which the blue wavelength saturated was considerably less than the saturation ratio for the red wavelength for both the brown and red silt samples. The difference between the depolarization ratio at which the blue and red wavelengths saturate is greater for the red silt than it is for the brown silt. Though the scattering efficiencies and reflectivities of the different particles at both wavelengths no doubt contribute to the saturation level of the scattering process, these results strongly suggest that the absorbance of the particles at the measurement wavelengths also contributes to the depolarization ratio at the saturation point of the scattering process.

Size Distribution

The white clay and silt sediment samples used in these measurements represent particles that range in size from 40 μm down to less that 1 μm. Comparison of the depolarization ratio graphs for these two size ranges indicates that the depolarization ratio is not greatly affected by the different particle sizes for some concentration levels. Figures 30 and 31 are the composite depolarization ratios for both of these particles. At the higher concentration levels where multiple scatter is present, the depolarization ratio is almost independent of size distribution for both the red and blue wavelengths. At the lower concentrations where single scatter is predominant, the particle size does affect the depolarization ratio. Since this occurs at concentration levels where single scatter largely dominates the returns, this effect is similar to the shape effects. Similar to the effects on the backscattering caused by the particle shape, the size of the particles also affects the degree of depolarization of the incident radiation when single scatter dominates the returns.

The cross section curves shown in Figures 32 and 33 show that the actual backscattered energy is greater for the smaller clay particles at the higher concentration levels. The concentration of the sediment particles is graphed in milligrams per liter (mg/l). Since the smaller particles require more particles to equal a similar mass of the larger particles, the actual number of scattering particles is higher for the smaller size range at the same concentration level on these graphs. Though this high particle concentration causes more increased scattering, the like- and cross-polarized returns are equally affected so that the depolarization ratio remains unaffected.

Algae Measurements

The results of the backscatter measurements from algae with and without sediment are shown in the depolarization ratio graphs of Figures 34 and 35. The scattering from clear water and the tank, before any sediment or algae was introduced, is shown as the returns at a concentration of 1.0 mg/l. The depolarization ratio for just the algae alone changed very little from the value for the clear water sample. The cross section curves for this experiment given in Figures 36 and 37 show that the maximum concentration of algae decreased the scattering from the measurement tank at both the red and

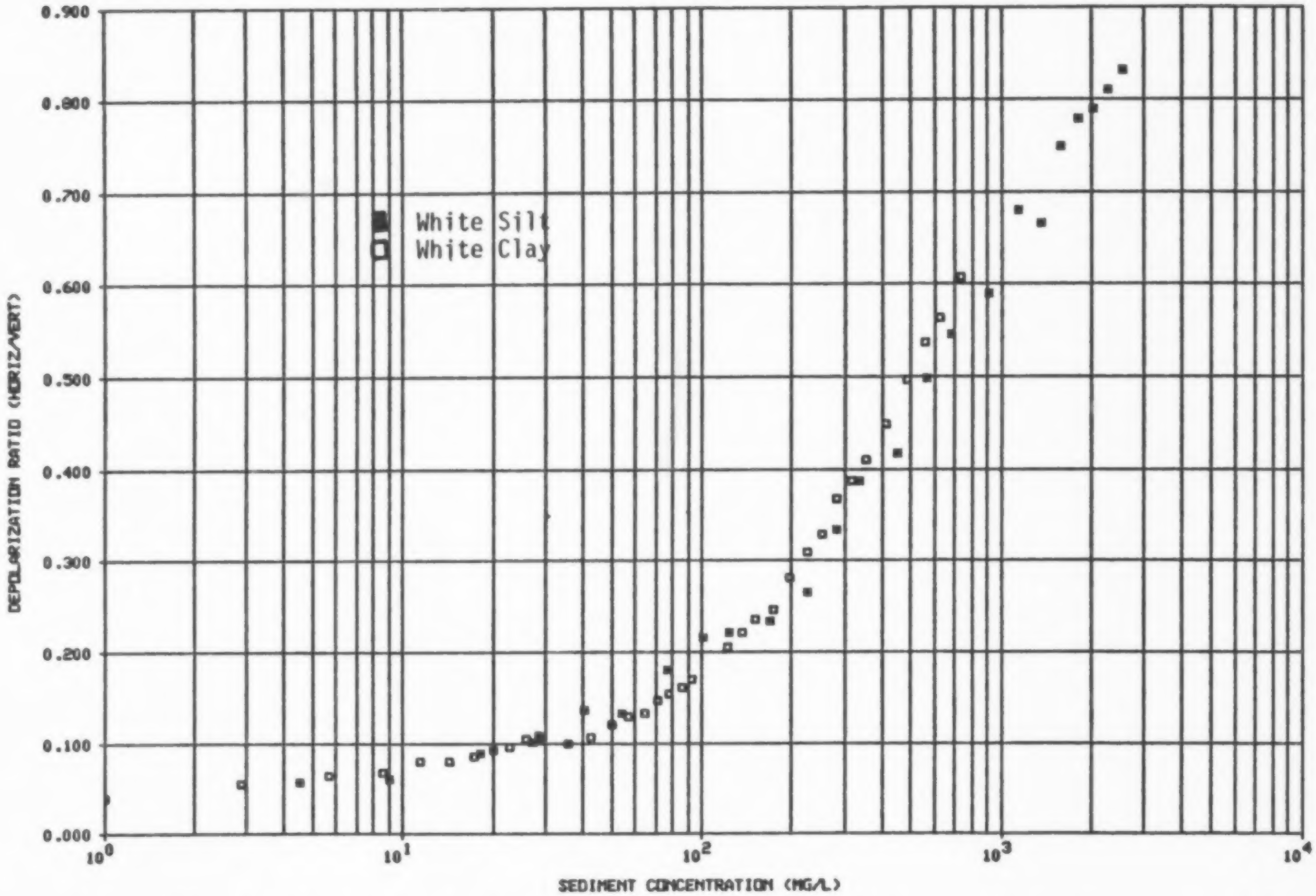

Figure 30. Depolarization Ratio Versus White Clay and Silt Concentration Measured at 632 nm

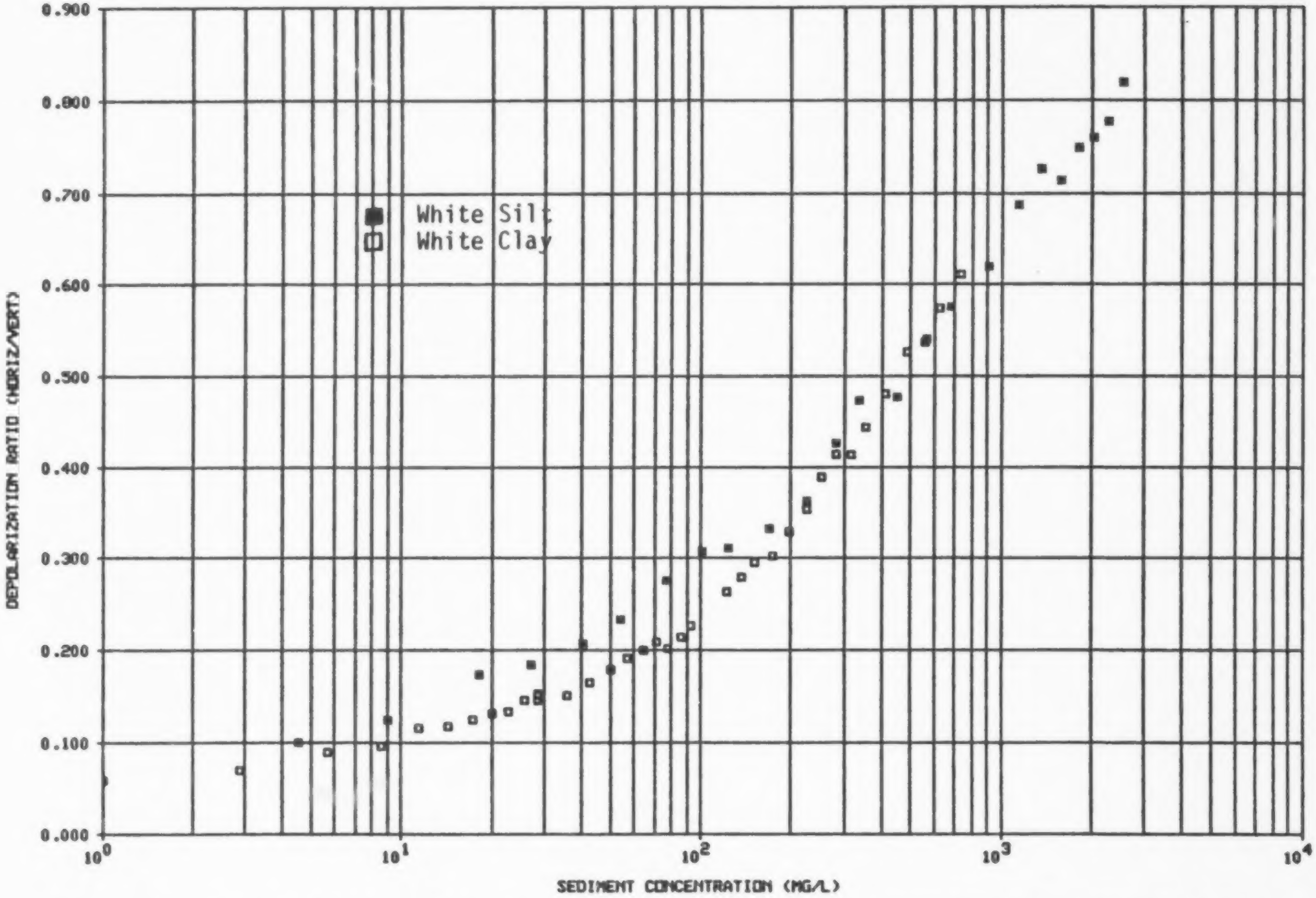

Figure 31. Depolarization Ratio Versus White Clay and Silt Concentration Measured at 442 nm

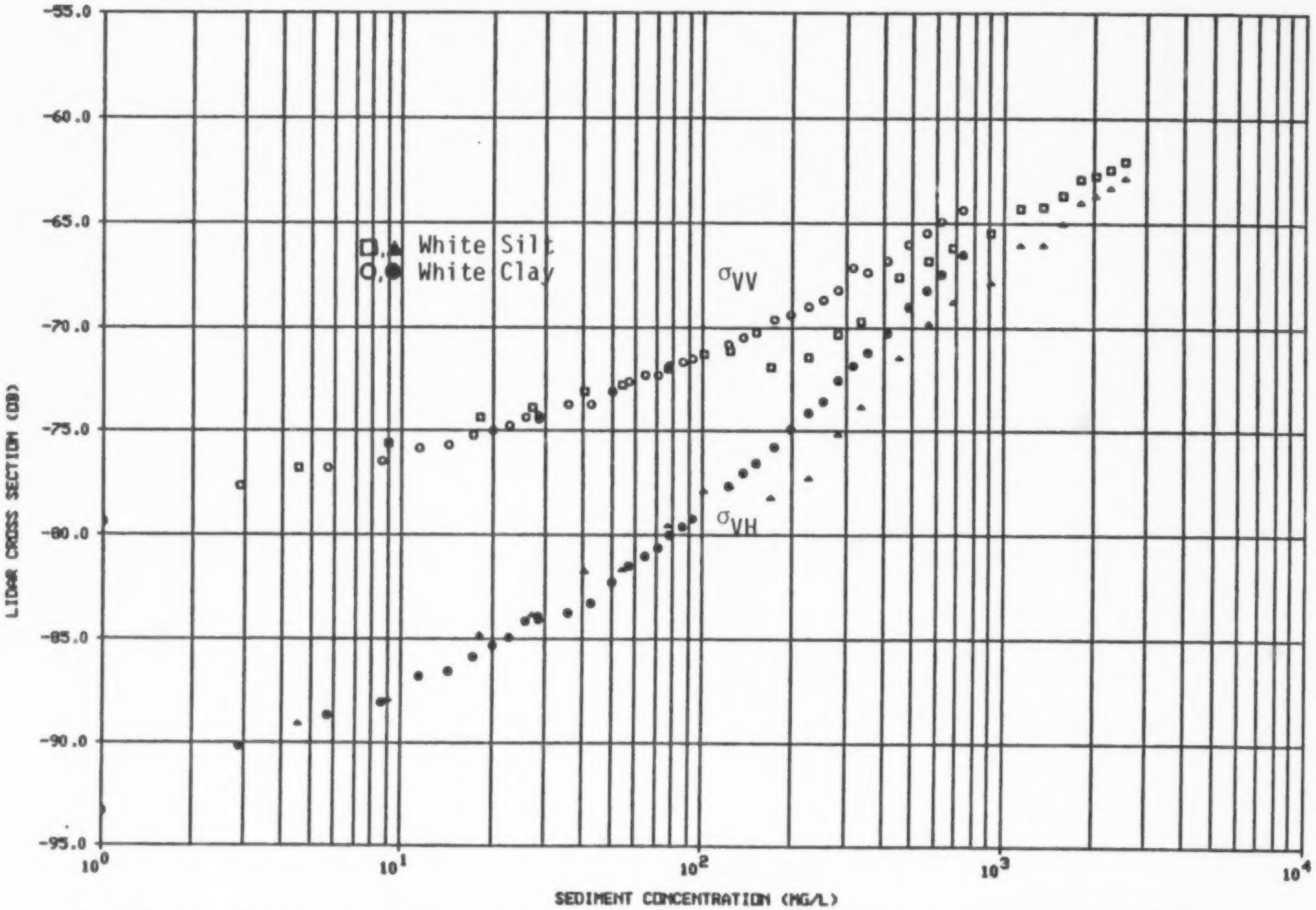

Figure 32. Cross Section Versus White Silt and Clay Concentration Measured at 632 nm

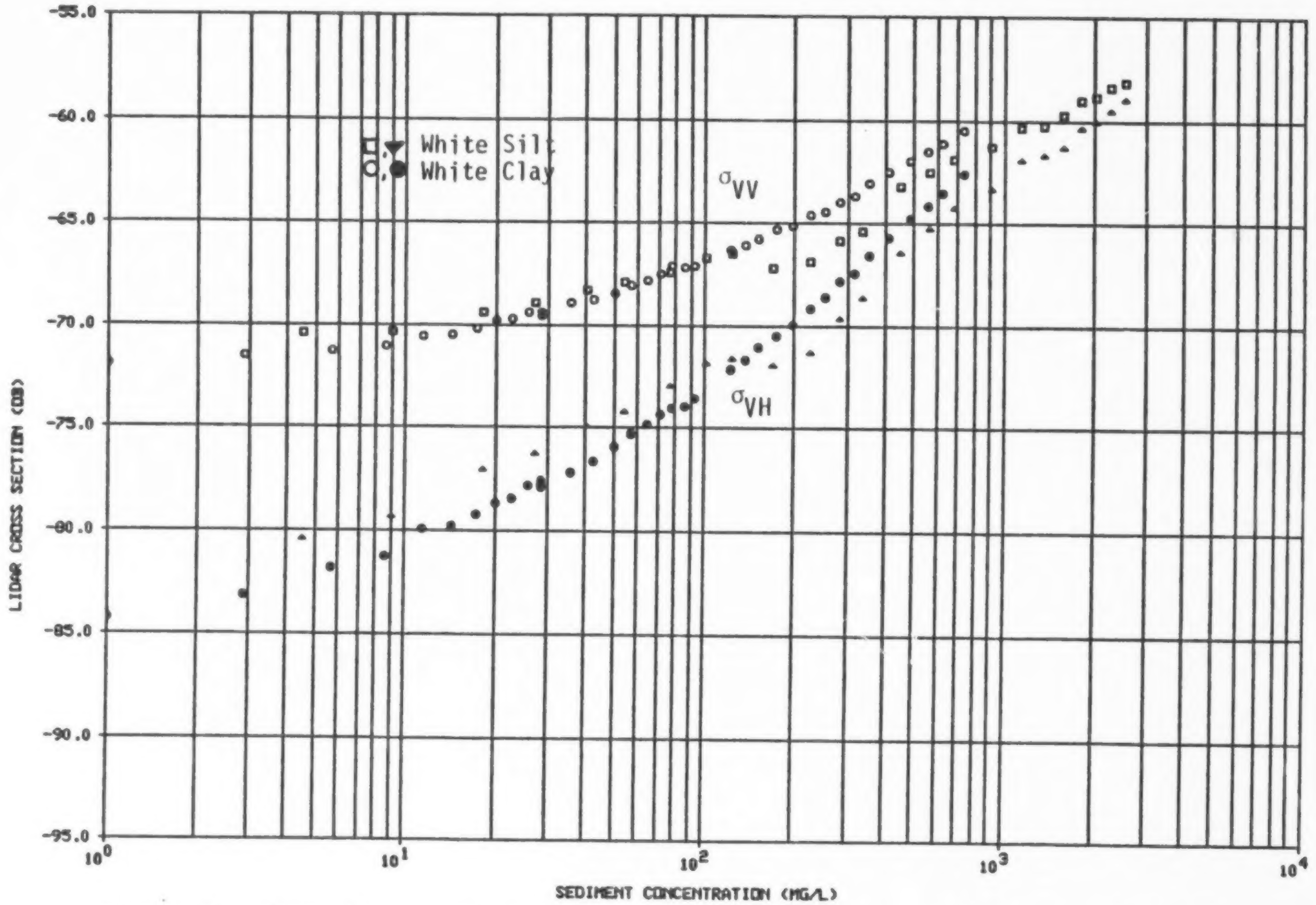

Figure 33. Cross Section Versus White Silt and Clay Concentration Measured at 442 nm

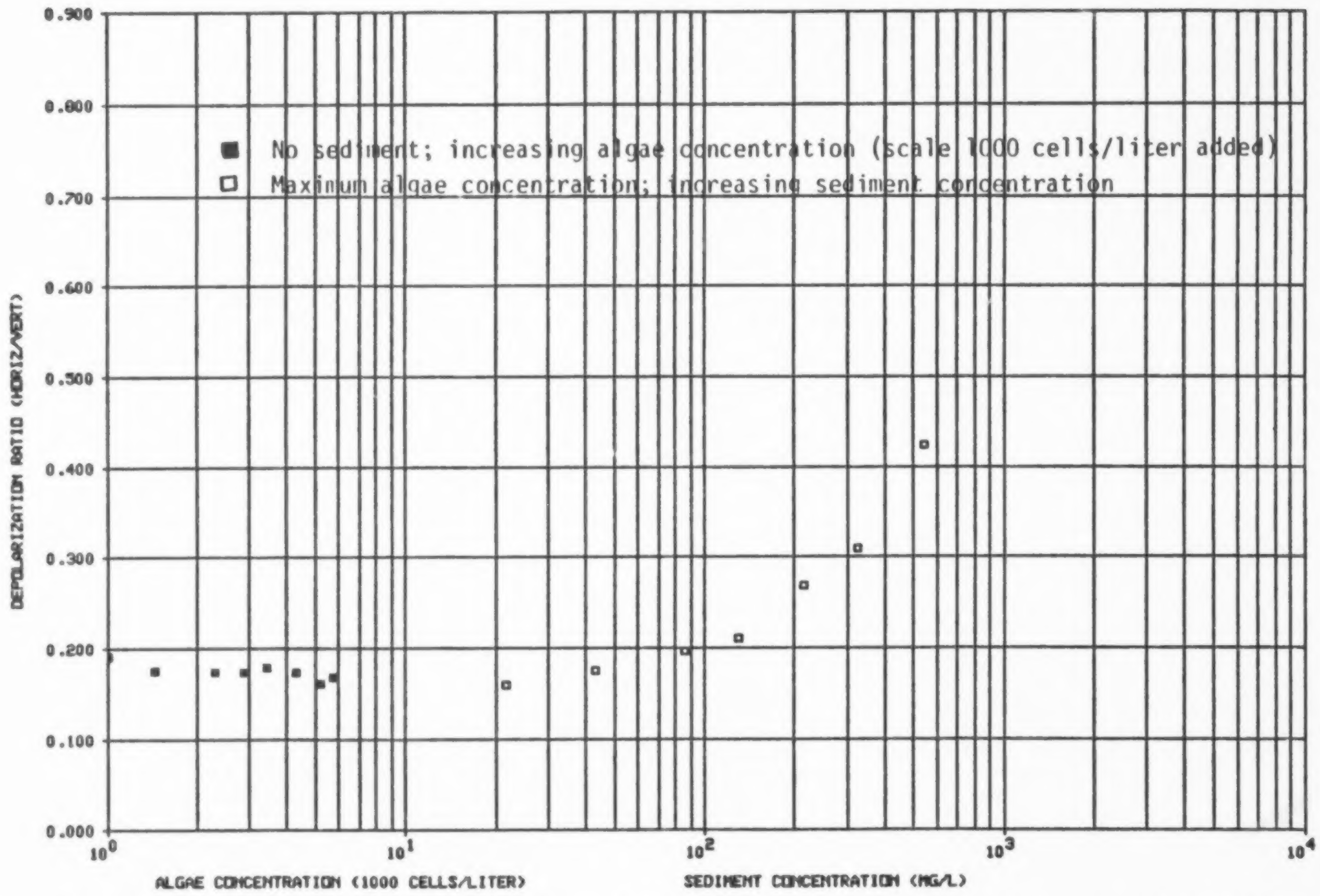

Figure 34. Depolarization Ratio Versus Algae and Sediment Concentration Measured at 632 nm

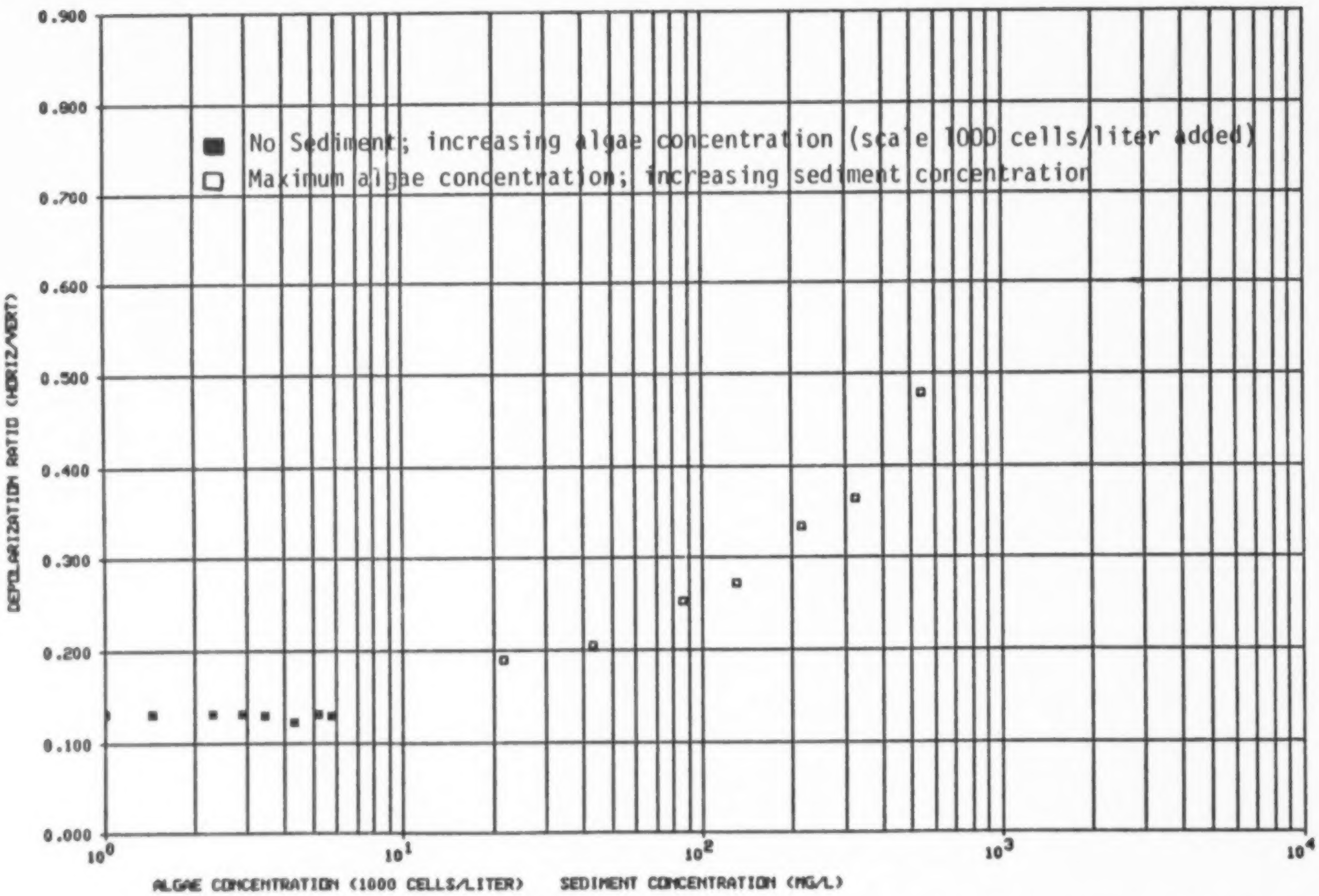

Figure 35. Depolarization Ratio Versus Algae and Sediment Concentration Measured at 442 nm

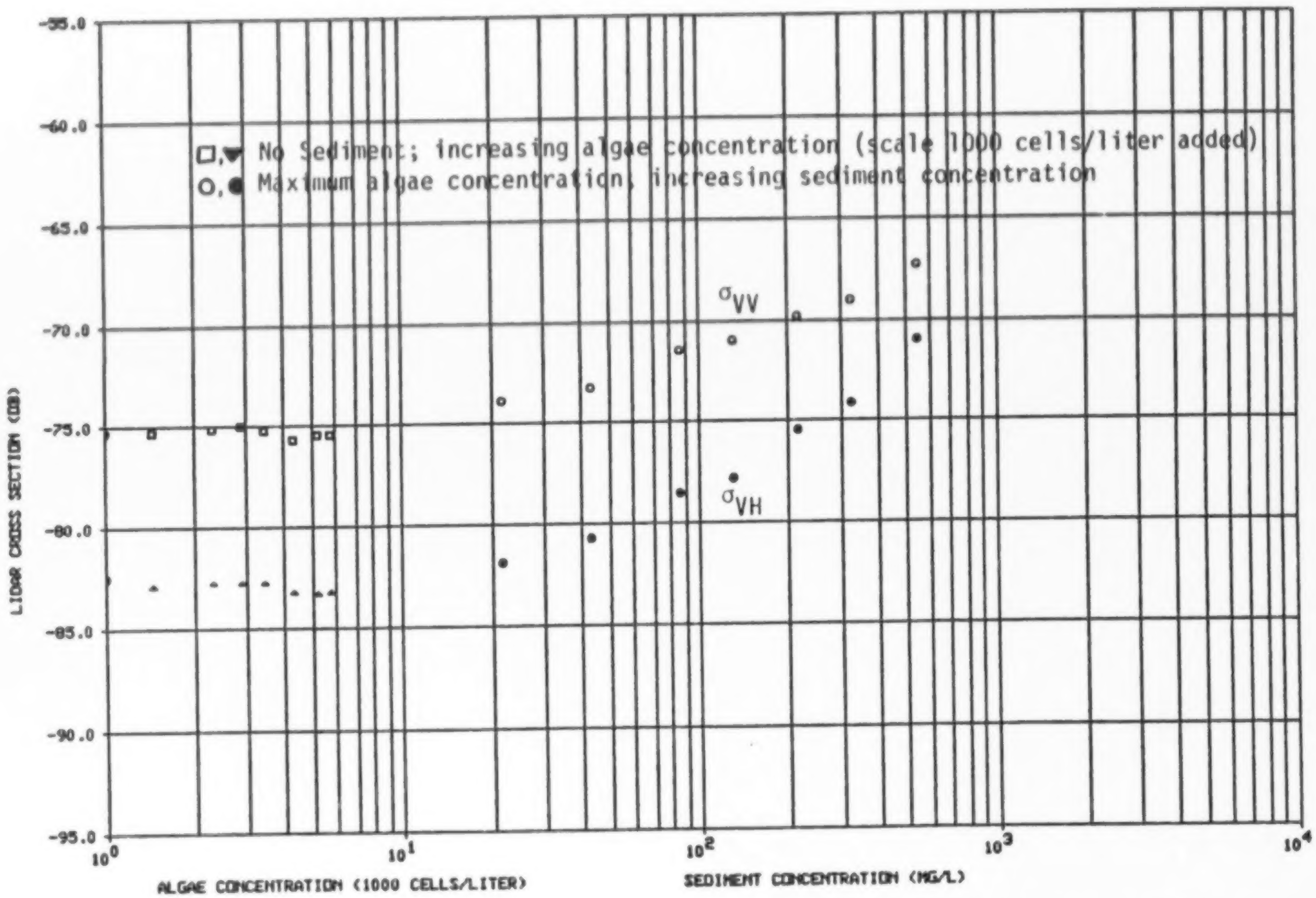

Figure 36. Cross Section Versus Algae and Sediment Concentration Measured at 632 nm

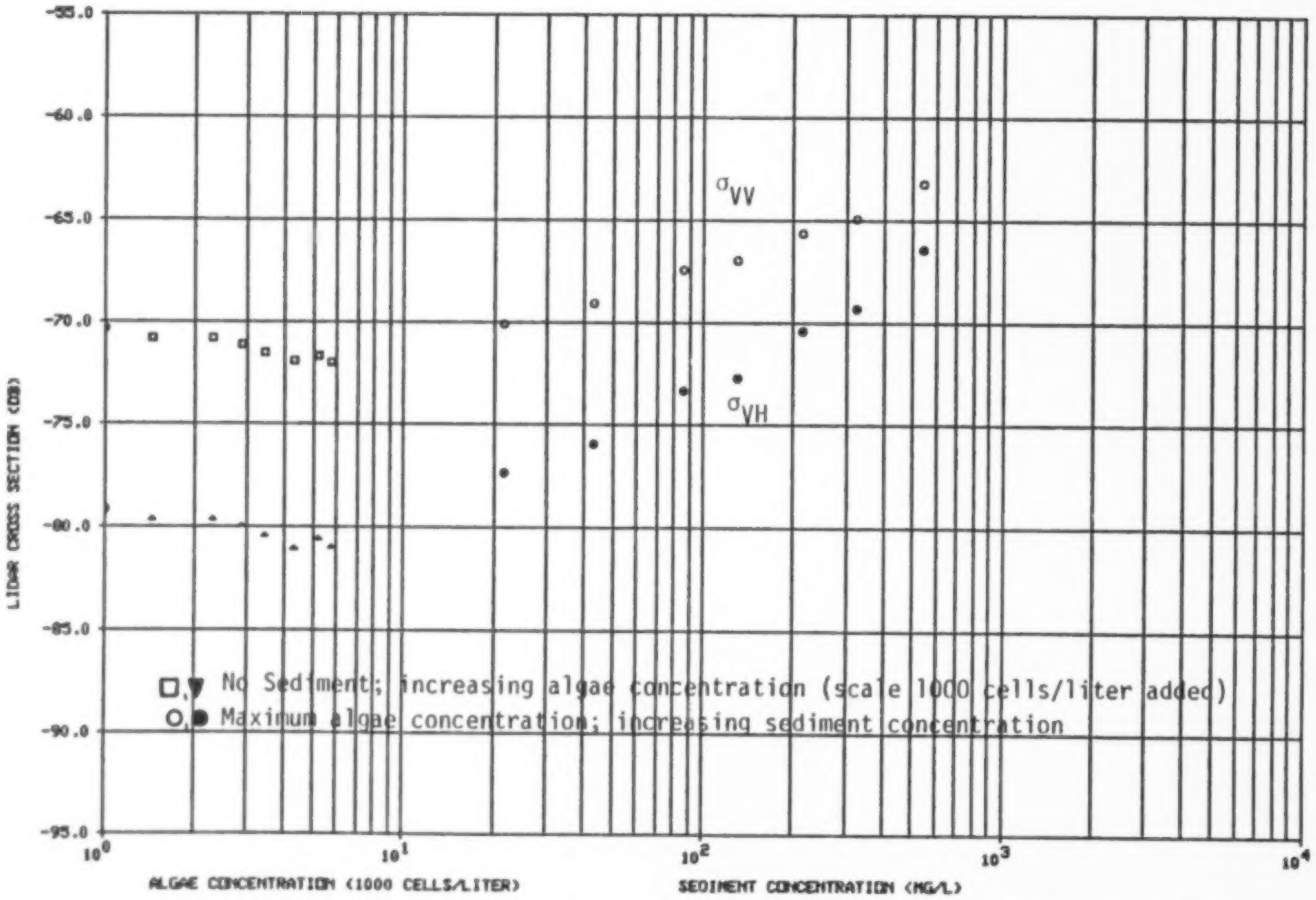

Figure 37. Cross Section Versus Algae and Sediment Concentration Measured at 442 nm

blue wavelengths. This decrease in the scattering indicates that this type of green algae has a high absorbance and a very low scattering efficiency.

The sediment used in these measurements was the white silt sample. Figures 17 and 18 shown previously are the depolarization ratio results for this particle type. A comparison of these results and the measurements made with algae indicate very little differece in the scattering from the sediment with and without algae. The depolarization for the blue returns is slightly lower but not significantly so. The returns for the red laser show no effects from the presence of the algae.

The algae used in this experiment were obtained from a 20-liter culture of Chlamydomonas grown to a bloom condition of approximately 2.0 x 10^5 cells/liter. When this algae concentration was introduced into the measurement tank, the final concentration of algae was 5.7 x10^3 cells/liter or approximately 3% of the maximum concentration of the algae at a bloom condition. Though this is not a high concentration of organic suspended solids, the water was tinted green by the algae even at the highest concentration of sediment measured. Since the growth of algae is geometric, a concentration of algae which is 3% of a bloom concentration would be indicative of a reasonable algae concentration encountered in ponds and lakes where algae is present, but not in a bloom condition.

The effect of higher concentrations of algae can be estimated by considering the scattering properties found to affect the backscattering from sediment particles. The measurements of the different colors of sediment particles have shown that the reflectivity, absorbance and scattering efficiencies of the particles at the measured wavelengths cause considerable variation in the scattering characteristics of sediment laden water. The complete lack of any backscattering from these organic suspended solids has shown that the reflectivity and scattering efficiencies for the algae cells are very low. The absorbance of organic suspended solids appears to be the dominant loss mechanism, as would be expected. Since absorbance affects the backscattering from sediment particles by causing the scattering to appear to saturate, the additional absorbance introduced by the presence of organic suspended solids would probably lower the concentration level as which the scattering from suspended sediments saturate. Very high concentration of algae could mask the detection of suspended sediment in this manner.

The absorbance and scattering efficiencies of different colors and types of algae could vary with wavelength. These characteristics would have to be measured to determine their effect on the scattering from different colors of suspended sediments.

Surface Roughness

As previously stated, the level of surface roughness generated for these measurements was limited by the measurement configuration. These low levels of surface roughness did not significantly affect the sedment scattering. The depolarization ratio and cross section graphs shown in Figures 38, 39, 40 and 41 for the surface roughness measurements from the white silt/clay

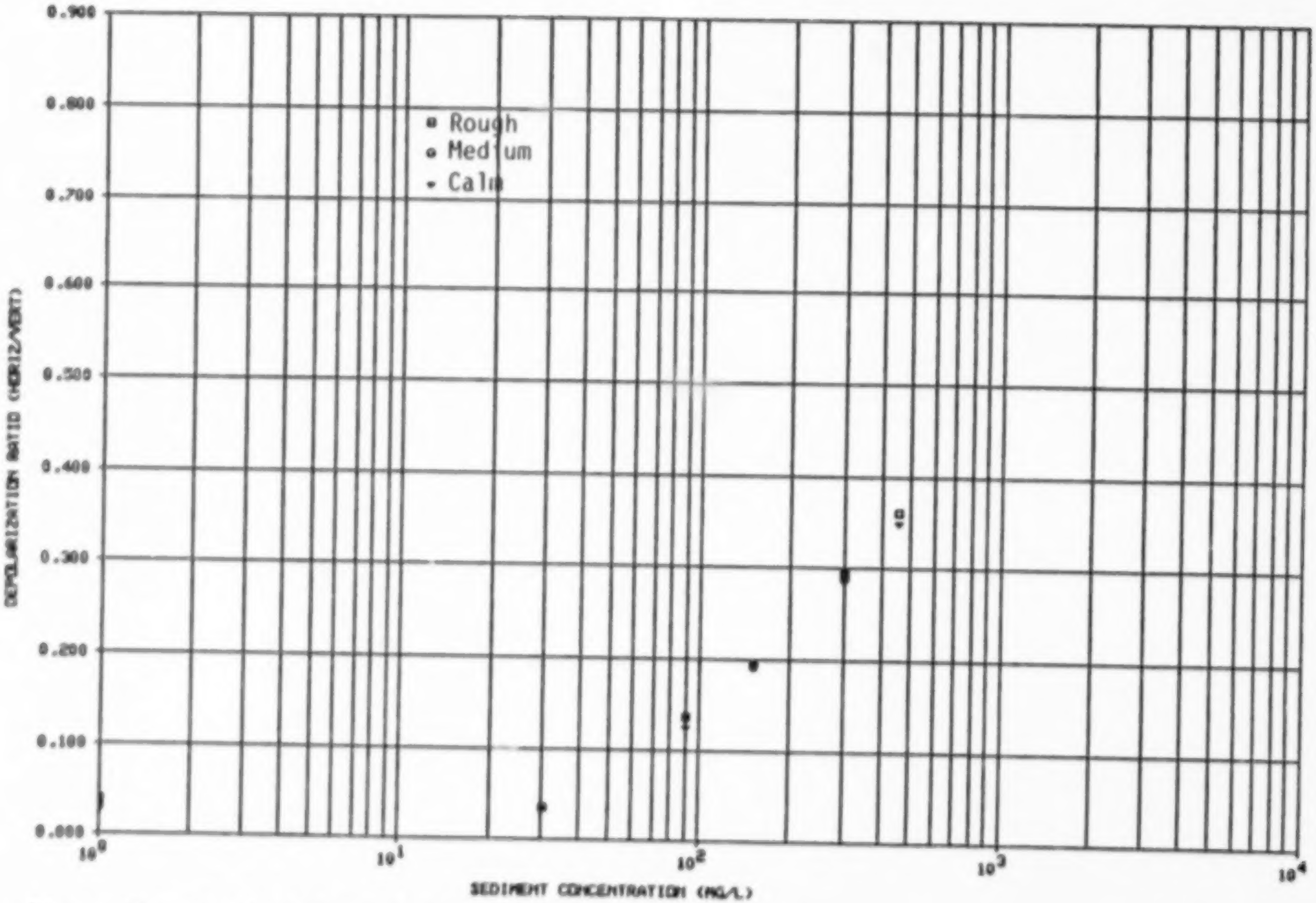

Figure 38. Depolarization Ratio Versus White Silt/Clay Sediment Concentration and Surface Roughness Measured at 632 nm

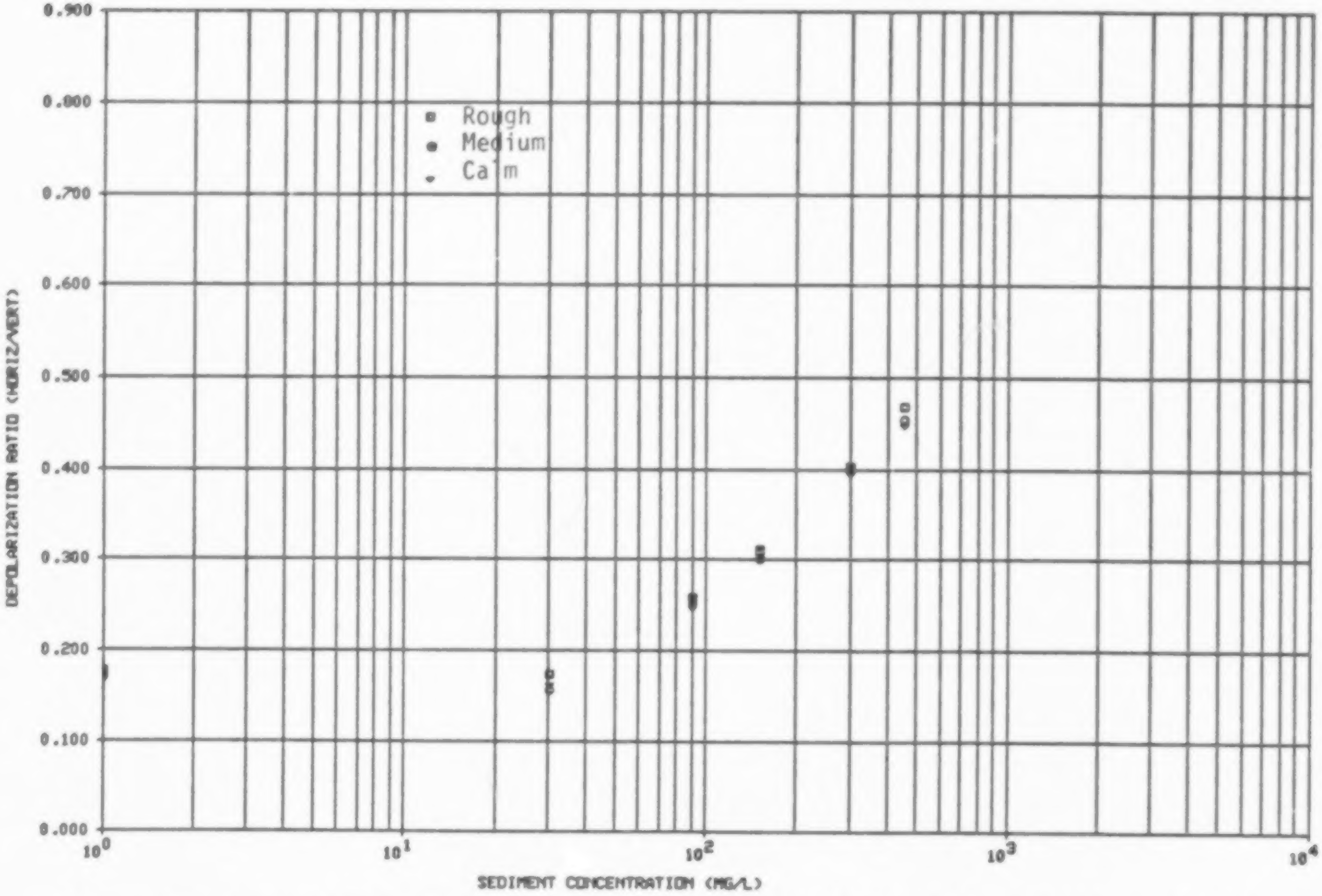

Figure 39. Depolarization Ratio Versus White Silt/Clay Sediment Concentration and Surface Roughness Measured at 442 nm

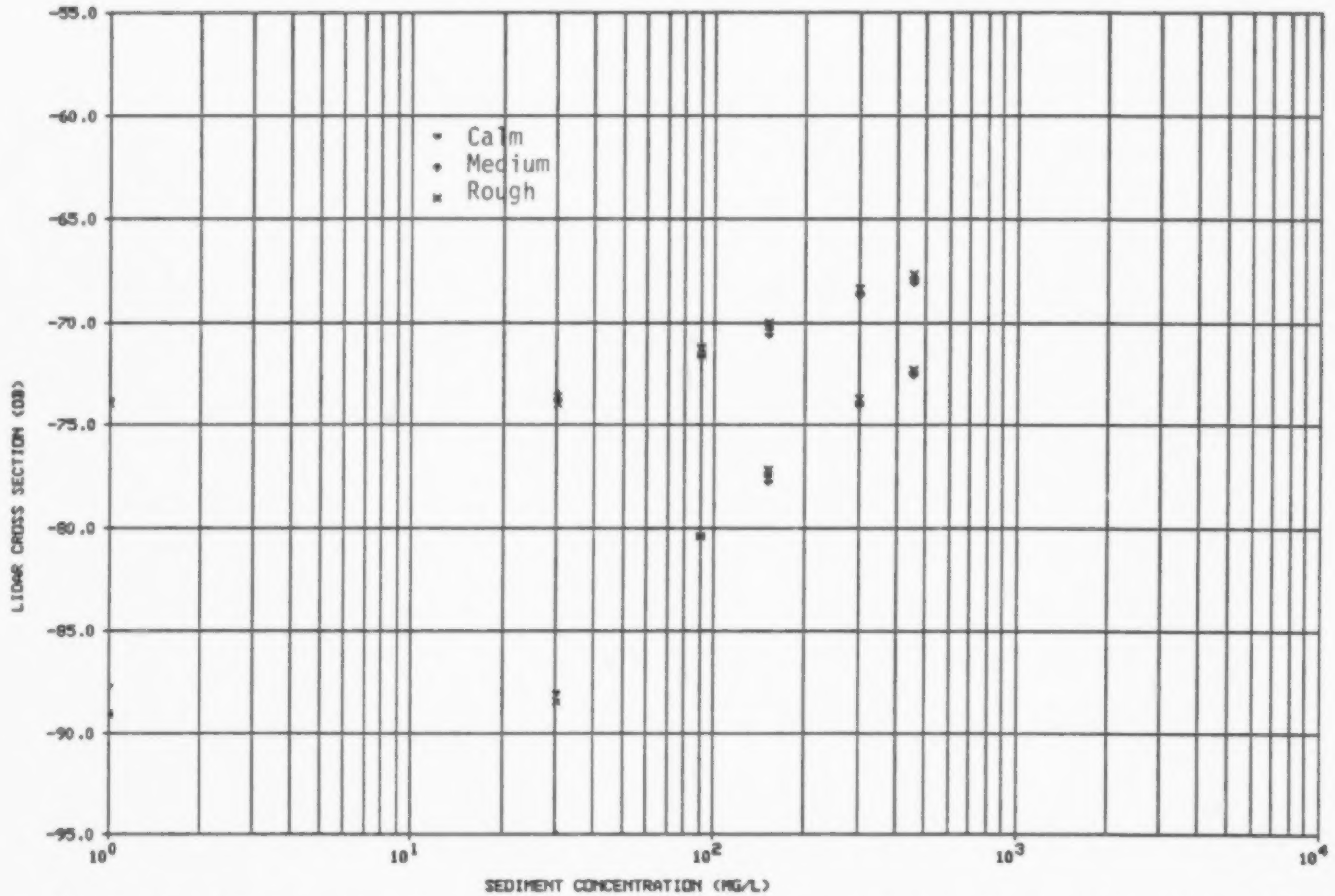

Figure 40. Cross Section Versus Sediment Concentration and Surface Roughness for White Silt/Clay Measured at 632 nm

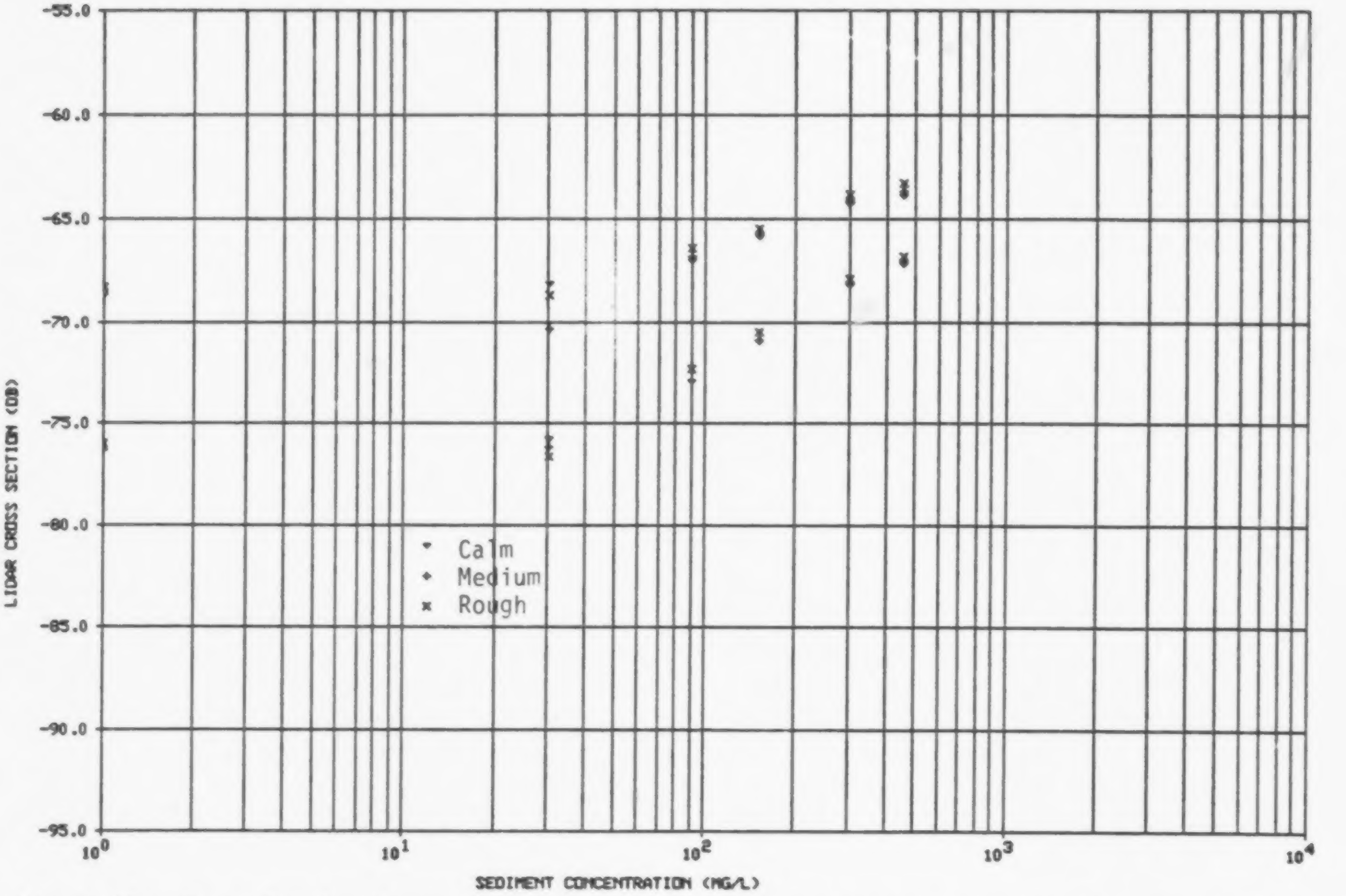

Figure 41. Cross Section Versus Sediment Concentration and Surface Roughness for White Silt/Clay at 442 nm

particles are typical of the results from the earlier (calm surface) measurements. The depolarization ratio for the different levels of surface roughness differs by 2% to 10%.

One effect that was mentioned in previous studies is also evident in these measurements. The depolarization ratio is less affected by surface roughness than either individual component of the backscattered returns. These measurements were made at an incidence angle beyond the Brewster angle. At this incidence angle, the transmission coefficients are fairly small and prevent an efficient transfer of the incident energy across the air-water interface. For the rough surface, the angles at which the laser beam strikes the air-water interface include a wide range of angles. The lower angles of incidence have considerably more efficient transmission coefficients. As a result, more energy is available to be scattered in the volume. This increase in efficiency causes an increase in both the like- and cross-polarized backscattering, in a manner similar to a power increase. However, both terms of the depolarization ratio are similarly affected and the net effect on the depolarization ratio is less than that on either individual component. This self-correcting characteristic of the depolarization ratio is therefore a significant advantage when normalizng the lidar returns.

INSTRUMENTAL AND MEASUREMENT ARTIFACTS

Several unusual characteristics in the results of the measurements are related to problems encountered during the data acquisition. This section explains some of these problems and how their effects may be prevented in subsequent experiments.

Clear Water Offsets

The backscattering from the measurement tank was usually measured before any scattering particles were introduced into the water. These returns which are the scattering from only the water and the black absorber in the bottom of the tank, are shown in the plots of both the cross sections and depolarization ratios at the nominal concentation level of 1.0 mg/l (i.e., at the left axis of the grid). A comparison of the many measurements shows that this backscattering from the measurement tank before sediment was added is not consistent for all of the measurements. For example, the cross section measurements for the white clay sample are given in Figures 42 and 43. The cross section measurements for the red silt particles are shown in Figures 23 and 24. For both the blue and red wavelengths at both the like- and cross-polarized returns, the cross sections of just the measurement tank before the red silt particles were added (-70.3, -80.1, -75.3, and -82.7, respectively) is greater than the cross sections for the measurement tank before the white clay particles were added (-71.9, -84.2, -79.3, and -93.3, respectively). The measurement sequence using the white calibration target corrected the measurements for both laser power fluctuations and any system gain changes. Any offset in the instrument electronics was checked prior to each measurement series due to previous problems with data transmission errors. Therefore, these offsets are due to some difference in the initial

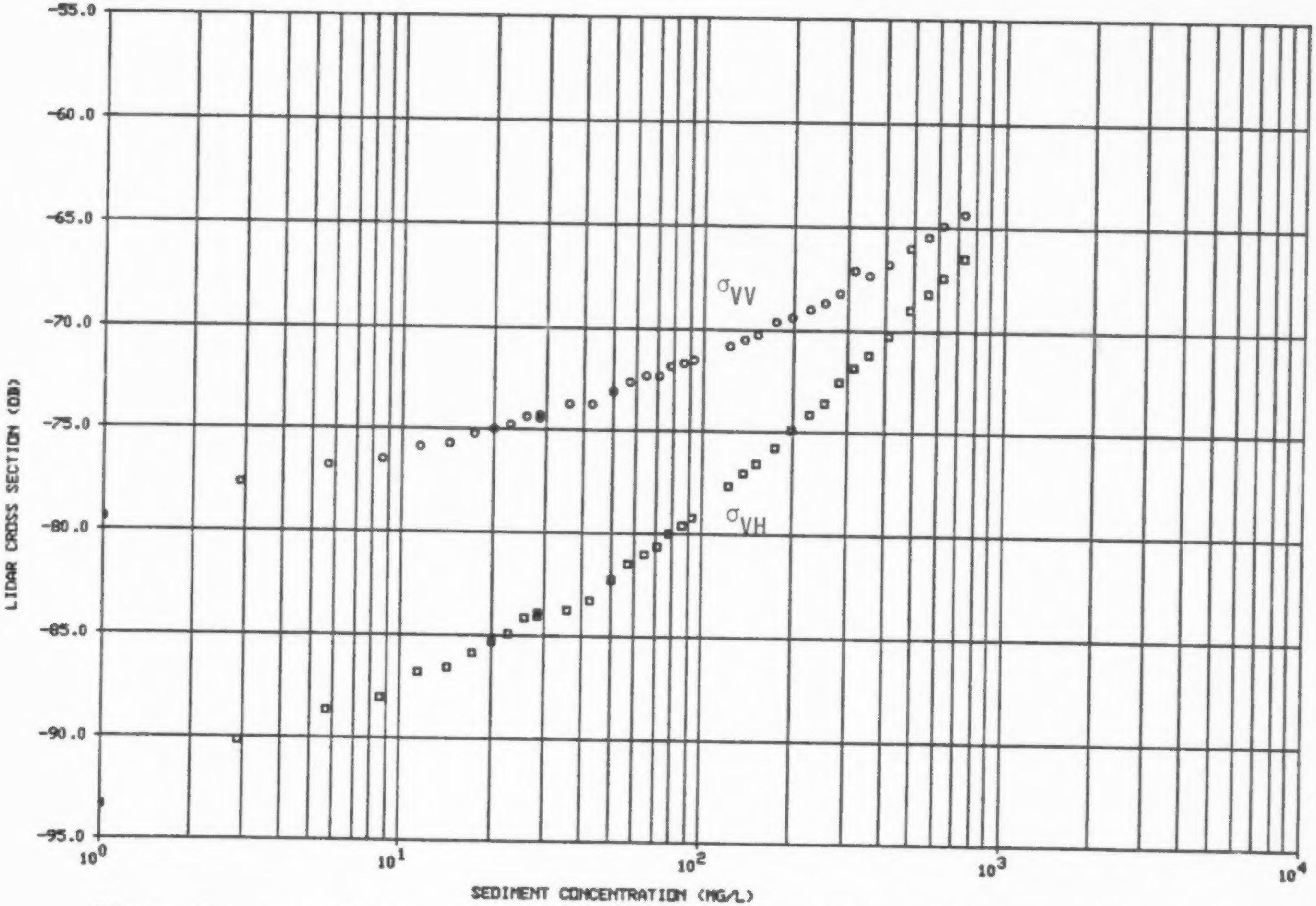

Figure 42. Cross Section Versus White Clay Sediment Concentration Measured at 632 nm

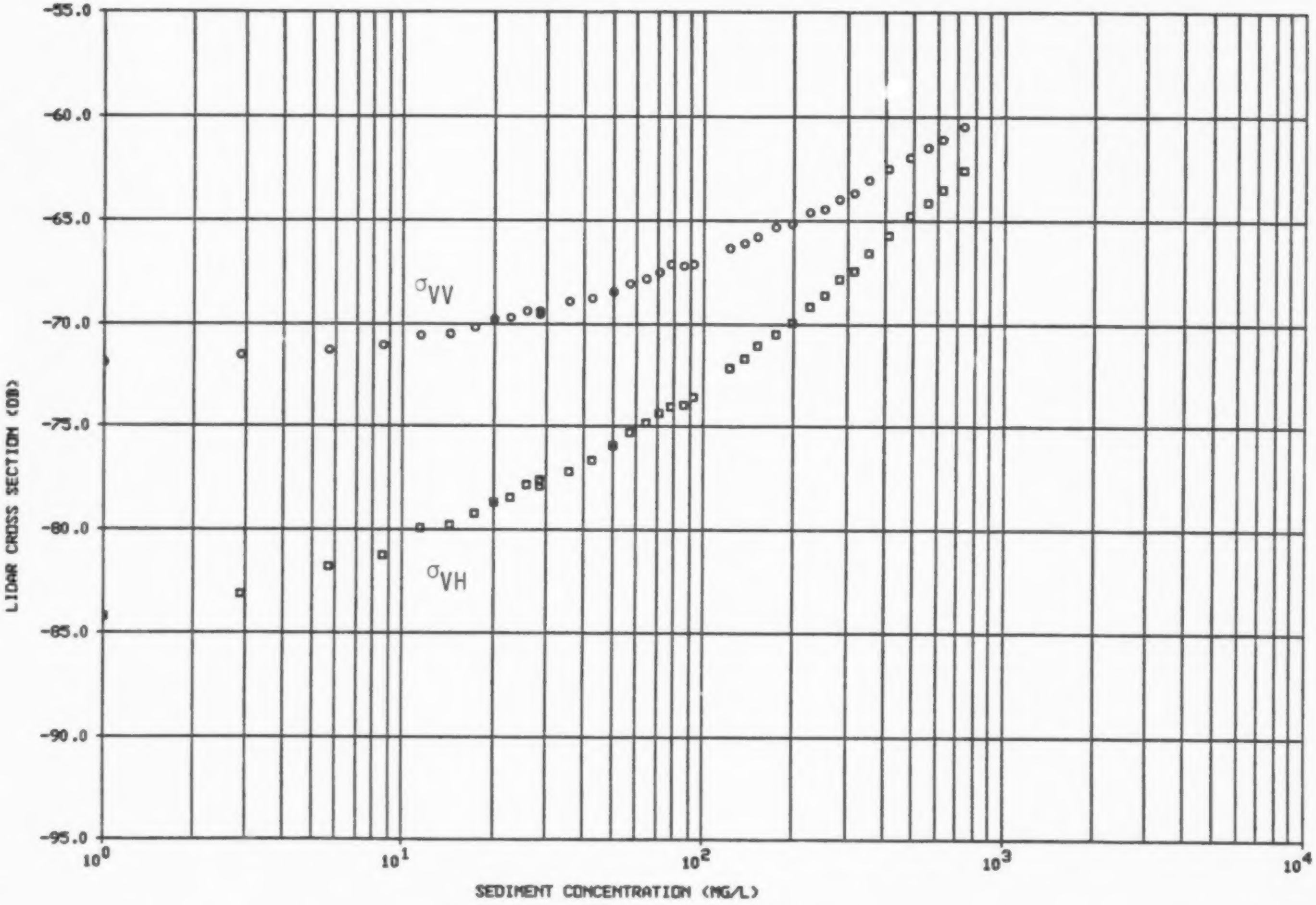

Figure 43. Cross Section Versus White Clay Sediment Concentration Measured at 442 nm

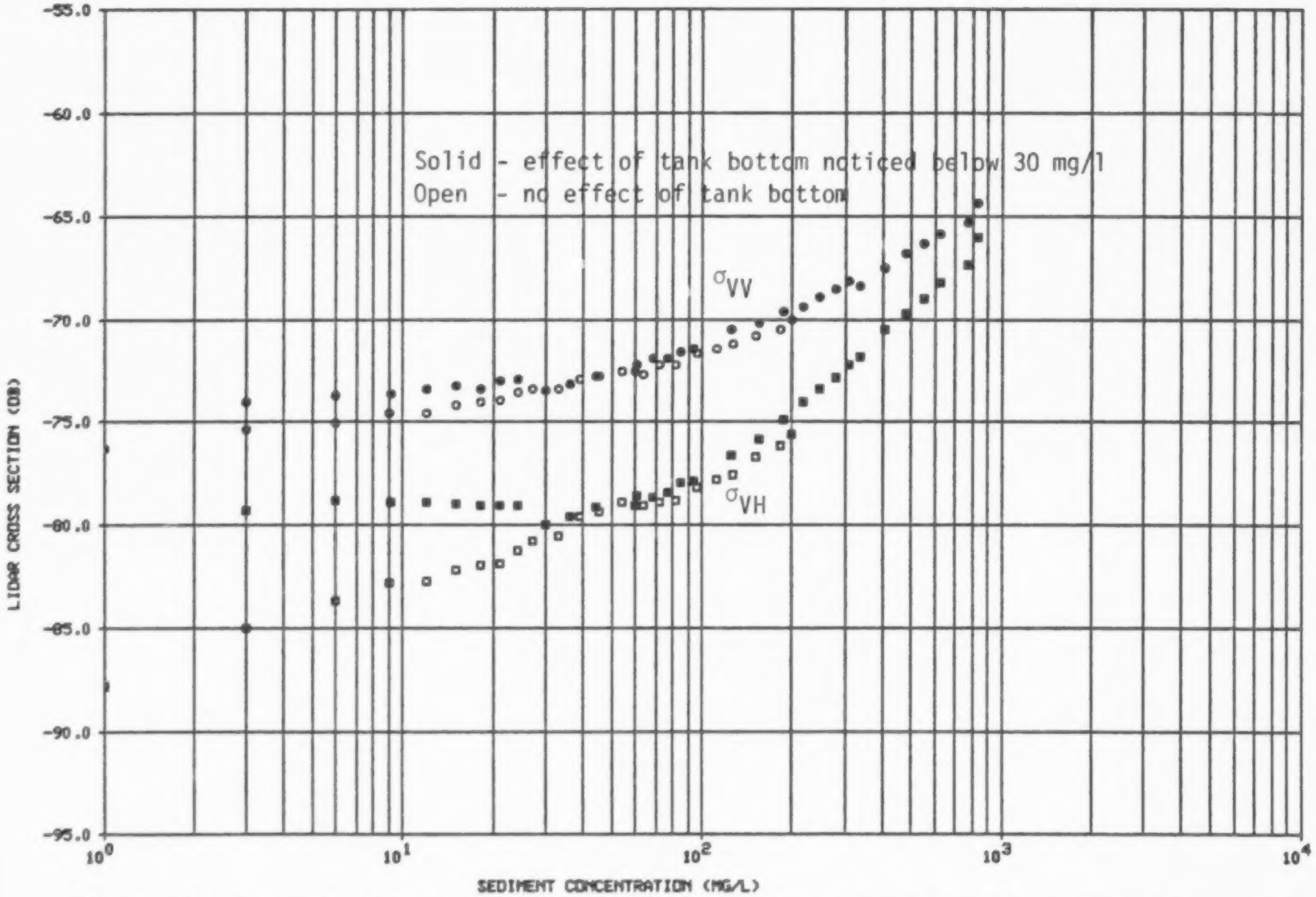

Figure 44. Cross Section Versus White Silt/Clay Sediment Concentration Measured at 632 nm

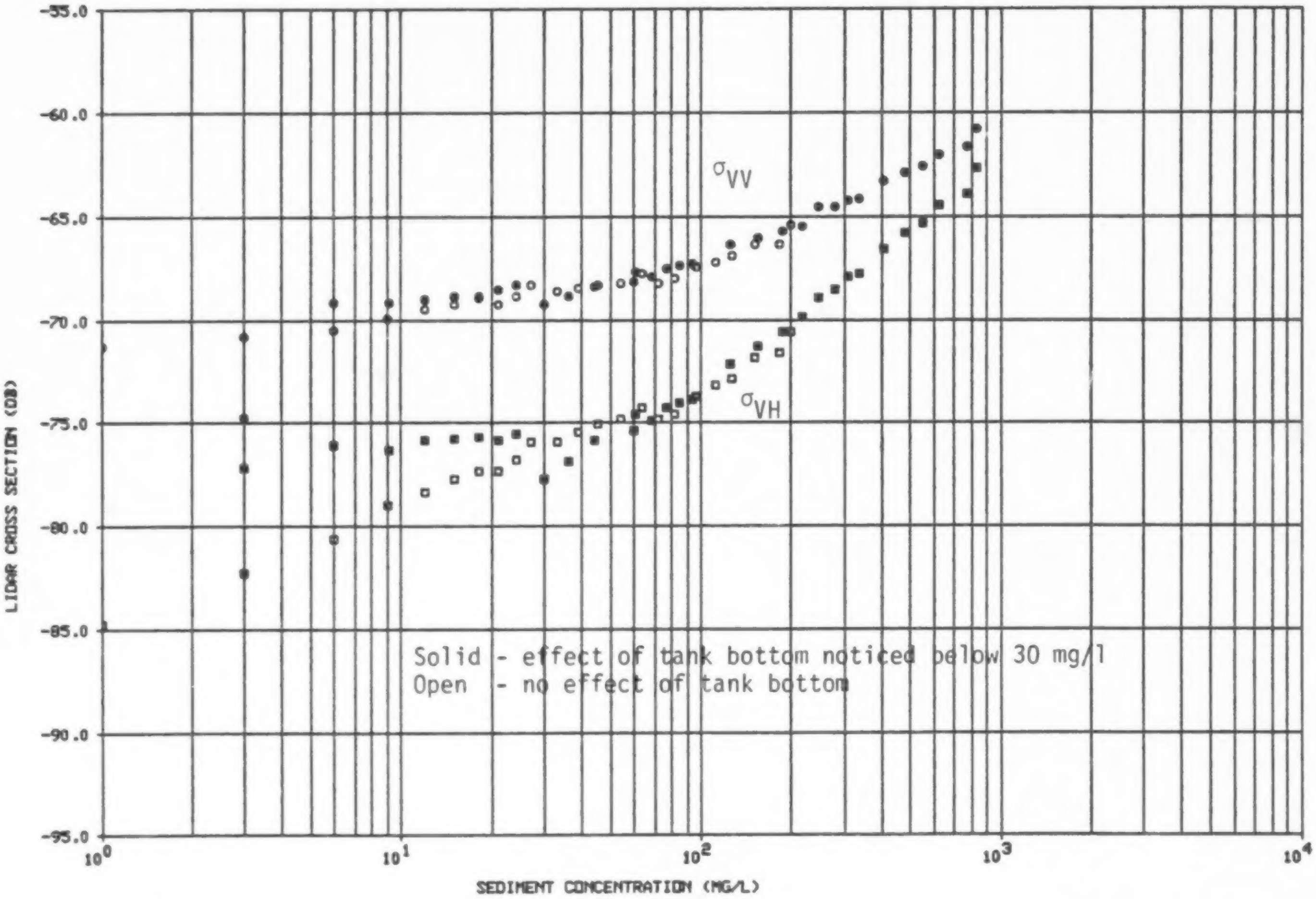

Figure 45. Cross Section Versus White Silt/Clay Sediment Concentration Measured at 442 nm

scattering from the "clear" water and the black absorber.

Because of the large amount of water used in these measurements, it was necessary to use tap water for all of the measurements. Since these measurements were made over a period of several months, inconsistencies in the purity of the tap water could easily have contributed to these returns. Failure to completely remove the residual sediment particles from the measurement tank and black absorber between measurement series was no doubt another contributing factor.

This effect can be minimized by careful cleaning and filling of the measurement tank and black absorber between measurement series. Tap water should be filtered to remove any suspended particles. An analysis of water sample taken before any suspended particles is introduced could be helpful in determining the chemical content and the presence of residual suspended solids in the tap water. The cause of the offsets from the measurement tank could be better identified and minimized in this manner.

It should be noted that the difference between most initial measurements was not significant. The close agreement between the brown silt cross section curves shown in Figures 25 and 26 and between the white silt/clay cross section plots shown in Figures 44 and 45, which are both actually the results of two different measurement series combined, shows that the offsets did not greatly affect the measurements.

Effects of Tank Bottom

The depolarization ratio curves for the scattering from the white silt/clay sample are shown in Figures 46 and 47. These measurements are the result of two different series of measurements using this particle type. In the first measurement series, the concentration was increased in very small increments and the maximum concentration reached in these measurements was not very high. A second series of measurements were made using an increasing increment in the concentration levels to more quickly reach a higher concentration.

In the second series of measurements, it appears that the black absorber was not in the proper position to absorb the unscattered laser beam and the scattering from the bottom of the tank contributed to the backscattering at low concentration levels. As the concentration of the sediment particles was increased, less energy reached the bottom of the tank decreasing the scattered returns. When the particle concentrations became high enough, the laser no longer reached the bottom of the tank and only scattering from the sediment particles was present. The measurement depth plot for the white silt particles given in Figure 27 shows a slightly lower measurement depth than the maximum depth of the tank for the concentration where scattering from the tank ceased. A slightly higher concentration of sediment particles is needed to extinguish the scattering from the bottom of the tank than the corresponding measurement depth, due to the greater scattering from the bottom of the tank. These measurements were the only series made in the large measurement tank which indicated any effects from scattering by the bottom of the tank.

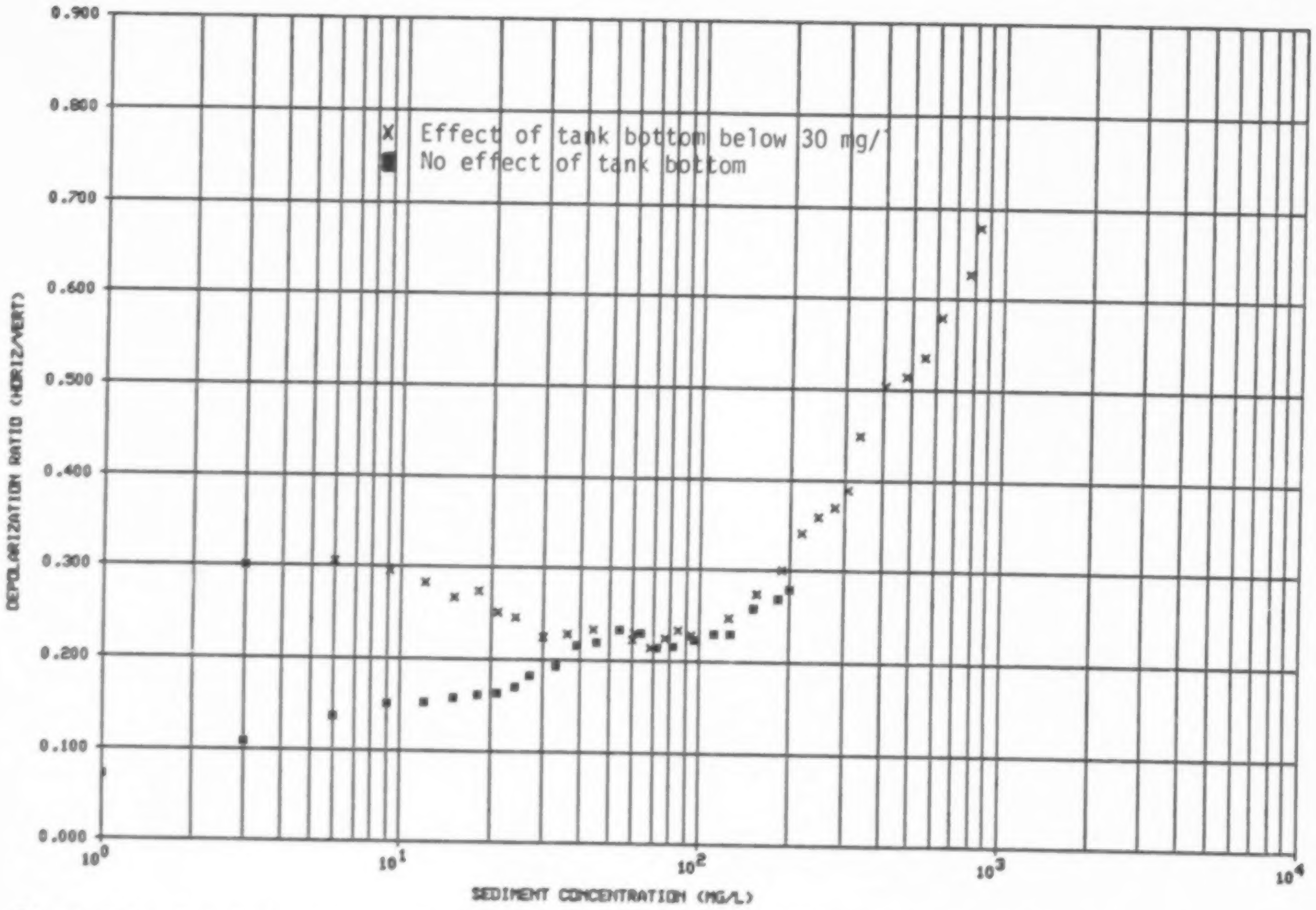

Figure 46. Depolarization Ratio Versus White Silt/Clay Sediment Concentration Measured at 632 nm

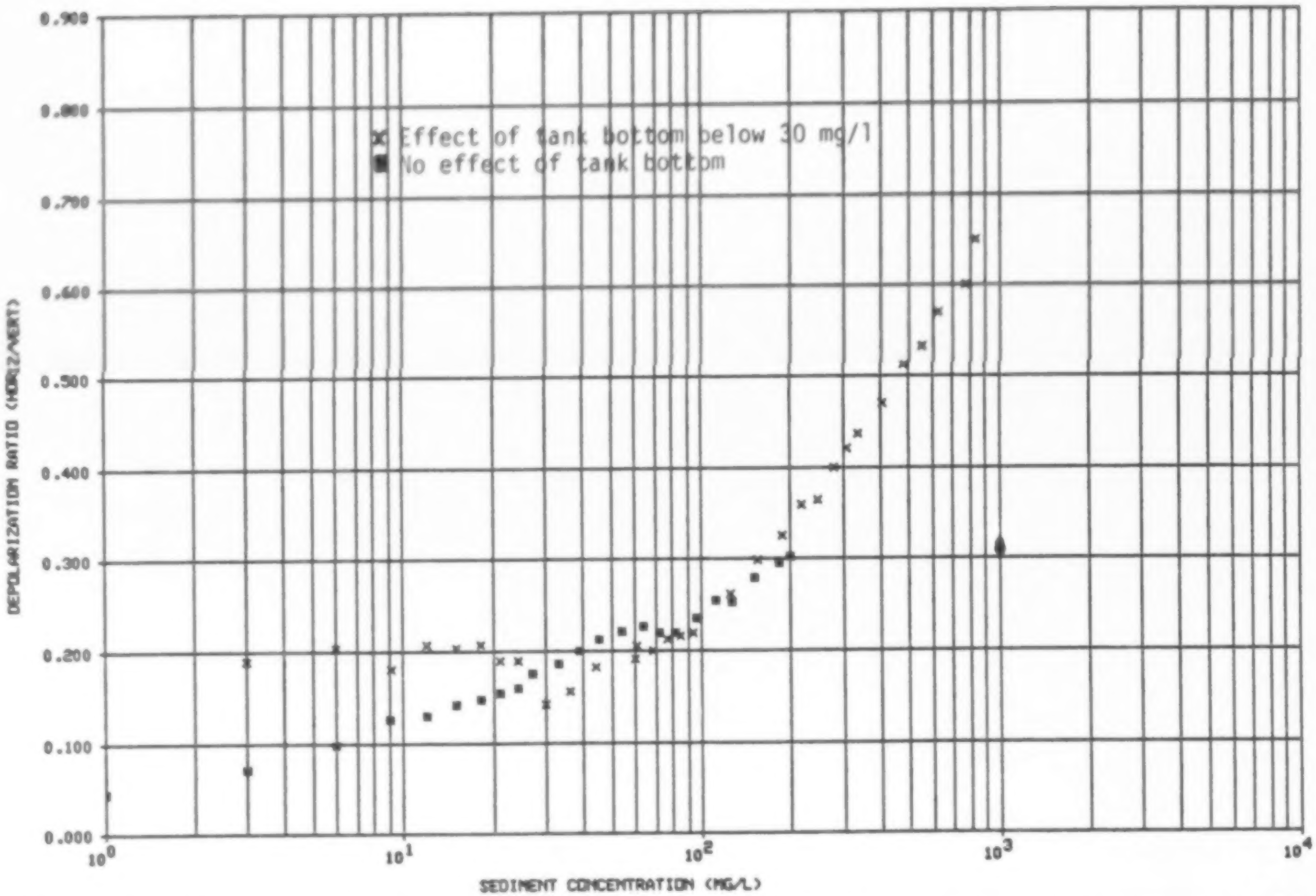

Figure 47. Depolarization Ratio Versus White Silt/Clay Sediment Concentration Measured at 442 nm

Particle Settling

The effects of settling by the sediment particles during the measurements can be seen in some of the returns. These settling characteristics are particularly evident in the results of the measurements from the white sand particles and the white silt sample.

The cross section plots for the scattering from the white sand particles are shown in Figures 48 and 49. The variability in the cross sections, such as the lowered scattering from the highest concentration level, is due to the rapid settling rate of this very large particle. The circulation pump used to keep the particles mixed was not quite sufficient to maintain the large sediment particles in suspension. Several times during the measurements of this particular particles type, the settled particles were remixed and backscatter measurements were repeated. The concentration levels where two returns are shown correspond to these double measurements.

Due to this rapid settling rate, a small fraction of the particles continually settled out of the suspension. This settling decreased the concentration especially at the higher concentration levels. The concentration levels reported on the graphs were computed from the amount of sediment added to the tank, and actually represent the maximum concentration of sediment that could be achieved when all of the added particles were in suspension. Due to this effect, the concentration reported for the white sand particles is slightly higher than the actual concentration of particles which contributed to the backscatter measurements. From the double measurements where the backscatter measurement was repeated after mixing the suspension, this error is probably less than 10% of the reported particle concentration.

After the backscatter measurements had been made at the highest concentration of the sand particles, the circulation pump was turned off. Backscatter measurements were taken at approximately one minute intervals as the particles settled out of the water. In less than ten minutes the depolarization ratio at both wavelengths had decreased to a value below 0.2. Only the settling of the large white sand particles presented such a substantial problem over the time period required to make a series of measurements.

Another effect of particle settling is evident in the cross section for the scattering from the white silt particles shown in Figures 50 and 51. The dip in the returns at approximatley 200 mg/l shows that the scattering decreased for an increase in the concentration of scattering particles. This decrease in scattering was apparently the result of a decrease in particle concentration due to settling. During the measurement sequence, data acquisition was halted at intervals to measure additional samples to be added to the measurement tank. The circulation pump was always left running during these periods. The dip in the white silt returns corresponds to one of these instances. Due possibly to a slightly longer delay than usual, a certain amount of sediment settled out of the water. When measurements were continued, the next two samples replaced the settled particles and the measurements continued without further settling. By comparing the slope of

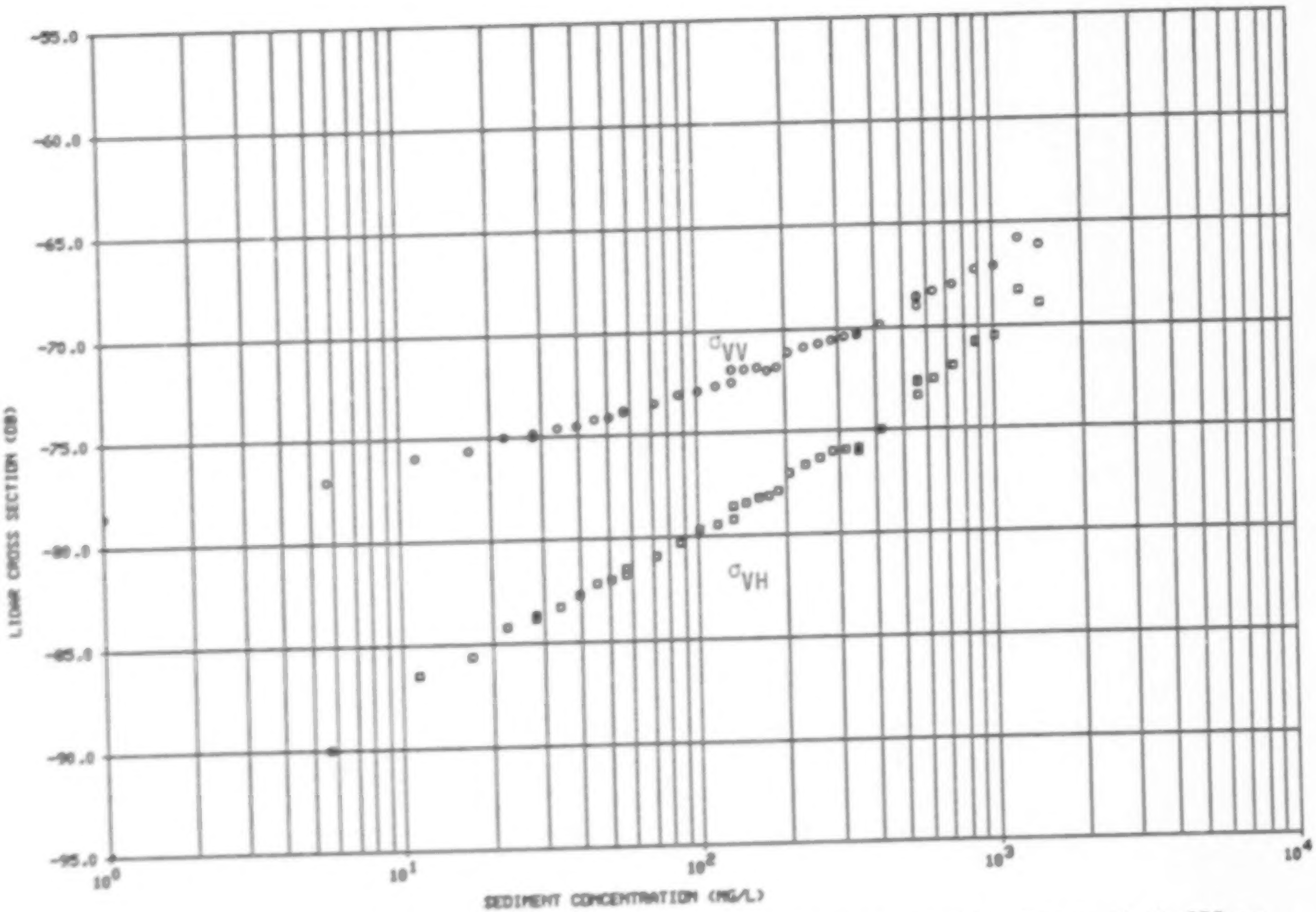

Figure 48. Cross Section Versus White Sand Sediment Concentration Measured at 632 nm

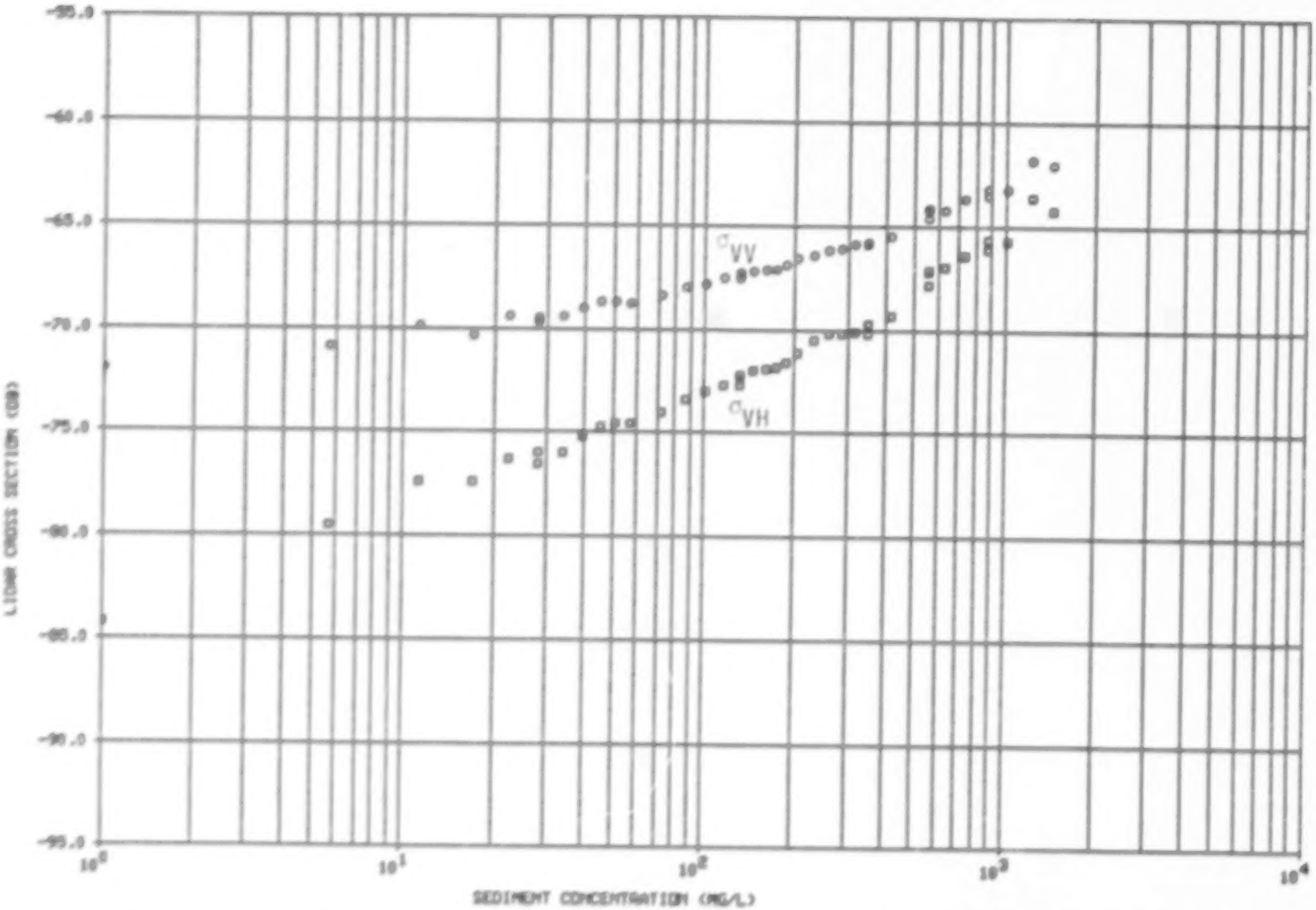

Figure 49. Cross Section Versus White Sand Sediment Concentration Measured at 442 nm

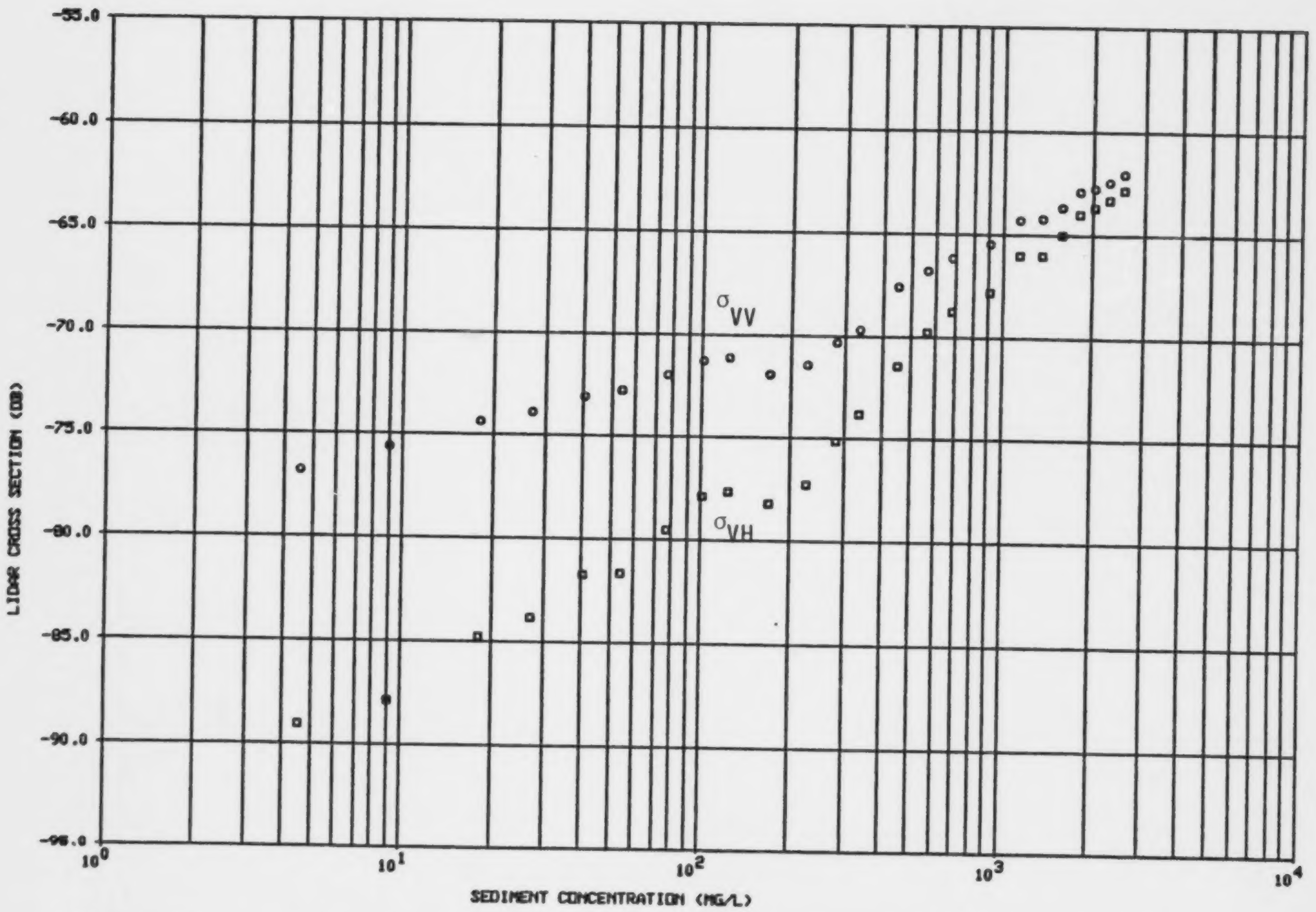

Figure 50. Cross Section Versus White Silt Sediment Concentration Measured at 632 nm

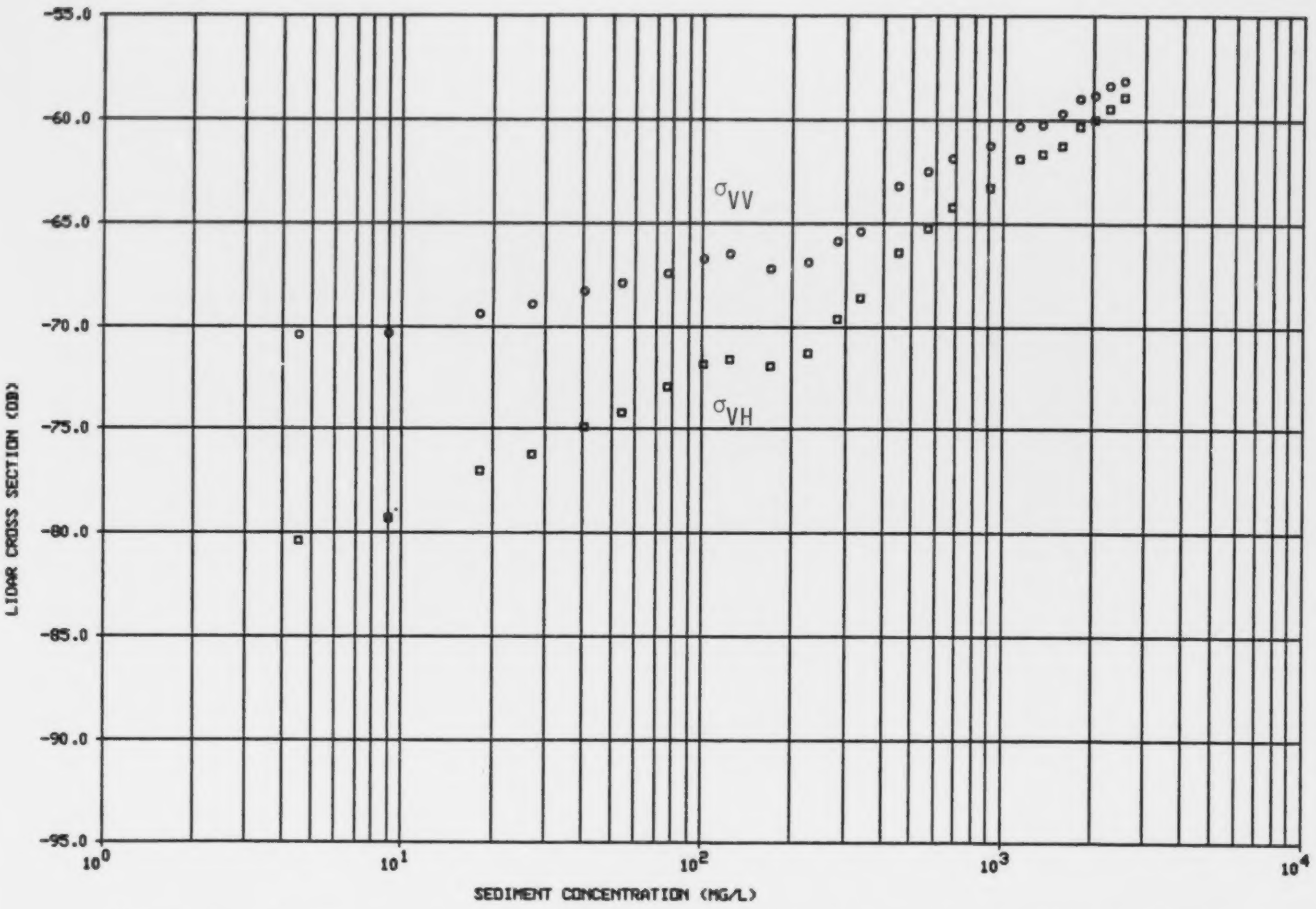

Figure 51. Cross Section Versus White Silt Sediment Concentration Measured at 442 nm

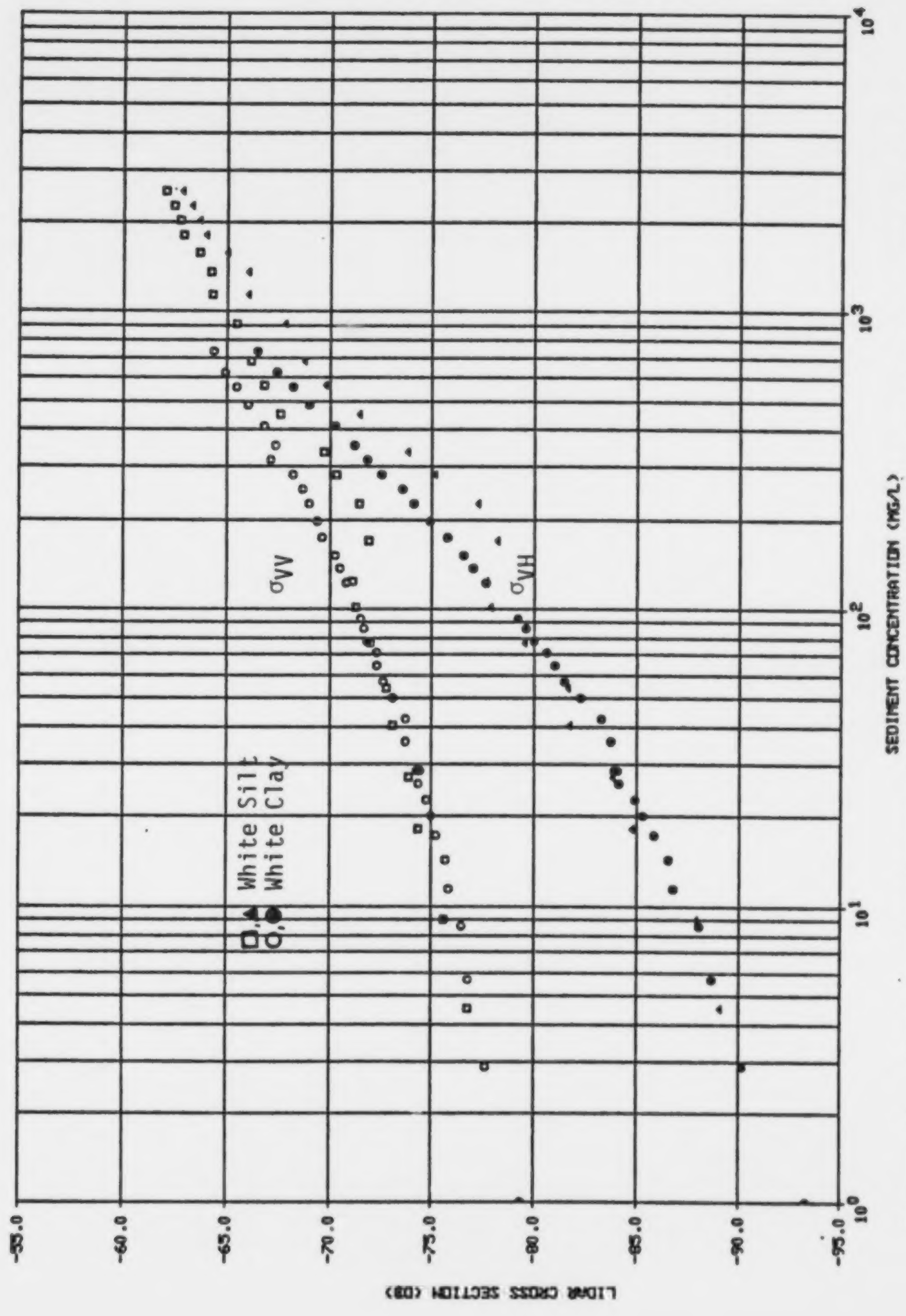

Figure 52. Cross Section Versus White Silt and Clay Concentration Measured at 632 nm

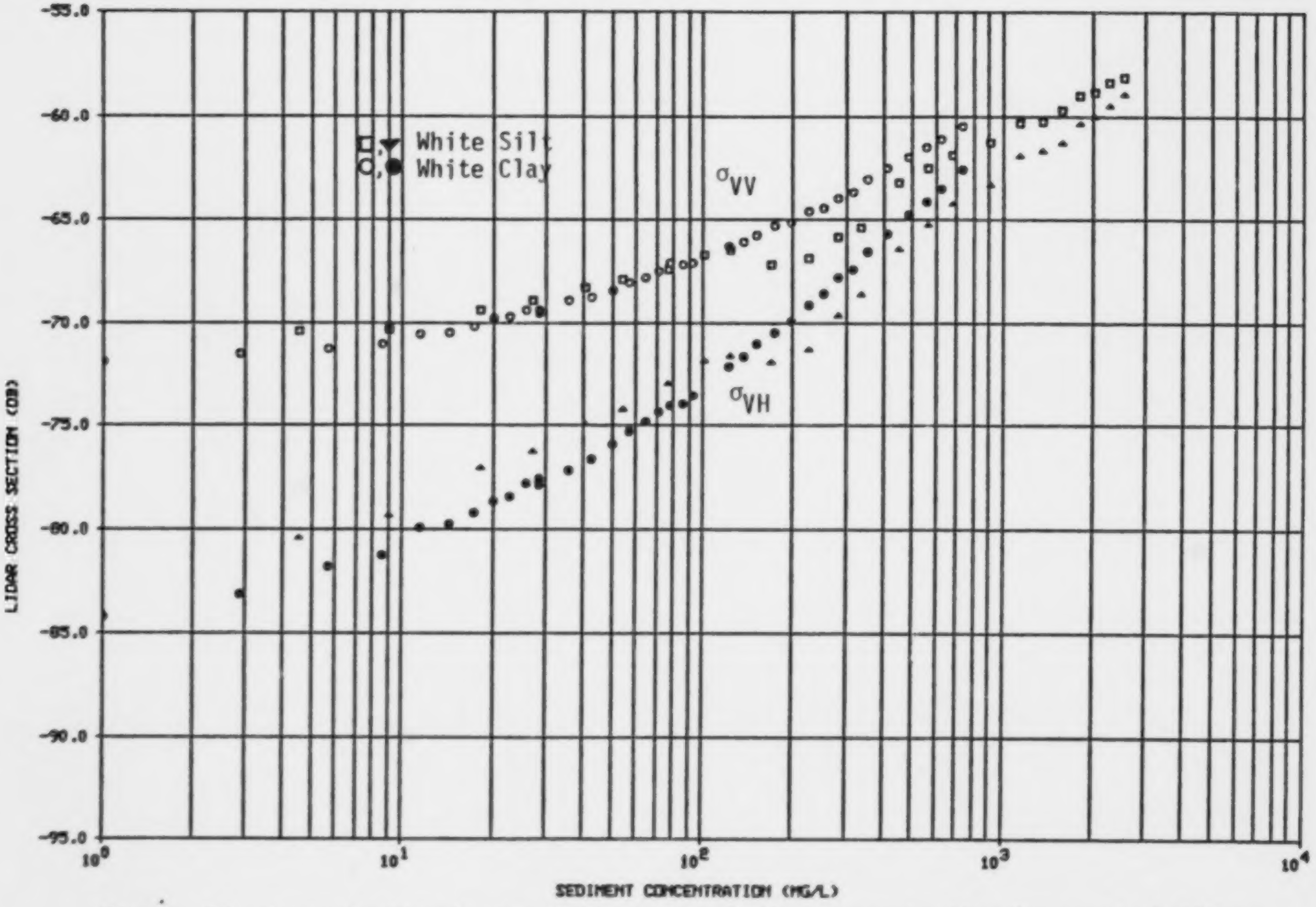

Figure 53 Cross Section Versus White Silt and Clay Concentration Measured at 442 nm

the white silt cross sections with the white clay cross section in the composite graphs shown in Figures 52 and 53, the error in the concentration can be verified.

These settling effects can be corrected by several methods. A larger circulation pump or better ciruclation flow would keep the particles in suspension better. A samling method to verify the concentration of the sediment particles actually contributing to the backscattering would also be useful. A quick, efficient measurement sequence is always necessary to provide consistently high quality data.

CHAPTER VI

CONCLUSION AND RECOMMENDATIONS

This study describes a measurement program to examine the effect of different measurement conditions on the backscattered laser energy from sediment laden water. A dual wavelength, lidar polarimeter was used to concurrently measure orthogonally polarized components of the backscattered return for both red (632 nm) and blue (442 nm) wavelengths. The measurement conditions which were examined included particle color, size distribution and concentration. The effects of water surface roughness and the presence of organic suspended solids (algae) were also examined. The volume of water that contributes to the lidar backscattering was determined for most of the different combinations of the above measurement conditions. The data were reduced to lidar cross section and depolarization ratio values by using a white calibration target to normalize the measurements for laser power fluctuations and slight optical misalignment of the system. The conclusions of this investigation are summarized below.

CONCLUSIONS

The cross- and like-polarized components of the backscattered energy from sediment laden water are directly dependent on the concentration of the suspended particles for a wide range of soil colors and particle size ranges. This dependence shows that a lidar polarimeter system can provide useful information concerning the concentration of the suspended sediments.

The spectral response of the particle has a significant effect on the backscattering process, especially at high particle concentrations. The reflectivity of the particles at the measurement wavelength directly influences not only the amount of energy reflected from the particle, but also the efficiency of the depolarization of the incident energy caused by multiple scattering. The sensitivity of the depolarization ratio to the sediment concentration is increased by a higher sediment particle reflectivity.

The absorbance and scattering efficiencies of the particles influence the value of particle concentration at which the scattering process saturates. An increase in particle concentration above the saturation level does not have an effect on the cross- and like-components of backscattered energy. As a result, the absorbance and scattering efficiences actually influence the maximum concentration of 800-900 mg/l could be measured for the brown and red scattering particle used in this study. No saturation effect was observed for the white sediment up to the maximum concentration measured, approximately 2500 mg/l.

The irregular shape of the scattering particle depolarizes the incident energy even for very low particle concentrations. As a result, the sensitivity of a lidar system to very low concentrations of scattering particles is affected by the particle shape. For a given maximum sensitivity the depolarization due to particle shape could determine the lowest detectable concentration. The measurements of this study indicate that concentrations lower than 10.0 mg/l should be measurable with this type of system.

The depolarization ratio is not greatly affected by the size range of the particles for high concentrations of scattering particles. Although at a given concentration in mg/l the clay size sediment has more scatterers within the scattering volume than the larger size sediment, the cross- and like-polarized returns are equally affected which results in little change in the depolarization ratio for a given mass of scattering particles. This result appears valid for particles less than 40 μm in size and concentrations above 100 mg/l.

Algae behave primarily as absorbers. As a result, absorbance by algae of a particular color group at the measurement wavelength could reduce the maximum concentration of suspended sediment that could be measured. It is believed, however, that the concentration of algae encountered in most ponds and lakes where the algae is not in a bloom condition would probably have little effect on backscatter measurements of suspended solids.

Small scale water surface roughness has little effect on the backscattered returns. The levels of surface roughness examined in the study were not representative of large scale conditions or of foaming conditions. However, it can be concluded based on this and other studies [6] that the depolarization ratio is less affected than either the cross- or like-polarized return due to the cancelation of effects common to both terms.

The depth of water that contributes to the backscattering is an exponentially decreasing function of the sediment concentration. A high absorbance by the sediment particle at the measurement wavelength decreases the depth that contributes to the backscattered returns. For the particle types measured in this study, the measurement depth at 100 mg/l varied from 15 cm for the red silt at the blue wavelength to 42 cm for the white silt at both the blue and red wavelengths.

RECOMMENDATIONS

From the results and problems encountered in this investigation, several recommendations can be made to further examine the capability of a lidar polarimeter to measure the concentration of suspended solids in water.

Laboratory Measurements

Further laboratory measurements are necessary to continue to develop a thorough understanding of the more subtle characteristics of scattering by natural sediment particles. A more complete characterization of the scattering process based on these additional laboratory measurements would permit the formulation of an analytical development to predict the amount of scattering for the wide variety of conditions encountered in field measurements. Such an analytical tool would be extremely useful in developing a sensor system for field application. In addition, the quality of the data acquired in subsequent examinations can be improved by noting the problems encountered in the experiments of the present study.

Scattering Measurements

Several particle characteristics directly affect the dependence of the backscattering process on the concentration of scattering particles. These particle characteristics influence the backscattering process for different regions of particulate concentration. The shape, reflectivity and absorbance of the particles should be further examined in experiments designed to isolate the effects of these particular characteristics on the single and multiple scattering processes. Specific measurements are also needed to verify some of the results shown in this study and in previous investigations concerning the effects of particle size distribution and the incident angle of the measurements.

The shape of the scattering particle from spherical to non-spherical has been shown to affect the backscattered returns at low concentrations of scattering particles. The amount of depolarization of the incident energy and the resulting dependency of the depolarization ratio on the particle concentration at low concentration levels is determined by the shape characteristics of the scattering particles. Additional measurements are needed to determine if the effect of particle shape between soil types and size ranges on the depolarization measurement at low concentrations is significant. The measurements should be designed to permit a comparison of the actual amount of cross-polarized backscattering for the different particle types, at concentration levels from 50 mg/l down to less than 1.0 mg/l. Careful attention to the scattering caused by the tap water and the measurement tank will be necessary to permit the maximum benefit from these measurements.

The sensitivity of the lidar backscattering to particle concentration is greatly affected by the reflectivity of the particle, especially at high concentration levels where multiple scattering is present. Spectrometer measurements of dry or dampened soil samples would indicate the spectral response of the particles. Nigrosine dye or colored dyes could be used to vary this spectral response by actually dyeing the particles different colors. A wide variety of sediment types could possibly be simulated in this manner. Unrealistic colors might also be useful in examining the response of the different wavelengths (for example, a blue particle).

The absorbance and scattering efficiences of the particles affect the saturation of the scattering process. This saturation level determines the maximum particle concentration that can be detected by a lidar system. The effect of the particle absorbance or the presence of an absorbing material such as algae on the saturation level and very low particle concentrations should be further examined. The actual absorbance of the scattering particles can be determined by measuring the attenuation caused by the particles for transmission through a diluted suspension of the particles. An absorbing material such as nigrosine dye should be introduced to change the absorption of the medium. These measurements would determine the limiting case of how an absorbing material such as algae could mask the detection of sediment particles from backscatter measurements.

The saturation point for both the brown and red silt particles occurred at approximately the same concentration level for both the blue and red wavelengths. A saturation was not observed for the white particles. The saturation level should be further examined to determine the effects of both particle characteristics and the measurement configuration on the scattering at high levels of particle concentration, since this effect limits the highest concentration of particles that can be measured.

The indication that the depolarization ratio is not affected by the size of the particles reduces the number of variables that must be considered for estimating the concentration of suspended solids from backscatter measurements. This result is particularly useful since it is the silt and clay size ranges and concentration levels above 10 mg/l which exhibit this characteristic which are the most important measurement regions. However, the measurements of the different size ranges were made on only the white particles. This result should be verified for the brown and red soil samples by making measurements similar to those made in this study for the white particle type. The size separation and measurement processes must be performed carefully to ensure that the size ranges are acquired accurately. Also, the slight differences in the color and shape of the particles for different size ranges from the same soil type should be documented.

The scattering model derived by Blanchard [31] calculates the scattering from a rough surface as a function of incident angle. Backscatter measurements from sediment laden water for a range of angles would permit the verification of this model. A wide range of angles could then be simulated, using the model, to determine the effects of incident angle on the measurement of suspended solids. The best range of incident angles for sediment measurements could then be determined.

Scattering Model

The many variables that contribute to the different scattering characteristics identified in this study accentuate the need for an analytical description of the scattering process. However, the large number of variables also greatly increases the complexity of the mathematical model to describe the many scattering characteristics. An accurate estimate of the concentration of suspended solids from backscatter measurements depends on the ability to distinguish the different effects of the many variables on the scattering process. An analytical development which accurately predicts the backscattered returns for a wide range of measurement conditions would necessarily include the effects of the many variables. The ability to include the effects of the different measurement conditions on the backscattered returns would be prerequisite to the ability to correct the backscatter measurements for the effects of the measurement conditions and thus isolate the effects of particle concentration. As a result, a complete development of the scattering process would be helpful in developing a technique of accurately predicting the concentration of suspended sediments from backscatter measurements.

A simulation program of the scattering process would permit the examination of different measurement effects without time consuming laboratory measurements. A wide range of conditions encountered in the field could then be quickly simulated using the program, verified by limited laboratory measurements and extended to accurately predict the backscattering under field conditions. The optimum measurement configuration for a set of field conditions can be determined from the program simulation without having to complete a wide range of laboratory measurements.

Measurement Procedures

The measurement procedure utilized for the measurements of this study could be improved in several areas. As mentioned previously, the measurement tank and black absorber should be cleaned very thoroughly between measurements of different particle types. Distilled water or filtered tap water should be used to permit measurements from very low concentration of scattering particles. A consistent and efficient measurement procedure in both the laboratory preparation and measurement execution will assure data of a high quality.

The concentration of the suspended particles that actually contributes to the backscattered returns should be verified during the measurements. However, the sampling methods used in the field have certain disadvantages. The volume of water that must be dried or filtered to obtain a measurable amount of suspended particles can be restrictive, especially at low concentration levels. A flocculant to remove the particles from suspension would be helpful. At higher concentration levels, where settling presented a problem in the measurements of this study an independent verification of the particle concentration would be very useful. The experience gained in the area of the laboratory measurements would prove useful in later field measurements.

Another consideration involving the use of tap water in these measurements concerns the flocculation of the sediment particles. A peptizer was used as a deflocculant in the pipette analysis used to determine the size distribution of the particles. The sediment sample recovered after the pipette analysis showed considerably different settling characteristics than samples which did not include the peptizer. This fact reveals two slight problems. First, since no peptizer was present in the measurement tank, the size distribution measured for the different particles does not accurately indicate the size distribution of the scattering particles actually used for the measurements. From the settling of the samples with and without the deflocculant, it is clear that the concentration of the smaller particles in the reported size distributions are slightly exaggerated. Since the white particles were more easily broken up into smaller particles, the white clay and silt/clay samples were the most susceptible to this problem. Secondly, some flocculation during the backscatter measurements was indicated by the settling characteristics of the samples. In subsequent measurements, the use of a very small amount of peptizer in the sample should be considered in order to properly simulate field conditions. In either case, determination of the actual size distribution of the scattering particles encountered in the backscatter measurements should only be done with distilled water.

Field Measurements

Field measurements are necessary to relate the limited number of conditions examined in the controlled laboratory measurements to the wide variety of natural conditions that can be encountered in field measurements. Initial field measurements should resemble the conditions examined in the laboratory as closely as possible so that the knowledge of the scattering process gained from the laboratory measurements can be applied to the results of the field measurements. Complete documentation of the ground truth information will permit meaningful interpretation of the data.

Location

The location of the field measurements should be planned to closely resemble the laboratory measurements. The characteristics of the data that have been observed in the laboratory measurements can then be related to the results of the field measurements with a minimum of additional variables.

The brown and red silt samples used in this study were removed from soil samples that are characteristic of two different locations in Texas. The brown silt sample was chosen to correspond to the suspended sediment encountered in the Brazos River. The red silt sample used in these measurements closely resembled the suspended solids found in the tributaries and reservoirs of the Colorado River in West and Central Texas. Field measurements in the lakes and rivers of these two areas would cover a wide range of conditions for the same type of particles measured in the laboratory.

Additional measurement conditions can be examined by the proper choice of different field measurement locations. The inability to properly measure the effects of algae and water surface roughness in the laboratory can be circumvented by making these measurement in the field. Different ponds could be located by aerial observation which represent a wide range of different algae types and concentrations. A well protected pond would permit the measurement of the effects caused by different amounts of water surface roughness.

Ground Truth Information

The actual conditions encountered encountered in the field which affect the backscatter measurements must be carefully documented to permit complete analysis of the data. Besides the measurement of the concentration of suspended solids, samples should also be taken to determine the shape and possibly the size distribution of the scattering particles. The concentration and type of algae will be difficult to determine. Large samples of the water should be taken to assure that an accurate measurement of the algae concentration can be made. The water surface roughness characteristics should be carefully documented, possibly by photographs which include a reference measurement grid. The depth of penetration by the laser beam and the depth of the water which contributes to the backscattering would also be helpful in determining the absorbance of the particle. The ability to properly determine the effects of the many variables on the backscatter measurements depends on the careful documentation of the actual conditions encountered in the field.

Lidar Design Rationale

From the measurements of this study and the field measurentns made in previous investigations, several recommendations can be made concerning the design of a lidar system to measure suspended solids in water.

The sensitivity of the system to changes in suspended particle concentration can be increased by several methods. The reflectivity and absorbance characteristics indicated in the results of these measurements show that the red laser is more sensitive to the concentration of suspended sediment particles and less influenced by the presence of algae.

The effects of noise can be reduced by several methods. A chopped or modulated continuous wave laser permits the effects of ambient light to be removed by the detection electronics. Spatial and optical filters prevent interference by unwanted water surface specular reflections. Immediately after being preamplified, the return signals can be bandpass filtered at the beam modulation frequency to further reduce noise. A reference signal from the beam chopper can also be used to synchronously demodulate the return signals.

The environmental constraints of operating both the laser and any electronics in field conditions which include a wide range of temperatures must be considered very carefully. Particular problems of power or laser type must be considered for the particular application. The trade-offs between component selection, ease of operation, cost, and measurement capability must be well defined to produce an effective, usable sensor.

The proven versatility of micro-processors, especially in the implementation of algorithms for field applications, would greatly aid in data reduction for this type of in situ sensor to provide real time data analysis.

Field measurements are also necessary to identify any other variables which might have an effect on the measurement capabilities or operation of this type of sensor. Particular requirements to produce a rugged, dependable and operational lidar system to be used to measure the suspended solids in water must be identified in the actual field conditions which will be the normal operational environment of the sensor.

REFERENCES

1. Wruble, D. R., J. D. Koutsandreas and B. Pijanowski, (editors), Proceedings of the Automated In Situ Water Quality Workshop, U. S. Environmental Protection Agency, Environmental Monitory and Support Laboratory, Las Vegas, Nevada, February 1978.

2. Mayo, Jr., W. T., G. J. Wilhelmi and J. W. Rouse, Jr., "A Dual Polarization Laser Backscatter System for Water Quality Studies," Proceedings of Electro-optical Systems Design Conference, New York, New York, pp. 250-256, Sepetember 1972.

3. Wilhelmi, G. J., W. T. Mayo, Jr., and J. W. Rouse, Jr., "Remote Water Quality Measurements with a Lidar Polarimeter," Laser and Unconventional Optics Journal, Vol. 43, pp. 3-16, January/February, 1973.

4. Mayo, Jr., W. T., G. J. Wilhelmi and J. W. Rouse, Jr., "Lidar Polarimeter: Experimental Feasibility Study," Technical Report RSC-40, Remote Sensing Center, Texas A&M Universty, College Station, Texas, September 1972.

5. Wilhelmi, G. J., "An investigation of the Depolarization of Back-scattered Electromagnetic Waves Using a Lidar Polarimeter," Technical Report RSC-45, Remote Sensing Center, Texas A&M University, College Station, Texas, August 1973.

6. Sheives, T. C., "A Study of a Dual Polarization Laser Backscatter System for Remote Identification and Measurement of Water Pollution," Technical Report RSC-53, Remote Sensing Center, Texas A&M University, College Station, Texas, May 1974.

7. Rouse, Jr., J. W., W. C. Hulse, A. J. Blanchard, and H. Malek, "Development of a Lidar Polarimeter Sensor for Remote Detection and Monitoring of Oil and Other Hazardous Materials in Water," Final Report RSC 984-1, Remote Sensing Center, Texas A&M Univeristy, College Station, Texas, April 1975.

8. Blanchard, A. J., J. A. Schell and S. Ramsawer, "Polarized Lidar Cross Section Measurements of Two Natural Water Samples," Technical Memorandum RSC-125, Remote Sensing Center, Texas A&M University, College Station, Texas, November 1975.

9. Rouse, Jr., J. W., "Development of an Active Spill Detection System (ASDS) for Remote Detection of Oil Spills," Final Report RSC 3233, Remote Sensing Center, Texas A&M University, College Station, Texas June 1978.

10. Kim, H. H. an P. T. Ryan, (editors), "The Use of Lasers for Hydrographic Studies" Symposium Proceedings, Wallops Flight Center, Wallops Island, Virginia, September 1973.

11. Carlson, P. R., and D. S. McCulloch, "Aerial Observation of Suspended Sediment Plumes in San Francisco Bay and the adjacent Pacific Ocean," *U.S. Geological Survey Research Journal*, Vol. 2, No. 5, pp. 519-526, September/October 1974.

12. Curran, R. J., "Ocean Color Determination Through a Scattering Atmosphere," *Applied Optics*, Vol. 11, No. 8, pp. 1857-1866, August 1972.

13. Kattawar, G. W. and T. J. Humphreys, "Remote Sensing of Chlorophyll in an Atmosphere-Ocean Environment: A theoretical Study," *Applied Optics*, Vol. 15, No. 1, pp. 273-282, January 1976.

14. Ritchie, J. C., F. R. Schiebe and J. R. McHenry, "Remote Sensing of Suspended Sediments in Surface Water," *Photogrametric Engineering and Remote Sensing*, Vol. 42. No. 12, pp. 1539-1545, December 1976.

15. Merry, C. J., "The Correlation and Quantification of Airborne Spectroradiometer Data to Turbidity Measurements at Lake Powell, Utah," CRREL Special Report 77-28, Cold Regions Research and Engineering Laboratory, Corps of Engineers, Hanover, New Hampshire, 1978.

16. Bristow, M., D. Nielsen and R. Furtek, "A Laser-Fluorosensor Technique for Water Quality Assessment," in *Proceedings of the Thirteenth International Symposium on Remote Sensing of Environment*, Ann Arbor, Michigan, April 1979, pp. 397-417.

17. Brown, C. A., F. H. Farmer, O. Jarrett and W. L. Staton, "Laboratory Studies in In Vivo Fluorescence of Phytoplankton," *Proceedings of Fourth Joint Conference on Sensing of Environmental Pollutant*, New Orleans, Louisiana, November 1977, pp. 782-788.

18. Kuo, C. Y. and R. Y. K. Cheng, "Laboratory Requirements for In Situ and Remote Sensing of Suspended Material," Technical Report 76-CZ, School of Engineering, Old Dominion Universty, Norfolk, Virginia, March 1976.

19. Allen, P. B., "Turbidimeter Measurement of Suspended Solids," Agricultural Research Results, Southern Series No. 4, Science and Education Administration, U. S. Department of Agriculture, Chickasha, Oklahoma, October, 1979.

20. Austin, R. W., "Instrumentation Used in Turbidity Measurement," *Proceedings of the NOAA Turbidity Workshop*, National Oceanic Instrumentation Center, May 1974.

21. Hahn, H. H. and R. Klute, "Pollutional Effects of Suspended, Sedimented and Eroded Particulate Material in the Aqueous Environment," Institut for Siedlungsivasserwirtschaft, University of Karlsruhe, 75 Karlsruhe, West Germany, 1974.

22. Oliver, B. G., "Heavy Metal Levels of Ottawa and Rideau River Sediments," *Environmental Science and Technology*, Vol. 7, No. 2, pp. 135-136, February 1973.

23. Cranston, R. E., and D. E. Buckley, "Mercury Pathways in a River and Estuary," *Environmental Science and Technology*, Vol. 6, No. 3, pp. 274-278, March 1972.

24. Sibbs, R. J. "Mechanisms of Trace Metal Transport in Rivers," *Science*, Vol. 180, pp. 71-73, April 1973.

25. Van Vleet, E. S. and J. G. Quinn, "Input and Fate of Petroleum Hydrocarbons Entering the Providence River and Upper Narragansett Bay from Wastewater Effluents," *Environmental Science and Technology*, Vol. 11, No. 12, pp. 1086-1091, November 1977.

26. Coleman, N. L., "A New Examination of Suspended Sedimentation in Open Channels," *Journal of Hydraulic Research*, Vol. 1, No. 7, pp. 67-82, 1969.

27. Hulse, W. C., "A Multichannel, Synchromous Laser Signal Processing System," Technical Report RSC-59, Remote Sensing Center, Texas A&M University, College Station, Texas, December 1974.

28. Milford, M. H., Personal Communication, Soil and Crop Sciences. Texas A&M University, College Station, Texas, February 1980.

29. Folk, R. L., *Petrology of Sedimentary Rocks*, Hemphill Publishing Company, Austin, Texas, 1974, pp. 37-43.

30. Wyman, P. W., "Definition of Laser Radar Cross Section," *Applied Optics*, Vol. 7, No. 1, p. 207, January 1968.

31. Blanchard, A. J., "Volumetric Effects in the Depolarization of Electromagnetic Waves Scattered by Rough Surfaces," Technical Report RSC-83, Remote Sensing Center, Texas A&M University, College Station, Texas, May 1977.

APPENDIX A

Sediment Concentration

REDUCED MEASUREMENTS

REDUCED DATA FOR WHITE CLAY
RED

CONCENTRATION	LIDAR CROSS SECTION		DEPOLARIZATION
(MG/L)	LIKE(VV,DB)	CROSS(VH,DB)	RATIO
0.0	79.32	93.32	.040
2.9	77.63	90.21	.055
5.7	76.80	88.65	.065
8.6	76.42	88.09	.068
11.4	75.83	86.80	.080
14.3	75.63	86.58	.081
17.2	75.21	85.88	.086
20.0	74.96	85.30	.092
22.9	74.76	84.93	.096
25.7	74.35	84.12	.105
28.6	74.26	83.94	.108
28.6	74.26	84.05	.105
28.6	74.38	84.04	.108
35.8	73.71	83.72	.099
42.9	73.72	83.24	.107
49.9	73.09	82.25	.121
56.9	72.59	81.49	.129
64.1	72.26	81.00	.134
71.1	72.32	80.61	.148
78.2	71.82	79.98	.154
85.9	71.66	79.57	.162
93.1	71.52	79.22	.170
121.7	70.77	77.65	.205
137.1	70.50	77.03	.222
151.4	70.25	76.50	.236
174.3	69.65	75.75	.246
195.8	69.37	74.89	.281
224.9	69.01	74.11	.309
253.4	68.69	73.52	.330
282.1	68.24	72.56	.368
317.9	67.12	71.84	.387
353.6	67.36	71.22	.411
410.8	66.77	70.24	.449
482.3	65.99	69.03	.496
553.8	65.49	68.18	.538
625.3	64.96	67.46	.563
732.5	64.36	66.51	.608

REDUCED DATA FOR WHITE CLAY
BLUE

CONCENTRATION	LIDAR CROSS SECTION		DEPOLARIZATION
(MG/L)	LIKE(VV,DB)	CROSS(VH,DB)	RATIO
0.0	71.90	84.22	.059
2.9	71.52	83.10	.069
5.7	71.28	81.80	.089
8.6	71.05	81.20	.096
11.4	70.55	79.93	.116
14.3	70.46	79.77	.118
17.2	70.18	79.18	.125
20.0	69.77	78.62	.131
22.9	69.69	78.40	.134
25.7	69.42	77.77	.146
28.6	69.44	77.58	.153
28.6	69.40	77.61	.151
28.6	69.56	77.85	.146
35.8	68.91	77.13	.151
42.9	68.74	76.57	.165
49.9	68.43	75.92	.179
56.9	68.06	75.24	.191
64.1	67.82	74.77	.201
71.1	67.52	74.31	.209
78.2	67.11	74.04	.202
85.9	67.23	73.91	.215
93.1	67.11	73.55	.227
121.7	66.32	72.12	.263
137.1	66.10	71.63	.280
151.4	65.77	71.05	.296
174.3	65.31	70.51	.302
195.8	65.16	69.97	.330
224.9	64.60	69.12	.354
253.4	64.48	68.57	.390
282.1	64.00	67.85	.413
317.9	63.64	67.46	.414
353.6	63.06	66.58	.444
410.8	62.50	65.69	.48
482.3	61.96	64.74	.527
553.8	61.45	64.14	.538
625.3	61.11	63.52	.574
732.6	60.47	62.60	.612

REDUCED DATA FOR WHITE SILT/CLAY (6/19/79)

RED

CONCENTRATION	LIDAR CROSS SECTION		DEPOLARIZATION
(MG/L)	LIKE(VV,DB)	CROSS(VH,DB)	RATIO
0.0	76.33	87.83	.071
3.0	75.37	85.00	.109
6.0	75.01	83.67	.136
9.0	74.57	82.82	.150
12.1	74.58	82.74	.153
15.1	74.17	82.18	.158
18.2	74.04	81.95	.162
21.1	73.98	81.83	.164
24.2	73.55	81.20	.171
27.2	73.39	80.79	.182
33.2	73.39	80.53	.193
39.3	72.94	79.59	.216
45.3	72.75	79.35	.219
54.4	72.56	78.89	.233
63.4	72.69	79.06	.231
72.5	72.24	78.92	.215
81.5	72.20	78.80	.217
96.6	71.7	78.20	.223
112.6	71.4	77.78	.231
127.3	71.16	77.54	.230
151.5	70.80	76.67	.259
182.3	70.46	76.15	.270
198.1	70.00	75.55	.279

REDUCED DATA FOR WHITE SILT/CLAY (6/19/79)
BLUE

CONCENTRATION (MG/L)	LIDAR CROSS SECTION LIKE(VV,DB)	CROSS(VH,DB)	DEPOLARIZATION RATIO
0.0	71.30	84.76	.045
3.0	70.80	82.24	.0712
6.0	70.49	80.57	.098
9.0	59.97	78.97	.126
12.1	69.48	78.30	.130
15.1	59.21	77.67	.142
18.2	68.96	77.28	.147
21.1	69.23	77.35	.154
24.2	68.81	76.80	.159
27.2	63.33	75.90	.175
33.2	68.60	75.88	.187
39.3	63.44	75.42	.200
45.3	68.29	75.03	.212
54.4	68.21	74.77	.221
63.4	67.78	74.25	.226
72.5	68.21	74.82	.219
81.5	67.97	74.54	.220
96.6	67.41	73.67	.236
112.6	67.22	73.15	.255
127.3	66.86	72.81	.254
151.5	66.30	71.84	.279
182.3	66.30	71.60	.295
198.1	65.39	70.57	.303

REDUCED DATA FOR WHITE SILT/CLAY (6/26/79)
RED

CONCENTRATION (MG/L)	LIDAR CROSS SECTION LIKE(VV,DB)	CROSS(VH,DB)	DEPOLARIZATION RATIO
3.0	74.03	79.26	.301
6.0	73.71	78.83	.307
9.1	73.59	78.88	.295
12.1	73.42	78.90	.283
15.1	73.22	78.95	.267
18.1	73.43	79.05	.274
21.1	73.02	79.01	.252
24.2	72.92	79.01	.246
30.2	73.47	79.95	.225
36.2	73.13	79.56	.228
44.4	72.77	79.10	.233
59.5	72.54	79.04	.224
60.4	72.20	78.58	.230
68.7	71.94	78.61	.215
77.2	71.90	78.39	.225
85.5	71.62	77.96	.233
93.9	71.44	77.86	.228
124.7	70.52	76.58	.248
156.0	70.18	75.79	.275
186.0	69.64	74.85	.301
217.0	69.38	74.05	.341
247.0	68.95	73.40	.359
278.0	68.55	72.87	.369
308.0	68.14	72.20	.389
338.0	68.34	71.8	.450
407.0	67.49	70.48	.503
481.0	66.81	69.69	.515
552.0	66.33	69.03	.536
627.0	65.86	68.24	.579
773.3	65.31	67.34	.627
826.1	64.34	66.03	.678

NOTE: Effect of tank bottom below 30 mg/l

REDUCED DATA FOR WHITE SILT/CLAY (6/26/79)
BLUE

CONCENTRATION (MG/L)	LIDAR CROSS SECTION LIKE(VV,DB)	CROSS(VH,DB)	DEPOLARIZATION RATIO
3.0	74.73	77.15	.189
6.0	69.16	76.07	.204
9.1	69.19	76.25	.180
12.1	68.99	75.82	.207
15.1	68.83	75.73	.204
18.1	68.81	75.64	.207
21.1	68.56	75.90	.189
24.2	68.30	75.54	.189
30.2	69.24	77.71	.142
36.2	68.84	76.88	.157
44.4	68.40	75.80	.182
59.5	68.14	75.32	.191
60.4	67.70	74.57	.206
68.7	67.90	74.89	.200
77.2	67.54	74.28	.212
85.5	67.34	74.00	.217
93.9	67.30	73.87	.220
124.7	66.33	72.14	.262
156.0	66.03	71.27	.299
186.0	65.69	70.56	.325
217.0	65.44	69.90	.359
247.0	64.56	68.95	.364
278.0	64.55	68.54	.400
308.0	64.19	67.94	.421
338.0	64.15	67.75	.436
407.0	63.29	66.56	.471
481.0	62.89	65.80	.512
552.0	62.56	65.28	.534
627.0	61.99	64.42	.571
773.3	61.66	63.88	.601
826.1	60.76	62.63	.651

NOTE: Effect of tank bottom below 30 mg/l

REDUCED DATA FOR WHITE SILT (1/80)
RED

CONCENTRATION (MG/L)	LIDAR CROSS SECTION LIKE (VV,DB)	CROSS (VH,DB)	DEPOLARIZATION RATIO
4.5	76.8	89.1	.058
9.0	75.6	87.9	.060
18.1	74.3	84.8	.089
27.1	73.9	83.8	.101
40.7	73.1	81.7	.137
54.2	72.8	81.6	.133
76.8	72.0	79.5	.180
101.7	71.3	77.9	.216
124.3	71.1	77.6	.221
169.5	71.9	78.2	.234
226.0	71.4	77.2	.265
282.5	70.3	75.1	.335
339.0	69.7	73.8	.387
452.0	67.6	71.4	.418
565.0	66.8	69.8	.498
678.0	66.2	68.8	.547
904.0	65.5	67.8	.591
1130.0	64.3	66.0	.680
1356.0	64.2	66.0	.567
1582.0	63.7	65.0	.749
1808.0	62.9	64.0	.780
2034.0	62.7	63.7	.789
2260.0	62.4	63.3	.810
2543.0	62.0	62.8	.832

REDUCED DATA FOR WHITE SILT (1/80)

BLUE

CONCENTRATION (MG/L)	LIDAR CROSS SECTION LIKE (VV, DB)	LIDAR CROSS SECTION CROSS (VH, DB)	DEPOLARIZATION RATIO
4.5	70.4	80.4	.100
9.0	70.3	79.3	.124
18.1	69.4	77.0	.174
27.1	68.9	76.2	.184
40.7	68.3	74.9	.208
54.2	67.9	74.2	.233
76.8	67.4	72.9	.277
101.7	66.7	71.8	.308
124.3	66.5	71.6	.311
169.5	67.2	71.9	.333
226.0	66.9	71.3	.362
282.5	65.9	69.6	.427
339.0	65.4	68.6	.473
452.0	63.2	66.4	.477
565.0	62.5	65.2	.541
678.0	61.9	64.2	.577
904.0	61.2	63.3	.621
1130.0	60.3	61.9	.687
1356.0	60.2	61.6	.727
1582.0	59.7	61.2	.713
1808.0	59.0	60.3	.749
2034.0	58.8	60.0	.760
2260.0	58.3	59.4	.777
2543.0	58.1	58.9	.820

REDUCED DATA FOR WHITE SAND BED

CONCENTRATION (MG/L)	LINEAR CROSS SECTION LIKE(VV,DB)	CROSS(VH,DB)	DEPOLARIZATION RATIO
0.0	78.6	99.9	.002
5.7	77.00	90.00	.052
11.3	75.90	86.50	.087
17.0	75.60	85.60	.100
22.6	75.00	84.20	.121
28.3	75.00	83.90	.129
28.3	74.80	83.70	.130
34.0	74.60	83.30	.137
39.6	74.50	82.70	.154
45.3	74.20	82.20	.158
50.9	74.10	82.00	.161
56.6	73.90	81.80	.160
56.6	73.80	81.50	.167
71.9	73.50	80.90	.182
87.4	73.10	80.30	.192
101.6	72.90	79.70	.206
115.7	72.70	79.40	.211
131.3	72.50	79.20	.214
131.3	71.90	78.60	.212
145.5	71.50	78.40	.229
160.0	71.80	78.20	.232
173.9	72.00	78.10	.242
188.0	71.80	77.90	.246
203.0	71.10	77.00	.255
231.0	70.90	76.60	.272
260.0	70.70	76.30	.278
287.0	70.60	76.00	.285
316.0	70.40	75.90	.281
348.0	70.20	75.80	.280
348.0	70.30	76.00	.269
417.0	69.90	75.20	.305
560.0	69.00	73.30	.374
560.0	68.60	72.60	.405
560.0	68.50	72.70	.384
631.1	68.30	72.50	.382
730.1	68.00	71.90	.404
871.6	67.30	70.70	.453
871.6	67.30	70.80	.456
1013.1	67.10	70.50	.460
1225.4	65.80	68.30	.561
1437.6	66.10	68.90	.526

REDUCED DATA FOR WHITE SAND
BLUE

CONCENTRATION (MG/L)	LIDAR CROSS SECTION LIKE(VV,DB)	CROSS(VH,DB)	DEPOLARIZATION RATIO
0.0	72.00	84.20	.060
5.7	70.90	79.50	.136
11.3	69.90	77.40	.175
17.0	70.30	77.40	.195
22.6	69.40	76.30	.208
28.3	69.50	76.00	.223
28.3	69.70	76.50	.212
34.0	69.40	76.00	.222
39.6	69.00	75.20	.240
45.3	68.70	74.70	.250
50.9	68.70	74.60	.256
56.6	68.80	74.60	.267
56.6	68.80	74.60	.259
71.9	68.40	74.00	.279
87.4	68.00	73.40	.288
101.6	67.80	73.00	.297
115.7	67.50	72.70	.303
131.3	67.50	72.70	.305
131.3	67.30	72.20	.325
145.5	67.20	72.00	.330
160.0	67.10	71.90	.333
173.8	67.10	71.80	.342
188.0	66.90	71.60	.345
203.0	66.60	71.10	.358
231.0	66.40	70.50	.386
260.0	66.20	70.20	.392
287.0	66.10	70.20	.390
316.0	65.90	70.10	.384
348.0	65.80	69.70	.408
348.0	65.90	70.20	.376
417.0	65.50	69.30	.419
560.0	64.60	67.90	.478
560.0	64.20	67.10	.512
560.0	64.10	67.20	.496
631.1	64.20	67.00	.526
730.1	63.70	66.40	.541
871.6	63.20	65.60	.568
871.6	63.50	66.10	.544
1013.1	63.20	65.70	.556
1225.4	61.80	63.60	.654
1437.6	62.00	64.20	.601

REDUCED DATA FOR RED SILT (HIGH CONCENTRATION)

CONCENTRATION (MG/L)	RED LIDAR CROSS SECTION LIKE(VV,DB)	CROSS(VH,DB)	DEPOLARIZATION RATIO
0.0	82.8	84.0	.754
14.8	69.00	74.00	.318
29.6	67.80	72.10	.374
44.4	66.90	70.50	.430
59.2	66.10	69.20	.484
74.0	65.50	68.40	.517
88.9	65.10	67.60	.560
148.0	63.60	65.40	.668
185.0	63.10	64.60	.720
222.0	61.80	62.90	.781
296.0	61.30	62.20	.812
407.0	60.60	61.40	.829
555.0	60.10	60.90	.840
703.0	59.90	60.70	.836
814.0	59.80	60.40	.863
962.0	59.60	60.30	.863
1110.0	59.50	60.10	.867
1295.0	59.40	60.10	.863
1480.0	59.30	60.00	.864
1850.0	59.30	60.00	.851
2220.0	59.20	59.90	.848

REDUCED DATA FOR RED SILT (HIGH CONCENTRATION)
BLUE

CONCENTRATION (MG/L)	LIDAR CROSS SECTION LIKE(VV,DB)	CROSS(VH,DB)	DEPOLARIZATION RATIO
0.0	77.20	80.00	.525
14.8	64.50	69.80	.295
29.6	63.90	68.70	.329
44.4	63.60	68.30	.336
59.2	63.20	67.30	.385
74.0	62.70	66.80	.394
88.8	62.40	66.20	.410
148.0	61.80	64.90	.482
185.0	61.40	64.50	.485
222.0	60.50	63.20	.535
296.0	60.30	62.90	.554
407.0	60.60	61.00	.554
555.0	60.30	62.90	.558
703.0	60.60	63.10	.557
814.0	60.60	63.20	.559
962.0	60.50	63.00	.562
1110.0	60.40	62.80	.569
1295.0	60.10	62.50	.572
1480.0	60.10	62.40	.577
1850.0	60.30	63.00	.539
2220.0	60.30	62.90	.542

REDUCED DATA FOR RED SILT

RED

CONCENTRATION (MG/L)	LIDAR CROSS SECTION LIKE(VV,DB)	CROSS(VH,DB)	DEPOLARIZATION RATIO
0.0	75.30	82.70	.183
3.7	71.70	77.40	.265
7.3	70.60	76.10	.278
11.0	69.90	75.10	.302
14.6	69.30	74.10	.331
18.3	68.90	73.50	.345
22.0	68.50	72.90	.364
25.6	68.20	72.50	.372
29.3	68.00	72.20	.379
32.9	67.70	71.90	.387
36.6	67.70	71.60	.405
45.8	66.80	70.30	.403
54.9	66.60	70.20	.430
64.1	66.40	69.90	.453
73.2	66.10	69.30	.479
82.4	65.80	68.70	.510
91.5	65.30	68.40	.493
100.7	65.20	68.10	.511
109.8	64.90	67.70	.529
119.0	64.60	67.20	.547
128.1	64.60	67.10	.564
146.4	64.10	66.50	.580
164.7	63.90	66.00	.617
183.0	63.60	65.50	.642
201.3	63.40	65.30	.652
228.8	62.90	64.70	.666
256.2	62.70	64.30	.687
283.7	62.40	63.90	.716
320.3	62.10	63.40	.740
393.5	61.70	62.80	.790

REDUCED DATA FOR RED SILT
BLUE

CONCENTRATION (MG/L)	LIDAR CROSS SECTION LIKE(VV,DB)	CROSS(VH,DB)	DEPOLARIZATION RATIO
0.0	70.30	80.10	.105
3.7	67.80	74.40	.219
7.3	66.90	73.00	.246
11.0	66.30	72.10	.263
14.6	66.00	71.70	.272
18.3	65.70	71.10	.291
22.0	65.30	70.50	.303
25.6	65.40	70.60	.300
29.3	65.10	70.20	.311
32.9	65.00	70.10	.309
36.6	64.90	69.70	.329
45.8	64.00	68.90	.330
54.9	64.00	68.60	.347
64.1	64.10	68.40	.364
73.2	63.80	68.00	.380
82.4	63.50	67.50	.391
91.5	63.10	67.20	.389
100.7	63.10	67.20	.393
109.8	63.20	67.10	.403
119.0	62.90	66.60	.424
128.1	62.90	66.60	.419
146.4	62.60	66.30	.429
164.7	62.40	66.00	.435
183.0	62.20	65.70	.451
201.3	62.10	65.40	.467
228.8	61.80	65.20	.465
256.2	61.70	64.90	.478
283.7	61.50	64.60	.493
320.3	61.30	64.30	.503
393.5	61.10	64.00	.511

REDUCED DATA FOR BROWN SILT (HIGH CONCENTRATION)
RED

CONCENTRATION (MG/L)	LIDAR CROSS SECTION LIKE (VV, DB)	CROSS (VH, DB)	DEPOLARIZATION RATIO
35.2	66.8	70.5	.411
70.4	67.00	71.00	.405
105.6	66.4	69.9	.448
140.8	65.5	68.7	.492
211.2	65.	67.7	.534
316.8	64.00	66.1	.618
422.4	63.3	65.	.68
528.0	63.3	64.5	.746
704.0	62.5	63.8	.731
880.0	62.1	63.4	.734
1144.	61.7	62.9	.758
1408.	61.4	62.6	.756
1760.	61.3	62.5	.755
2200.	61.2	62.4	.770
2640.	61.	62.2	.753
3520.	61.0	62.1	.755
4400.0	60.8	62.00	.762
5280.	60.8	62.1	.745
6160.0	60.7	62.00	.741

REDUCED DATA FOR BROWN SILT (HIGH CONCENTRATION)
BLUE

CONCENTRATION (MG/L)	LIDAR CROSS SECTION LIKE(VV,DB)	CROSS(VH,DB)	DEPOLARIZATION RATIO
35.2	64.5	70.1	.278
70.4	63.5	68.7	.312
105.6	63.3	68.00	.340
140.8	62.7	67.00	.37
211.2	62.3	66.1	.397
316.8	61.7	65.2	.449
422.4	61.3	64.6	.469
528.0	61.2	64.3	.493
704.0	61.1	64.2	.494
880.0	61.00	63.9	.512
1144.	60.4	63.3	.514
1408.	60.3	63.1	.519
1760.	60.7	63.5	.526
2200.	60.3	63.2	.516
2640.	60.5	63.3	.516
3520.	60.1	63.0	.511
4400.0	60.0	62.9	.511
5280.	60.0	63.0	.504
6160.0	59.9	62.8	.494

REDUCED DATA FOR BROWN SILT
RED

CONCENTRATION (MG/L)	LIDAR CROSS SECTION LIKE(VV,DB)	CROSS(VH,DB)	DEPOLARIZATION RATIO
0.00	76.50	85.75	.119
3.9	73.20	80.45	.192
7.8	71.97	78.49	.223
11.5	71.05	77.31	.237
15.5	70.55	76.51	.254
19.4	70.24	75.94	.269
23.3	69.70	75.49	.264
27.2	69.51	75.01	.282
31.0	69.17	74.48	.295
40.7	68.34	73.62	.319
50.4	68.20	72.90	.339
60.1	67.85	72.34	.356
69.8	67.34	71.74	.363
79.5	67.20	71.31	.388
89.2	66.91	70.87	.402
98.9	66.75	70.51	.420
108.5	66.49	70.29	.417
118.3	66.33	69.99	.431
128.0	66.11	69.59	.448
137.7	66.12	69.45	.464
157.1	65.63	68.89	.473
176.5	65.43	68.51	.492
195.9	65.19	68.08	.514
215.3	64.75	67.63	.516
234.7	64.67	67.48	.523
254.1	64.53	67.34	.523
302.6	64.07	66.72	.543
351.1	63.57	66.09	.573
399.5	63.30	65.50	.604
448.1	63.15	64.89	.670
496.6	63.01	64.78	.664
545.1	62.88	64.71	.656
642.1	62.93	64.82	.647
739.1	62.87	64.57	.675

REDUCED DATA FOR BROWN SILT
BLUE

CONCENTRATION (MG/L)	LIDAR CROSS SECTION LIKE(VV,DB)	CROSS(VH,DB)	DEPOLARIZATION RATIO
0.00	71.53	82.33	.083
3.9	69.04	76.32	.187
7.8	67.61	74.23	.218
11.6	66.90	73.15	.237
15.5	66.91	72.92	.251
19.4	66.42	72.34	.256
23.3	65.82	71.79	.253
27.2	65.72	71.58	.259
31.0	65.50	71.14	.273
40.7	65.15	70.61	.284
50.4	64.94	70.19	.299
60.1	64.53	69.57	.313
69.8	64.04	69.14	.309
79.5	64.21	69.01	.331
89.2	63.92	68.62	.339
98.9	63.69	68.30	.346
108.6	63.53	68.15	.345
118.3	63.35	67.82	.357
128.0	63.19	67.59	.363
137.7	63.29	67.60	.371
157.1	62.97	67.23	.374
175.5	62.75	66.90	.385
195.9	62.73	66.77	.395
215.3	62.44	66.48	.394
234.7	62.45	66.44	.399
254.1	62.53	66.35	.414
302.5	62.17	65.93	.421
351.1	62.11	65.73	.435
399.6	61.85	65.40	.443
448.1	61.68	65.12	.452
495.6	61.50	64.85	.462
545.1	61.71	64.99	.469
642.1	61.88	65.24	.461
739.1	61.97	65.05	.492

RAW MEASUREMENTS

RAW MEASUREMENT OF WHITE CLAY

CONC. (MG/L)	PMT	SEDIMENT RETURNS (X.001)				WHITE TARGET RETURNS (X.001)			
		RV	RH	BV	BH	RV	RH	BV	BH
0	1150/850	3.42	3.54	5.97	5.49	.171	.007	.544	.029
2.86	1150/850	.246	.014	.610	.039	3.33	3.46	6.14	5.65
5.72	1150/850	.298	.020	.668	.053	3.33	3.46	6.14	5.65
8.58	1150/850	.328	.024	.702	.063	3.34	3.55	6.33	5.94
11.44	1150/850	.373	.032	.787	.084	3.34	3.55	6.33	5.94
14.30	1150/850	.396	.034	.829	.091	3.38	3.56	6.51	6.11
17.16	1150/850	.436	.039	.884	.010	3.38	3.56	6.52	6.11
20.02	1150/850	.463	.045	.959	.117	3.39	3.53	6.45	6.03
22.88	1150/850	.485	.049	.976	.123	3.39	3.53	6.45	6.03
25.74	1150/850	.522	.058	1.06	.143	3.32	3.47	6.57	6.07
28.60	1150/850	.549	.063	1.11	.158	3.42	3.65	6.91	6.42
28.60	1150/850	.549	.062	1.12	.157	3.42	6.65	6.91	6.42
28.60	1150/850	.543	.060	1.07	.148	3.48	3.54	6.85	6.39
35.75	1150/850	.599	.063	1.23	.176	3.29	3.54	6.79	6.44
42.90	1150/850	.652	.074	1.34	.204	3.44	3.63	7.11	6.56
49.91	1150/850	.722	.093	1.44	.237	3.44	3.63	7.11	6.56
56.91	1150/850	.776	.109	1.58	.278	3.29	3.59	7.17	6.59
64.06	1150/850	.836	.122	1.67	.310	3.29	3.59	7.17	6.59
71.07	1150/850	.878	.135	1.69	.325	3.50	3.63	6.76	6.22
78.22	1150/850	.920	.154	1.70	.336	3.27	3.58	6.20	6.04
85.94	1150/850	.969	.170	1.71	.350	3.32	3.60	6.40	6.10
93.09	1150/850	1.02	.185	1.81	.384	3.38	3.61	6.60	6.17
107.4									
121.7	1150/850	1.23	.266	2.23	.545	3.43	3.62	6.77	6.30
137.1	1150/850	1.32	.311	2.37	.615	3.46	3.67	6.84	6.34
151.4	1150/850	1.41	.355	2.58	.706	3.49	3.71	6.91	6.38
174.3	1150/850	1.53	.418	2.74	.797	3.30	3.67	6.59	6.35
195.8	1150/850	1.69	.498	2.93	.911	3.42	3.59	6.81	6.42
224.9	1150/850	1.84	.597	3.33	1.11	3.42	3.59	6.81	6.42
253.5	1150/850	2.03	.706	3.57	1.26	3.51	3.71	7.10	6.43
282.1	1150/850	2.24	.839	4.01	1.51	3.49	3.53	7.14	6.52
317.9	1150/850	2.42	.973	4.19	1.65	3.34	3.47	6.86	6.56
353.6	1150/850	2.68	1.15	4.74	1.97	3.41	3.56	6.80	6.36
410.8	1150/850	3.07	1.44	5.39	2.42	3.41	3.56	6.80	6.36
482.3	1150/850	3.59	1.84	5.14	2.97	3.33	3.44	6.84	6.27
553.8	1150/850	4.10	2.27	6.96	3.58	3.39	3.49	6.39	6.59
625.3	1150/850	4.67	2.72	7.92	4.26	3.42	3.54	7.25	6.77
732.6	1150/850	5.44	3.40	20.6	5.38	3.45	3.58	7.64	7.09
732.6	1100/850	3.77	2.38	6.74	3.83	3.45	3.58	7.64	7.09

RAW MEASUREMENT OF WHITE SILT/CLAY (6/19/79)

CONC. (MG/L)	PMT	SEDIMENT RETURNS (X.001) RV	RH	BV	BH	WHITE TARGET RETURNS (X.001) RV	RH	BV	BH
00.00	1150/850	.332	.022	.545	.022	3.33	3.15	5.17	4.64
3.02	1150/850	.414	.043	.612	.039	3.33	3.15	5.17	4.64
6.04	1150/850	.450	.058	.651	.057	3.33	3.15	5.17	4.64
9.06	1150/850	.498	.071	.734	.083	3.33	3.15	5.17	4.64
12.08	1150/850	.510	.073	.790	.096	3.42	3.20	4.91	4.50
15.10	1150/850	.552	.084	.823	.109	3.37	3.22	4.96	4.52
18.12	1150/850	.571	.089	.876	.119	3.38	3.25	4.99	4.51
21.14	1150/850	.596	.091	.882	.123	3.42	3.22	5.23	4.73
24.15	1150/850	.628	.104	.862	.129	3.32	3.20	4.58	4.34
27.18	1150/850	.655	.117	1.01	.164	3.34	3.28	4.87	4.52
30.20	1150/850	.584	.124	1.02	.172	3.54	3.35	5.36	4.81
33.22	1150/850	.683	.125	1.01	1.72	3.48	3.30	5.19	4.72
36.24	1150/850	.736	.147	.966	.175	3.54	3.29	4.27	3.81
39.26	1150/850	.753	.153	1.01	.183	3.46	3.25	5.00	4.52
42.28	1150/850	.753	.156	1.01	.187	3.50	3.31	4.94	4.43
45.30	1150/850	.738	.164	1.11	.212	3.51	3.30	5.31	4.73
48.32	1150/850	.807	.173	1.20	.236	3.58	3.38	5.34	4.80
51.34	1150/850	.820	.175	1.18	.231	3.54	3.29	5.25	4.70
54.36	1150/850	.840	.182	1.17	.231	3.56	3.21	5.49	4.91
57.38	1150/850	.860	.178	1.16	2.29	3.52	3.32	5.13	4.65
60.40	1150/850	.851	.181	1.22	2.41	3.49	3.41	5.51	5.05
63.42	1150/850	.875	.186	1.31	.286	3.40	3.50	5.57	5.05
129.9	1150/850	.893	.184	1.33	.271	3.59	3.33	5.49	5.31
69.46	1150/850	.910	.186	1.24	.248	3.66	3.45	5.36	5.36
72.48	1150/850	.913	.186	1.19	.234	3.57	3.39	5.50	5.03
72.48	1150/850	.913	.186	1.19	.234	3.57	3.39	5.59	5.03
75.50	1150/850	.932	.194	1.26	.252	3.55	3.35	5.43	4.92
78.52	1150/850	.947	.191	1.30	.261	3.54	3.41	5.09	4.60
81.54	1150/850	.954	.192	1.32	.266	3.70	3.43	5.85	5.36
89.39	1150/850	.980	.207	1.34	.277	3.65	3.43	6.01	5.44
95.64	1150/850	1.03	.214	1.46	.311	3.65	3.43	6.01	5.44
104.6	1150/850	.052	.000	.066	.000	3.57	3.33	5.70	5.13
112.6	1150/850	1.10	.236	1.50	.342	3.57	3.31	5.60	5.00
120.0	1150/850	1.15	.253	1.53	.346	3.42	3.39	4.80	4.46
127.3	1150/850	1.16	.252	1.56	.362	3.54	3.34	5.37	4.90
135.6	1150/850	1.19	.269	1.63	.387	3.46	3.30	5.33	4.86
142.8	1150/850	1.21	.278	1.57	.370	3.57	3.32	5.14	4.62
151.5	1150/850	1.27	.306	1.70	.427	3.57	3.32	5.14	4.62
156.3	1150/850	1.32	.330	1.82	.475	3.51	3.35	5.36	4.85
182.3	1150/850	1.40	.355	1.93	.517	3.64	3.42	5.83	5.23
198.1	1150/850	1.51	.411	2.14	.611	3.53	3.45	5.24	4.94

RAW MEASUREMENT OF WHITE SILT/CLAY (6/26/79)

CONC. (MG/L)	PMT	SEDIMENT RETURNS (X.001)				WHITE TARGET RETURNS (X.001)			
		RV	RH	BV	BH	RV	RH	BV	BH
3.02	1150/850	.551	.159	.387	.066	3.26	3.13	2.69	2.43
6.04	1150/850	.605	.178	.408	.075	3.26	3.13	2.69	2.43
9.06	1150/850	.622	.176	.405	.072	3.32	3.18	2.39	2.16
12.08	1150/850	.529	.172	.431	.080	3.23	3.12	2.42	2.17
15.10	1150/850	.658	.170	.447	.082	3.23	3.12	2.42	2.17
18.12	1150/850	.662	.166	.494	.093	3.41	3.12	2.66	2.40
21.14	1150/850	.671	.165	.358	.062	3.14	3.07	1.82	1.63
24.16	1150/850	.686	.165	.380	.066	3.14	3.07	1.82	1.63
27.18	1150/850	.638	.148	.256	.031	3.46	3.05	1.59	1.44
27.18	1150/850	.632	.141	.288	.036	3.37	3.23	1.79	1.59
30.20	1150/850	.654	.142	.296	.037	3.40	3.28	1.76	1.56
33.22	1150/850	.700	.155	.338	.048	3.33	3.19	1.81	1.61
36.24	1150/850	.705	.151	.334	.047	3.39	3.19	1.81	1.61
44.39	1150/850	.756	.168	.369	.060	3.39	3.19	1.81	1.61
51.94	1150/850	.798	.171	.390	.067	3.35	3.20	1.80	1.62
60.40	1150/850	.854	.190	.431	.080	3.15	3.20	1.80	1.62
68.71	1150/850	.877	.191	.428	.078	3.20	3.24	1.87	1.71
77.16	1150/850	.928	.201	.458	.087	3.36	3.24	1.84	1.66
85.47	1150/850	.990	.222	.474	.093	3.36	3.24	1.84	1.66
93.92	1150/850	1.02	.227	.473	.094	3.32	3.24	1.80	1.63
124.7	1150/850	1.20	.301	.594	.143	3.16	3.20	1.81	1.66
155.7	1150/850	1.35	.371	.644	.176	3.29	3.29	1.83	1.67
186.5	1150/850	1.53	.461	.697	.207	3.29	3.29	1.83	1.67
217.0	1150/850	1.57	.542	.754	.240	3.38	3.22	1.87	1.66
247.5	1150/850	1.81	.624	.883	.300	3.32	3.19	1.79	1.67
277.7	1150/850	1.95	.711	.905	.329	3.26	3.22	1.83	1.66
308.5	1150/850	2.14	.823	.984	.376	3.26	3.22	1.83	1.66
338.4	1150/850	2.25	.916	1.01	.399	3.59	3.25	1.86	1.68
407.1	1150/850	2.63	1.17	1.35	.583	3.31	3.05	2.04	1.87
481.1	1150/850	2.99	1.47	1.40	.646	3.35	3.20	1.93	1.74
552.1	1150/850	3.27	1.69	1.59	.769	3.28	3.16	2.03	1.84
626.8	1150/850	3.56	2.01	1.76	.832	3.30	3.13	1.97	1.75
773.3	1150/850	4.28	2.54	2.04	1.11	3.40	3.22	2.12	1.92
826.1	1150/850	5.36	3.44	2.51	1.48	3.38	3.12	2.14	1.93

PIA MEASUREMENT OF WHITE SILT (1/80)

CONC. (MG/L)	PMT	SEDIMENT RETURNS (X.001)				WHITE TARGET RETURNS (X.001)			
		RV	RH	BV	BH	RV	RH	BV	BH
4.52	1150/700	.197	.011	1.76	.166	.425	.412	2.91	2.65
9.04	1150/700	.242	.014	1.92	.212	.425	.412	2.91	2.65
18.08	1150/700	.327	.028	2.20	.361	.425	.412	2.91	2.65
27.12	1150/700	.361	.035	2.37	.420	.423	.405	2.65	2.55
33.90	1150/700	.434	.057	2.80	.561	.423	.405	2.65	2.55
54.24	1150/700	.475	.069	2.97	.655	.436	.415	2.64	2.52
79.10	1150/700	.584.	.097	3.38	.871	.451	.411	2.69	2.50
101.7	1150/700	.630	.138	3.97	1.14	.451	.411	2.68	2.50
124.3	1150/700	.730	.147	4.12	1.20	.451	.411	2.68	2.50
169.5	1100/700	.593	.131	3.25	1.04	.440	.417	2.45	2.16
395.5	1100/700	.657	.163	3.46	1.14	.436	.410	2.46	2.32
282.5	1100/700	.841	.265	4.33	1.74	.436	.410	2.46	2.36
339.0	1100/700	.963	.348	4.91	2.14	.431	.403	2.47	2.29
452.0	1050/700	.732	.286	3.65	1.71	.426	.399	2.35	2.30
565.0	1050/700	.909	.424	4.42	2.30	.436	.409	2.43	2.31
678.0	1050/700	1.06	.544	5.23	2.87	.447	.418	2.45	2.33
904.0	1050/700	1.24	.694	5.84	3.48	.449	.426	2.34	2.26
1130.	1050/700	1.63	1.03	7.17	4.63	.447	.416	2.34	2.22
1356.	1050/700	1.73	1.11	7.56	5.09	.461	.443	2.42	2.23
1582.	1000/700	1.30	.897	5.52	3.78	.457	.422	2.37	2.27
1808.	1000/700	1.55	1.12	6.54	4.63	.457	.422	2.37	2.27
2034.	1000/700	1.54	1.22	6.79	4.95	.460	.432	2.35	2.26
2260.	1000/700	1.82	1.38	7.61	5.63	.469	.440	2.35	2.26
2543.	1000/700	2.31	1.57	8.09	6.32	.479	.449	2.35	2.24

RAW MEASUREMENT OF WHITE SAND

CONC. (MG/L)	PMT	SEDIMENT RETURNS (X.001)				WHITE TARGET RETURNS (X.001)			
		RV	RH	BV	BH	RV	RH	BV	BH
00.00	1150/850	.184	.000	.468	.027	3.13	3.43	5.28	5.05
5.66	1150/850	.246	.014	.616	.076	2.91	3.15	5.33	4.84
11.32	1150/850	.323	.031	.776	.123	2.91	3.15	5.33	4.84
16.98	1150/850	.372	.040	.799	.146	3.19	3.41	6.03	5.66
22.64	1150/850	.440	.056	.938	.183	3.24	3.44	5.84	5.48
28.30	1150/850	.449	.062	.399	.199	3.28	3.47	5.64	5.32
28.30	1150/850	.461	.064	.919	.191	3.29	3.53	6.15	5.72
33.96	1150/850	.486	.071	.988	.204	3.29	3.53	6.15	5.72
39.62	1150/850	.515	.082	1.03	.227	3.42	3.55	5.85	5.37
45.28	1150/850	.552	.091	1.12	.256	3.42	3.55	5.85	5.37
50.94	1150/850	.565	.096	1.14	.269	3.41	3.60	5.95	5.49
56.60	1150/850	.591	.102	1.12	.277	3.40	3.65	6.07	5.63
56.60	1150/850	.610	.109	1.18	.289	3.40	3.64	6.30	5.93
71.88	1150/850	.653	.123	1.25	.324	3.40	3.54	6.18	5.73
37.45	1150/850	.709	.140	1.41	.377	3.40	3.50	6.25	5.79
101.6	1150/850	.753	.157	1.49	.410	3.40	3.45	6.32	5.86
115.7	1150/850	.789	.169	1.59	.445	3.40	3.45	6.32	5.86
131.3	1150/850	.832	.185	1.62	.470	3.45	3.59	6.43	6.16
131.3	1150/850	.908	.208	1.75	.541	3.26	3.52	6.71	6.39
145.5	1150/850	.911	.217	1.84	.570	3.33	3.48	6.85	6.43
159.6	1150/850	.937	.226	1.87	.585	3.33	3.48	6.85	6.43
173.7	1150/850	.960	.234	1.92	.602	3.53	3.55	7.03	6.45
187.9	1150/850	.991	.246	2.01	.635	3.56	3.55	7.03	6.45
203.2	1150/850	1.03	.260	2.07	.665	3.52	3.67	7.11	6.70
203.2	1150/850	1.10	.303	2.19	.750	3.31	3.57	7.07	6.78
231.2	1150/850	1.17	.335	2.31	.830	3.40	3.58	7.10	6.60
259.5	1150/850	1.23	.360	2.42	.886	3.40	3.58	7.10	6.60
286.9	1150/850	1.28	.384	2.49	.922	3.40	3.59	7.18	6.81
315.6	1150/850	1.32	.392	2.60	.947	3.40	3.59	7.18	6.81
347.8	1150/850	1.39	.426	2.72	1.03	3.43	3.77	7.27	6.75
347.8	1150/850	1.31	.378	2.55	.927	3.26	3.51	7.10	6.85
417.4	1150/850	1.51	.484	2.92	1.14	3.43	3.61	7.32	6.83
488.2	1150/850	1.69	.596	3.32	1.40	3.43	3.61	7.32	6.93
560.3	1150/850	1.88	.729	3.59	1.59	3.49	3.62	7.37	6.83
560.3	1150/850	2.05	.860	3.95	1.87	3.49	3.62	7.37	6.93
560.3	1150/850	2.03	.829	3.82	1.79	3.37	3.59	7.03	6.63
348.1	1150/850	2.19	.944	4.00	1.91	3.49	3.93	7.42	6.75
730.1	1150/850	2.35	1.05	4.43	2.20	3.47	3.84	7.38	6.75
971.6	1150/850	2.75	1.35	5.00	2.62	3.44	3.74	7.33	6.75
871.6	1150/850	2.68	1.31	4.92	2.57	3.40	3.65	7.72	7.43
1013.	1150/850	2.81	1.39	5.10	2.63	3.38	3.62	7.51	6.98
1225.	1150/850	3.81	2.29	6.87	4.41	3.36	3.59	7.30	6.72
1437.	1150/850	3.65	2.09	6.56	3.76	3.44	3.75	7.38	7.03

RAW MEASUREMENT OF RED SILT (HIGH CONCENTRATION)

CONC. (MG/L)	PMT	SEDIMENT RETURNS (X.001)				WHITE TARGET RETURNS (X.001)			
		RV	RH	BV	BH	RV	RH	BV	BH
0	1000/750	.015	.011	.120	.058	.722	.697	5.05	4.63
14.8	1000/750	.340	.103	.209	.561	.714	.675	4.72	4.28
29.6	1000/750	.456	.166	2.50	.769	.725	.708	4.36	4.53
44.4	1000/750	.555	.231	2.87	.949	.709	.683	5.27	5.18
59.2	1000/750	.666	.311	3.18	1.20	.709	.683	5.27	5.18
74.0	1000/750	.763	.381	3.48	1.35	.716	.692	5.23	5.13
98.8	1000/750	.849	.459	3.81	1.54	.716	.692	5.23	5.13
88.8	1000/750	1.01	.595	42.1	1.77	.713	.688	5.23	4.94
148.	1000/750	1.17	.756	4.36	1.98	.713	.688	5.23	4.94
185.	1000/750	1.35	.920	4.76	2.21	.728	.691	5.22	4.99
148.	1000/750	1.54	1.10	4.91	2.41	.728	.691	5.22	4.99
222.	1000/750	1.84	1.40	5.49	2.74	.737	.716	4.87	4.54
296.	1000/750	2.09	1.64	5.66	2.93	.737	.716	4.87	4.54
407.	1000/750	2.40	1.94	5.86	3.08	.727	.707	5.36	5.10
555.	1000/750	2.69	2.20	6.21	3.30	.727	.707	5.36	5.10
703.	1000/750	2.92	2.37	6.64	3.52	.756	.734	6.07	5.78
814.	1000/750	3.02	2.52	6.55	3.49	.756	.734	6.07	5.78
962.	1000/750	3.13	2.63	6.37	3.41	.755	.734	5.70	5.43
1110.	1000/750	3.25	2.74	6.54	3.54	.755	.734	5.70	5.43
1295.	1000/750	3.31	2.79	6.38	3.40	.761	.744	5.21	4.85
1480.	1000/750	3.38	2.85	6.45	3.46	.761	.744	5.21	4.85
1850.	1000/750	3.15	2.93	6.34	3.40	.776	.774	5.43	5.39
2220.	1000/750	3.53	2.99	6.36	3.43	.776	.774	5.43	5.39
2220.	950/750	2.34	1.99	4.31	2.29	7.87	7.61	5.36	4.96
2220.	900/750	1.52	1.31	2.74	1.49	7.87	7.61	5.36	4.96

RAW MEASUREMENT OF RED SILT

CONC. (MG/L)	PMT	SEDIMENT RETURNS (X.001)				WHITE TARGET RETURNS (X.001)			
		RV	RH	BV	BH	RV	RH	BV	BH
0.00	1150/850	.409	.075	.689	.070	3.24	3.21	5.21	5.04
3.66	1150/850	.932	.253	1.26	.259	3.19	3.26	5.41	5.06
7.32	1150/850	1.20	.341	1.57	.361	3.19	3.26	5.41	5.06
10.98	1150/850	1.41	.434	1.77	.436	3.19	3.26	5.41	5.06
14.64	1150/850	1.59	.523	1.96	.498	3.18	3.16	5.58	5.21
18.30	1150/850	1.75	.601	2.11	.574	3.18	3.16	5.58	5.21
21.96	1150/850	1.94	.701	2.32	.655	3.18	3.16	5.58	5.21
25.62	1150/850	2.05	.771	2.46	.709	3.17	3.21	6.04	5.83
29.28	1150/850	2.17	.834	2.62	.786	3.17	3.21	6.04	5.83
32.94	1150/850	2.28	.895	2.68	.797	3.17	3.21	6.04	5.83
36.60	1150/850	2.39	.974	2.78	.848	3.26	3.28	6.07	5.62
45.75	1150/850	2.71	1.18	3.21	1.04	3.05	3.30	5.77	5.67
54.90	1150/850	2.97	1.35	3.38	1.13	3.15	3.34	6.01	5.81
64.05	1150/850	3.18	1.50	3.46	1.20	3.25	3.39	6.25	5.95
73.20	1150/850	3.41	1.70	3.65	1.32	3.25	3.39	6.25	5.95
91.50	1150/850	3.91	2.09	4.10	1.56	3.11	3.38	5.87	5.76
100.7	1150/850	4.08	2.23	4.22	1.62	3.14	3.36	6.14	5.98
109.8	1150/850	4.34	2.42	4.35	1.68	3.16	3.32	6.39	6.13
119.0	1150/850	4.66	2.68	4.61	1.88	3.16	3.32	6.39	6.13
128.1	1150/850	4.75	2.76	4.56	1.84	3.20	3.30	5.24	5.99
155.6	800/350	5.22	3.18	4.80	2.01	3.13	3.30	6.25	6.10
164.7	1150/850	5.58	3.50	5.04	2.14	3.23	3.27	6.21	6.05
183.0	1150/850	6.00	3.91	5.28	2.32	3.23	3.27	6.21	6.05
201.3	1150/850	6.37	4.24	5.50	2.44	3.25	3.32	6.35	6.02
228.8	1150/850	6.95	4.84	5.65	2.60	3.20	3.35	6.11	6.04
256.2	1150/850	7.48	5.30	5.86	2.71	3.22	3.32	6.10	5.90
283.7	1150/850	7.69	5.77	6.05	2.84	3.24	3.28	6.03	5.78
320.3	1150/850	8.49	6.33	6.25	3.03	3.24	3.26	5.98	5.76
356.9	1150/850	31.0	6.85	7.05	3.43	3.38	3.27	6.35	6.10
393.5	1130/850	8.38	6.44	6.36	3.12	3.38	3.29	6.71	6.45

RAW MEASUREMENT OF BROWN SILT (HIGH CONCENTRATION)

CONC. (MG/L)	PMT	SEDIMENT RETURNS (X.001)				WHITE TARGET RETURNS (X.001)			
		RV	RH	BV	BH	RV	RH	BV	BH
39.08	1100/750	.569	.230	2.67	.711	.710	.698	6.03	5.77
78.16	1100/750	.540	.214	3.42	1.02	.720	.705	6.29	6.01
117.2	1100/750	.629	.274	3.82	1.23	.729	.710	6.57	6.25
140.8	1100/750	.756	.362	4.43	1.56	.729	.710	6.57	6.25
211.2	1100/750	.915	.483	4.65	1.74	.759	.751	6.33	5.95
316.8	1100/750	1.16	.707	5.34	2.25	.759	.751	6.33	5.95
422.4	1100/750	1.35	.885	5.79	2.54	.763	.736	6.19	5.82
528.0	750/750	.131	.094	.562	.261	.763	.736	6.19	5.82
704.0	1100/750	1.71	1.22	6.32	2.98	.798	.778	6.54	6.24
880.0	1100/750	1.89	1.35	6.54	3.19	.798	.778	6.54	6.24
1144.	1100/750	2.01	1.49	6.99	3.43	.779	.760	6.15	5.86
1408.	1100/750	2.14	1.58	7.26	3.59	.779	.760	6.15	5.86
1760.	1100/750	2.18	1.62	6.91	3.45	.774	.751	6.45	6.13
2200.	1100/750	2.23	1.66	7.13	3.52	.777	.751	6.12	5.86
3520.	1100/750	2.35	1.75	7.20	3.53	.772	.752	.583	.558
4400.	1100/750	2.43	1.80	7.32	3.58	.772	.752	.583	.558
5280.	1100/750	2.44	1.79	7.46	3.65	.776	.766	5.95	5.78
6160.	1100/750	2.50	1.83	7.86	3.78	.776	.766	5.95	5.78

RAW MEASUREMENT OF BROWN SILT

CONC. (MG/L)	PMT	SEDIMENT RETURNS (X.001)				WHITE TARGET RETURNS (X.001)			
		RV	RH	BV	BH	RV	RH	BV	BH
00.00	1150/850	.327	.039	.543	.042	3.41	3.45	5.54	5.19
3.88	1150/850	.684	.134	1.02	.179	3.41	3.48	5.80	5.44
7.76	1150/850	.927	.211	1.42	.290	3.41	3.48	5.80	5.44
11.64	1150/850	1.09	.269	1.54	.337	3.24	3.38	5.35	4.93
15.52	1150/850	1.26	.332	1.54	.357	3.34	3.47	5.35	4.95
19.40	1150/850	1.39	.383	1.72	.409	3.43	3.51	5.35	4.97
23.28	1150/850	1.50	.421	2.05	.501	3.27	3.48	5.54	5.36
27.16	1150/850	1.61	.473	2.22	.543	3.36	3.50	5.86	5.54
31.04	1150/850	1.74	.534	2.33	.602	3.36	3.50	5.86	5.54
40.74	1150/850	1.96	.641	2.64	.711	3.35	3.45	6.12	5.80
50.44	1150/850	2.17	.758	2.77	.734	3.35	3.45	6.12	5.80
60.14	1150/850	2.36	.872	3.06	.895	3.36	3.49	6.15	5.75
69.84	1150/850	2.55	.989	3.29	.995	3.23	3.45	5.91	5.79
79.54	1150/850	2.73	1.11	3.39	1.07	3.35	3.51	6.33	6.04
89.24	1150/850	2.92	1.23	3.62	1.17	3.35	3.51	6.33	6.04
98.94	1150/850	3.05	1.32	3.79	1.24	3.37	3.47	6.28	5.94
108.6	1150/850	3.20	1.42	4.03	1.35	3.33	3.54	6.44	6.26
118.3	1150/850	3.31	1.50	4.23	1.45	3.32	3.49	6.48	6.22
128.0	1150/850	3.48	1.64	4.39	1.53	3.32	3.49	6.48	6.22
137.7	1150/850	3.59	1.72	4.54	1.60	3.43	3.54	6.85	6.52
157.1	1150/850	3.91	1.97	4.80	1.75	3.34	3.56	6.73	6.56
176.5	1150/850	4.17	2.16	5.11	1.89	3.40	3.58	6.83	6.56
195.9	1150/850	4.48	2.39	5.22	1.95	3.46	3.59	6.94	6.57
215.3	1150/850	4.73	2.58	5.35	2.08	3.30	3.49	6.65	6.55
234.7	1150/850	4.94	2.78	5.58	2.18	3.38	3.64	6.95	6.80
254.1	1150/850	5.22	3.00	5.79	2.30	3.46	3.80	7.34	7.05
302.6	1150/850	5.73	3.43	5.71	2.32	3.42	3.77	6.67	6.44
351.1	1150/850	6.22	3.84	5.89	2.46	3.38	3.64	6.79	6.52
399.6	1150/850	6.56	4.25	6.36	2.69	3.33	3.52	6.92	6.61
448.1	1150/850	7.04	4.66	6.39	2.80	3.40	3.36	6.66	6.45
496.6	1150/850	7.39	4.95	6.81	3.02	3.45	3.48	6.82	6.55
545.1	1150/850	3.20	3.62	7.00	6.64	7.72	5.24	6.67	2.97
642.1	1150/850	7.12	4.99	6.22	2.97	3.27	3.54	6.79	6.80
739.1	1150/850	7.52	5.33	6.28	2.92	3.40	3.57	6.95	6.64

APPENDIX B

Algae Measurements

REDUCED MEASUREMENTS

REDUCED DATA FOR ALGAE & WHITE SILT

CONCENTRATION		LIDAR CROSS SECTION		DEPOLARIZATION
ALGAE (LITERS)	SILT (MG/L)	LIKE(VV,DB)	CROSS(VH,DB)	RATIO
		RED		
0.0	0.0	75.30	82.50	.192
5.0	0.0	75.30	82.90	.175
8.0	0.0	75.10	82.70	.173
10.0	0.0	75.00	82.70	.173
12.0	0.0	75.20	82.70	.179
15.0	0.0	75.70	83.20	.173
18.0	0.0	75.40	83.30	.161
20.0	0.0	75.40	83.20	.169
0.0	21.6	73.90	81.90	.160
0.0	43.2	73.20	80.70	.175
0.0	86.4	71.40	78.50	.197
0.0	129.6	71.00	77.80	.211
0.0	216.0	69.80	75.40	.270
0.0	324.0	69.00	74.10	.310
0.0	540.0	67.30	71.00	.425

REDUCED DATA FOR ALGAE & WHITE SILT

BLUE

CONCENTRATION ALGAE (LITERS)	CONCENTRATION SILT (MG/L)	LIDAR CROSS SECTION LIKE (VV,DB)	LIDAR CROSS SECTION CROSS (VH,DB)	DEPOLARIZATION RATIO
0.0	0.0	70.30	79.10	.132
5.0	0.0	70.80	79.60	.131
8.0	0.0	70.80	79.60	.131
10.0	0.0	71.10	79.90	.131
12.0	0.0	71.50	80.40	.130
15.0	0.0	71.90	81.00	.123
18.0	0.0	71.70	80.50	.131
20.0	0.0	72.00	80.90	.129
0.0	21.6	70.10	77.30	.190
0.0	43.2	69.10	75.90	.205
0.0	86.4	67.40	73.30	.254
0.0	129.6	67.00	72.70	.272
0.0	216.0	65.60	70.40	.334
0.0	324.0	64.90	69.30	.364
0.0	540.0	63.20	66.40	.479

RAW MEASUREMENTS

RAW MEASUREMENT OF ALGAE

CONC. (MG/L)	PMT	SEDIMENT RETURNS (X.001)				WHITE TARGET RETURNS (X.001)			
		RV	RH	BV	BH	RV	RH	BV	BH
00.00	1150/800	3.21	.060	1.26	.160	1.56	1.51	5.85	5.65
5.00	1150/800	3.32	.056	1.27	.162	1.60	1.54	6.58	6.36
8.00	1150/800	.343	.057	1.22	.155	1.57	1.52	6.34	6.17
10.00	1150/800	.338	.055	1.19	.148	1.54	1.45	6.62	6.25
12.00	1150/800	.335	.056	1.15	.141	1.59	1.50	7.09	6.66
15.00	1150/800	.338	.055	1.13	.132	1.77	1.66	7.58	7.26
18.00	1150/800	.345	.054	1.13	.146	1.71	1.66	7.22	7.05
20.00	1150/800	.342	.055	1.03	.130	1.71	1.63	7.05	6.90

RAW MEASUREMENT OF ALGAE WITH SEDIMENT

CONC. (MG/L)	PMT	SEDIMENT RETURNS (X.001)				WHITE TARGET RETURNS (X.001)			
		RV	RH	BV	BH	RV	RH	BV	BH
00.00	1150/800	3.21	.060	1.26	.160	1.56	1.51	5.85	5.65
1080.	1150/800	3.32	.056	1.27	.162	1.60	1.54	6.58	6.36
1728.	1150/800	.343	.057	1.22	.155	1.57	1.52	6.34	6.17
2160.	1150/800	.338	.055	1.19	.148	1.54	1.45	6.62	6.25
2592.	1150/800	.335	.056	1.15	.141	1.59	1.50	7.09	6.66
3240.	1150/800	.338	.055	1.13	.132	1.77	1.66	7.58	7.26
3888.	1150/800	.345	.054	1.13	.146	1.71	1.66	7.22	7.05
4320.	1150/800	.342	.055	1.03	.130	1.71	1.63	7.05	6.90

APPENDIX C

Surface Roughness Measurements

REDUCED MEASUREMENTS

REDUCED DATA FOR WHITE SILT

RED

CONCENTRATION (MG/L)	LIDAR CROSS SECTION LIKE(VV,DB)	CROSS(VH,DB)	DEPOLARIZATION RATIO
SURFACE: CALM			
0.0	73.79	87.74	.040
30.3	73.77	88.08	.037
90.9	71.76	80.43	.136
151.5	70.64	77.75	.195
303.0	68.78	74.08	.295
454.5	68..15	72.58	.360
SURFACE: MEDIUM			
0.0	73.78	89.07	.030
30.3	73.57	88.03	.036
90.9	71.58	80.26	.136
151.5	70.37	77.48	.194
303.0	68.58	73.97	.289
454.5	67.93	72.38	.361
SURFACE: ROUGH			
0.0	73.96	89.07	.031
30.3	73.92	88.43	.035
90.9	71.26	80.34	.124
151.5	70.01	77.15	.193
303.0	68.37	73.73	.292
454.5	67.69	72.26	.349

REDUCED DATA FOR WHITE SILT
BLUE

CONCENTRATION (MG/L)	LIDAR CROSS SECTION LIKE(VV,DB)	LIDAR CROSS SECTION CROSS(VH,DB)	DEPOLARIZATION RATIO
SURFACE: CALM			
0.0	68.71	76.21	.178
30.3	68.14	75.76	.173
90.9	67.02	72.89	.259
151.5	65.90	71.00	.309
303.0	64.30	68.25	.403
454.5	63.92	67.21	.468
SURFACE: MEDIUM			
0.0	68.60	76.27	.171
30.3	70.32	76.16	.156
90.9	66.82	72.85	.249
151.5	65.70	70.91	.301
303.0	64.10	68.10	.398
454.5	63.63	67.06	.454
SURFACE: ROUGH			
0.0	68.29	76.01	.169
30.3	68.69	76.62	.161
90.9	66.39	72.31	.255
151.5	65.46	70.49	.314
303.0	63.83	67.88	.394
454.5	63.30	66.78	.448

REDUCED DATA FOR RED SILT

CONCENTRATION (MG/L)	RED LIDAR CROSS SECTION LIKE(VV,DB)	CROSS(VH,DB)	DEPOLARIZATION RATIO
SURFACE: CALM			
8.2	68.62	74.63	.250
40.8	65.06	68.81	.422
122.3	62.26	64.35	.618
203.8	60.89	62.32	.719
SURFACE: CALM			
1.0	68.48	74.24	.265
8.2	68.33	74.27	.255
40.8	65.02	68.81	.418
122.3	62.20	64.32	.613
203.8	60.80	62.46	.683
SURFACE: MEDIUM			
1.0	68.47	74.38	.257
8.2	68.21	74.34	.244
40.8	65.00	68.79	.418
122.3	62.13	64.23	.617
203.8	60.80	62.24	.701
SURFACE: ROUGH			
1.0	68.68	74.69	.250
8.2	68.29	74.33	.249
40.8	64.68	68.53	.412
122.3	61.83	64.07	.597
203.8	60.72	62.26	.701

REDUCED DATA FOR RED SILT
BLUE

CONCENTRATION (MG/L)	LIDAR CROSS SECTION LIKE(VV,DB)	CROSS(VH,DB)	DEPOLARIZATION RATIO
SURFACE: CALM			
8.2	64.69	70.82	.244
40.8	62.24	67.03	.332
122.3	60.58	64.23	.431
203.8	59.86	63.08	.476
SURFACE: CALM			
1.0	64.62	70.41	.243
8.2	64.53	70.73	.240
40.8	62.22	66.98	.334
122.3	60.58	64.30	.425
203.8	59.98	63.12	.486
SURFACE: MEDIUM			
1.0	64.55	70.71	.242
8.2	64.09	70.32	.243
40.8	62.05	66.88	.329
122.3	60.45	64.10	.432
203.8	59.77	63.06	.470
SURFACE: ROUGH			
1.0	64.40	70.87	.225
8.2	64.16	70.39	.238
40.8	61.62	66.58	.319
122.3	60.11	63.54	.454
203.8	59.53	62.69	.482

REDUCED DATA FOR BROWN SILT
RED

CONCENTRATION (MG/L)	LIDAR CROSS SECTION LIKE(VV,DB)	CROSS(VH,DB)	DEPOLARIZATION RATIO
SURFACE: CALM			
8.2	69.78	79.66	.103
24.6	67.57	74.50	.203
41.0	66.48	72.45	.253
57.4	65.75	71.10	.291
106.7	64.73	69.35	.345
194.0	63.30	66.72	.455
291.0	62.40	65.39	.503
SURFACE: MEDIUM			
8.2	69.85	80.26	.091
24.6	67.42	74.36	.202
41.0	66.26	72.35	.246
57.4	65.72	71.05	.294
106.7	64.64	69.30	.345
194.0	63.20	66.57	.460
291.0	62.26	65.14	.516
SURFACE: ROUGH			
8.2	70.13	81.31	.074
24.6	67.33	74.10	.210
41.0	66.07	71.96	.258
57.4	65.31	70.88	.277
106.7	64.39	69.08	.339
194.0	63.02	66.37	.463
291.0	62.08	65.04	.505

REDUCED DATA FOR BROWN SILT
BLUE

CONCENTRATION	LIDAR CROSS SECTION		DEPOLARIZATION
(MG/L)	LIKE(VV,DB)	CROSS(VH,DB)	RATIO
SURFACE: CALM			
8.2	65.81	73.37	.175
24.6	63.54	70.02	.225
41.0	62.79	68.58	.264
57.4	62.28	67.88	.275
106.7	61.58	66.75	.304
194.0	00.00	00.00	.000
291.0	60.53	64.33	.417
SURFACE: MEDIUM			
8.2	65.47	73.20	.169
24.6	63.39	69.89	.224
41.0	62.58	68.61	.249
57.4	62.06	67.97	.257
106.7	00.00	00.00	.000
194.0	00.00	00.00	.000
291.0	60.01	64.19	.382
SURFACE: ROUGH			
8.2	64.80	72.29	.160
24.6	62.83	69.31	.225
41.0	61.99	68.19	.240
57.4	62.26	67.37	.308
106.7	00.00	00.00	.000
194.0	00.00	00.00	.000
291.0	59.61	63.91	.371

RAW MEASUREMENTS

RAW MEASUREMENT OF WHITE SILT

SURFACE ROUGHNESS: C-CALM M-MEDIUM R-ROUGH

CONC. (MG/L)	PMT	SEDIMENT RETURNS (X.001)				WHITE TARGET RETURNS (X.001)				
		RV	RH	BV	BH	RV	RH	BV	BH	
00.00	1150/800	.414	.013	1.77	.294	1.47	1.44	5.16	5.07	R
00.00	1150/800	.414	.013	1.66	.278	1.50	1.46	5.20	5.09	M
00.00	1150/800	.446	.018	1.63	.282	1.52	1.49	5.24	5.10	C
30.30	1150/800	.432	.015	1.64	.257	1.52	1.49	5.24	5.10	R
30.30	1150/800	.472	.017	1.72	.263	1.53	1.52	4.80	4.70	M
30.30	1150/800	.453	.017	1.58	.267	1.54	1.55	4.45	4.35	C
90.90	1150/800	.798	.099	3.11	.771	1.52	1.52	5.85	5.68	R
90.90	1150/800	.750	.100	2.85	.702	1.54	1.51	5.92	5.85	M
90.90	1150/800	.725	.096	2.79	.713	1.55	1.51	6.07	6.00	C
151.5	1150/800	1.05	.200	4.11	1.24	1.50	1.48	6.24	6.10	R
151.5	1150/800	.980	.188	3.89	1.15	1.52	1.50	6.25	6.13	M
151.5	1150/800	.938	.179	3.72	1.13	1.55	1.52	6.26	6.15	C
303.0	1150/800	1.54	.446	6.02	2.32	1.51	1.50	6.29	6.15	R
303.0	1150/800	1.48	.425	5.63	2.20	1.52	1.51	6.26	6.14	M
303.0	1150/800	1.43	.419	5.36	2.12	1.54	1.53	6.24	6.13	C
454.5	1150/800	1.84	.642	6.79	2.99	1.54	1.54	6.27	6.16	R
454.5	1150/800	1.76	.628	6.56	2.85	1.57	1.55	6.54	6.25	M
454.5	1150/800	1.72	.604	6.40	2.79	1.72	.604	6.40	2.79	C

RAW MEASUREMENT OF RED SILT

SURFACE ROUGHNESS: S-SMOOTH C-CALM M-MEDIUM R-ROUGH

CONC. (MG/L)	PMT	SEDIMENT RETURNS (X.001)				WHITE TARGET RETURNS (X.001)				
		RV	RH	BV	BH	RV	RH	BV	BH	
50.00	1150/850	1.05	.261	3.08	.747	1.73	1.62	6.32	5.82	C
50.00	1150/850	1.06	.261	3.16	.725	1.74	1.67	6.38	6.05	M
50.00	1150/850	1.01	.250	3.28	.723	1.74	1.72	6.40	1.08	R
50.00	1150/850	1.04	.259	3.35	.786	1.64	1.64	6.18	6.10	R
50.00	1150/850	1.06	.257	3.42	.820	1.64	1.63	6.22	6.13	M
50.00	1150/850	1.03	.261	3.09	.731	1.64	1.61	6.25	6.15	C
50.00	1150/850	.964*	.240	2.98	.716	1.64	1.61	6.26	6.15	S
250.0	1150/850	2.49	1.02	6.49	2.05	1.71	1.70	6.68	6.61	R
250.0	1150/850	2.31	9.55	5.85	1.90	1.71	1.69	6.65	6.57	M
250.0	1150/850	2.29	.940	5.61	1.85	1.70	1.68	6.63	6.54	C
250.0	1150/850	2.27	.941	5.59	1.83	1.70	1.68	6.63	6.54	S
750.0	1150/850	4.76	2.82	74.7	4.05	1.78	1.76	6.80	6.68	R
750.0	1150/850	4.46	2.68	94.5	3.36	1.77	1.76	6.75	6.70	M
750.0	1100/850	4.73	2.30	21.9	4.21	1.77	1.76	6.75	6.70	R
750.0	1100/850	4.39	2.65	86.9	3.63	1.77	1.76	6.75	6.70	M
750.0	1100/850	3.30	1.96	6.50	2.91	1.69	1.68	6.70	6.70	R
750.0	1100/850	3.10	1.89	6.02	2.58	1.70	1.68	6.80	6.75	M
750.0	1100/850	3.07	1.85	5.85	2.48	1.71	1.68	6.81	6.80	C
750.0	1100/850	3.03	1.84	5.86	2.52	1.71	1.68	6.81	6.80	S
1250.	1100/800	1.96	1.37	3.13	1.51	1.72	1.76	6.90	6.85	C
1250.	1100/800	1.96	1.39	3.25	1.52	1.72	1.74	6.83	6.80	M
1250.	1100/800	2.01	1.40	3.41	1.64	1.73	1.72	6.77	6.75	R
1250.	1100/800	1.93	1.38	3.16	1.50	1.73	1.72	6.77	6.75	S

RAW MEASUREMENT OF BROWN SILT

SURFACE ROUGHNESS: C-CALM M-MEDIUM R-ROUGH

CONC. (MG/L)	PMT	SEDIMENT RETURNS (X.001)				WHITE TARGET RETURNS (X.001)				
		RV	RH	BV	BH	RV	RH	BV	BH	
8.20	1150/850	.640	.047	2.44	.376	1.50	1.49	5.27	5.06	R
8.20	1150/850	.665	.060	2.21	.353	1.50	1.49	5.52	5.23	M
8.20	1150/850	.675	.069	2.10	.351	1.50	1.49	5.67	5.41	C
24.60	1150/850	1.25	.251	5.46	1.18	1.58	1.51	7.43	7.14	R
24.60	1150/850	1.21	.237	4.83	1.03	1.56	1.51	7.47	7.12	M
24.60	1150/850	1.16	.231	4.57	.977	1.55	1.52	7.31	7.10	C
41.00	1150/850	1.66	.417	6.83	1.59	1.57	1.53	7.65	7.42	R
41.00	1150/850	1.59	.384	5.95	1.43	1.57	1.54	7.64	7.36	M
41.00	1150/850	1.51	.375	5.66	1.43	1.57	1.54	7.62	7.30	C
57.40	1150/850	1.98	.538	6.57	1.99	1.57	1.54	7.83	7.69	R
57.40	1150/850	1.81	.518	6.91	1.73	1.58	1.54	7.87	7.68	M
57.40	1150/850	1.80	.508	6.59	1.76	1.58	1.53	7.90	7.66	C
90.20	1150/850	2.51	.836	123.	2.60	1.61	1.58	7.96	7.84	R
90.20	1150/850	2.35	.800	47.9	2.40	1.60	1.58	7.94	7.80	M
90.20	1150/850	2.29	.781	7.76	2.31	.59	1.57	7.91	7.75	C
164.0	1150/850	3.52	1.53	.010	3.68	1.65	1.55	7.74	7.65	R
164.0	1150/850	3.32	1.47	.125	3.43	1.62	1.56	7.69	7.58	M
164.0	1150/850	3.20	1.43	2.42	3.37	1.60	1.57	7.64	7.52	C
246.0	1050/850	2.05	.990	5.61	2.01	1.62	1.55	7.62	7.36	R
246.0	1050/850	1.95	.981	5.18	1.94	1.61	1.57	7.73	7.57	M
246.0	1050/850	1.89	.938	5.06	1.93	1.61	1.59	7.85	7.78	C

APPENDIX D

System Constants

This appendix documents the calibration procedure and equations necessary to convert measurements made by the Lidar Polarimeter System to absolute lidar cross sections. The discussion is separated into several calibration sections listed below.

1. Documentation of system efficiencies
2. Analysis of PMT sensitivity versus power supply voltage
3. Determination of power received
4. Calculation of the Lidar Cross Section from system parameters.

The final reduction equation for the red and blue wavelength system will allow calculation of measured lidar cross section from the basic system parameters; range, output power, PMT supply voltage and computer readout.

DOCUMENTATION OF SYSTEM EFFICIENCIES

Incoming energy which strikes the telescope receiving system is not completely converted to an output voltage. There are some losses associated with the lense system, the optical filter and the photo multiplier. In addition, these particular efficiencies are functions of the wavelength of the incoming radiation. The table below gives the optical efficiencies for both blue and red wavelengths.

	RED	BLUE
Optics	65%	65%
Filters	69%	47%
PMT Relative Sensitivity	40%	98%

ANALYSIS OF PMT SENSITIVITY VERSUS POWER SUPPLY VOLTAGE

The relationship between PMT sensitivity and power supply voltage can be written as follows:

$$\ln S = A \ln E + B$$

where: S - PMT sensitivity in amps per lumen
E - power supply voltage
A and B are constants associated with the particular tube of interest (in this case, the RCA 8645)

The constants A and B were solved using the typical data from the RCA 8645 data sheet. The equation for PMT sensitivity becomes:

$$\ln S = 8 \ln E - 56.03$$

Typical values of S (amps/lumen) for various PMT supply voltages are shown below.

E (volts)	S (amps/lumen)
950	0.31
1050	0.69
1100	1.00
1250	2.77
1350	5.12
1400	6.85
1500	11.89

DETERMINATION OF RECEIVED POWER

The power detected by the received PMT is written as follows:

$$P_{PMT} = P_{INC}(\eta)$$

where: P_{PMT} - power detected by the PMT

P_{INC} - power incident on the receiver

η_1 - optical efficiency of the receiver (optics and filters)

The voltage produced by the PMT

$$V_{OUT} = P_{PMT}(\eta_2)(S)(10^6\Omega)(429\ \text{lumen/watt})$$

where: η_2 - relative sensitivity in percent at the wavelength interest

S - absolute sensitivity in amps/lumen

The total power received can now be written in terms of the PMT output voltage and the various system efficiencies.

$$P_{inc} = \frac{V_{OUT}}{S(\eta_1)(\eta_2)(429\ \text{lumen/watt})(10^6\Omega)}$$

For the red system:

$$P_{inc} = \frac{V}{S}\,(7.67 \times 10^{-8})$$

For the blue system:

$$P_{inc} = \frac{V}{S}\,(7.67 \times 10^{-9})$$

CALCULATION OF MEASURED LIDAR CROSS SECTION FROM SYSTEM PARAMETERS

The lidar cross section is calculated to be:

$$\sigma^{\circ} = \pi R^2 (4\pi) \frac{A_B}{A_R} \frac{P_{INC}}{P_T}$$

where: σ° - normalized lidar cross section
R - range of target
A_B - area of the beam
A_R - area of the receiver
P_{inc} - power incident on the receiver
P_t - transmitted power.

For the blue system:

Beam Divergence = 1 milliradian
Beam Diameter = 0.8 mm

For the red system:

Beam Divergence = 1.7 milliradians
Beam Diameter = 1.0 mm

The area of the receiving optics is $\pi R^2 = 2.56 \times 10^{-3} m^2$. The calculation of A_B for red and blue lidar systems can be accomplished using the information above.

APPENDIX E

Reflectivity Measurements

SEDIMENT: WHITE CLAY

CONCENTRATION (MG/L)	RED LIDAR CROSS SECTION LIKE(VV,DB)	RED LIDAR CROSS SECTION CROSS(VH,DB)	DEPOLARIZATION RATIO
1.0	79.32	93.32	.040
2.9	77.63	90.21	.055
5.7	76.80	88.65	.065
8.6	76.42	88.09	.068
11.4	75.83	86.80	.080
14.3	75.63	86.58	.081
17.2	75.21	85.88	.086
20.0	74.96	85.30	.092
22.9	74.76	84.93	.096
25.7	74.35	84.12	.105
28.6	74.26	83.94	.109
28.6	74.26	84.05	.105
28.6	74.38	84.04	.108
35.8	73.71	83.72	.099
42.9	73.72	83.24	.107
49.9	73.09	82.25	.121
56.9	72.59	81.49	.129
64.1	72.26	81.00	.134
71.1	72.32	80.61	.148
78.2	71.82	79.98	.154
85.9	71.66	79.57	.162
93.1	71.52	79.22	.170
121.7	70.77	77.65	.205
137.1	70.50	77.03	.222
151.4	70.25	76.50	.236
174.3	69.65	75.75	.246
195.8	69.37	74.89	.281
224.9	69.01	74.11	.309
253.4	68.69	73.52	.330
282.1	68.24	72.56	.368
317.9	67.12	71.84	.387
353.6	67.36	71.22	.411
410.8	66.77	70.24	.449
482.3	65.99	69.03	.496
553.8	65.49	68.18	.538
625.3	64.96	67.46	.563
732.6	64.36	66.51	.608

SEDIMENT: WHITE CLAY

CONCENTRATION (MG/L)	BLUE LIDAR CROSS SECTION LIKE(VV,DB)	BLUE LIDAR CROSS SECTION CROSS(VH,DB)	DEPOLARIZATION RATIO
1.0	71.90	84.22	.059
2.9	71.52	83.10	.069
5.7	71.28	81.80	.089
8.6	71.05	81.20	.096
11.4	70.55	79.93	.116
14.3	70.46	79.77	.118
17.2	70.18	79.18	.125
20.0	69.77	78.62	.131
22.9	69.69	78.40	.134
25.7	69.42	77.77	.146
28.6	69.44	77.58	.153
28.6	69.40	77.61	.151
28.6	69.56	77.85	.146
35.8	68.91	77.13	.151
42.9	68.74	76.57	.165
49.9	68.43	75.92	.179
56.9	68.06	75.24	.191
64.1	67.82	74.77	.201
71.1	67.52	74.31	.209
78.2	67.11	74.04	.202
85.9	67.23	73.91	.215
93.1	67.11	73.55	.227
121.7	66.32	72.12	.263
137.1	66.10	71.63	.280
151.4	65.77	71.05	.296
174.3	65.31	70.51	.302
195.8	65.16	69.97	.330
224.9	64.60	69.12	.354
253.4	64.48	68.57	.390
282.1	64.00	67.85	.413
317.9	63.64	67.46	.414
353.6	63.06	66.58	.444
410.8	62.50	65.69	.48
482.3	61.96	64.74	.527
553.8	61.45	64.14	.538
625.3	61.11	63.52	.574
732.6	60.47	62.60	.612

SEDIMENT: WHITE SILT/CLAY (6/9/79)

CONCENTRATION (MG/L)	RED LIDAR CROSS SECTION LIKE(VV,DB)	RED LIDAR CROSS SECTION CROSS(VH,DB)	DEPOLARIZATION RATIO
1.0	76.33	87.83	.071
3.0	75.37	85.00	.109
6.0	75.01	83.67	.136
9.0	74.57	82.82	.150
12.1	74.58	82.74	.153
15.1	74.17	82.18	.158
18.2	74.04	81.95	.162
21.1	73.98	81.83	.164
24.2	73.55	81.20	.171
27.2	73.39	80.79	.182
33.2	73.39	80.53	.193
39.3	72.94	79.59	.216
45.3	72.75	79.35	.219
54.4	72.56	78.89	.233
63.4	72.69	79.06	.231
72.5	72.24	78.92	.215
81.5	72.20	78.80	.217
96.6	71.7	78.20	.223
112.6	71.4	77.78	.231
127.3	71.16	77.54	.230
151.5	70.80	76.67	.259
182.3	70.46	76.15	.270
198.1	70.00	75.55	.279

SEDIMENT: WHITE SILT CLAY (6/19/79)

CONCENTRATION (MG/L)	BLUE LIDAR CROSS SECTION LIKE(VV,DB)	CROSS(VH,DB)	DEPOLARIZATION RATIO
1.0	71.30	84.76	.045
3.0	70.80	82.24	.0712
6.0	70.49	80.57	.098
9.0	69.97	78.97	.126
12.1	69.48	78.30	.130
15.1	69.21	77.67	.142
18.2	68.96	77.29	.147
21.1	69.23	77.35	.154
24.2	68.81	76.80	.159
27.2	68.33	75.90	.175
33.2	68.60	75.88	.187
39.3	68.44	75.42	.200
45.3	68.29	75.03	.212
54.4	68.21	74.77	.221
63.4	67.78	74.25	.226
72.5	68.21	74.82	.219
81.5	67.97	74.54	.220
96.6	67.41	73.67	.236
112.6	67.22	73.15	.255
127.3	66.86	72.81	.254
151.5	66.30	71.84	.279
182.3	66.30	71.60	.295
198.1	65.39	70.57	.303

Reproduced from best available copy.

SEDIMENT: WHITE SILT/CLAY (6/21/79)

CONCENTRATION (MG/L)	RED LIDAR CROSS SECTION LIKE(VV,DB)	RED LIDAR CROSS SECTION CROSS(VH,DB)	DEPOLARIZATION RATIO
3.0	74.03	79.26	.301
6.0	73.71	78.83	.307
9.1	73.59	78.88	.295
12.1	73.42	78.90	.283
15.1	73.22	78.95	.267
18.1	73.43	79.05	.274
21.1	73.02	79.01	.252
24.2	72.92	79.01	.246
30.2	73.47	79.95	.225
36.2	73.13	79.56	.228
44.4	72.77	79.10	.233
59.5	72.54	79.04	.224
60.4	72.20	78.58	.230
68.7	71.94	78.61	.215
77.2	71.90	78.39	.225
85.5	71.62	77.96	.233
93.9	71.44	77.86	.228
124.7	70.52	76.58	.248
156.0	70.18	75.79	.275
186.0	69.64	74.85	.301
217.0	69.38	74.05	.341
247.0	68.95	73.40	.359
278.0	68.55	72.87	.369
308.0	68.14	72.20	.389
338.0	68.34	71.8	.450
407.0	67.49	70.48	.503
481.0	66.81	69.69	.515
552.0	66.33	69.03	.536
627.0	65.86	68.24	.579
773.3	65.31	67.34	.627
826.1	64.34	66.03	.678

NOTE: Effect of tank bottom below 30 mg/l

SEDIMENT: WHITE SILT/CLAY (6/26/79)

CONCENTRATION (MG/L)	BLUE LIDAR CROSS SECTION LIKE(VV,DB)	BLUE LIDAR CROSS SECTION CROSS(VH,DB)	DEPOLARIZATION RATIO
3.0	74.73	77.16	.189
6.0	69.16	76.07	.204
9.1	69.19	76.26	.180
12.1	68.99	75.82	.207
15.1	68.83	75.73	.204
18.1	68.81	75.64	.207
21.1	68.56	75.30	.199
24.2	68.30	75.54	.189
30.2	69.24	77.71	.142
36.2	68.84	76.88	.157
44.4	68.40	75.80	.182
59.5	68.14	75.32	.191
60.4	67.70	74.57	.206
68.7	67.90	74.39	.200
77.2	67.54	74.28	.212
85.5	67.34	74.00	.217
93.9	67.30	73.87	.220
124.7	66.33	72.14	.262
156.0	66.03	71.27	.299
186.0	65.69	70.56	.325
217.0	65.44	69.90	.359
247.0	64.56	68.95	.364
278.0	64.55	68.54	.400
308.0	64.19	67.94	.421
338.0	64.15	67.75	.436
407.0	63.29	66.56	.471
481.0	62.89	65.80	.512
552.0	62.56	65.28	.534
627.0	61.99	64.42	.571
773.3	61.66	63.88	.601
826.1	60.76	62.63	.651

NOTE: Effect of tank bottom below 30 mg/l

Reproduced from best available copy.

SEDIMENT: WHITE SILT (JANUARY 1980)

CONCENTRATION (MG/L)	RED LIDAR CROSS SECTION LIKE(VV,DB)	CROSS(VH,DB)	DEPOLARIZATION RATIO
4.5	76.8	89.10	.058
9.0	75.6	87.9	.060
18.1	74.30	84.80	.099
27.1	73.9	83.8	.101
40.7	73.1	81.7	.137
54.2	72.8	81.6	.133
76.8	72.0	79.5	.190
101.7	71.3	77.9	.216
124.3	71.1	77.6	.221
169.5	71.9	78.2	.234
226.0	71.4	77.2	.265
282.5	70.3	75.10	.335
339.0	69.7	73.8	.357
452.0	67.6	71.4	.418
565.0	66.8	69.8	.499
678.0	66.2	68.8	.547
904.0	65.5	67.3	.591
1130.0	64.3	66.0	.680
1356.0	64.2	66.0	.667
1582.0	63.7	65.0	.749
1808.0	62.9	64.0	.780
2034.0	62.7	63.7	.789
2260.0	62.4	63.3	.910
2543.0	62.0	62.8	.932

SEDIMENT: WHITE SILT (JANUARY 1980)

CONCENTRATION (MG/L)	BLUE LIDAR CROSS SECTION LIKE(VV,DB)	CROSS(VH,DB)	DEPOLARIZATION RATIO
4.5	70.40	80.40	.100
9.0	70.3	79.30	.124
18.1	69.4	77.0	.174
27.1	68.9	76.2	.184
40.7	68.3	74.3	.208
54.2	67.9	74.2	.233
76.8	67.4	72.9	.277
101.7	66.7	71.8	.308
124.3	66.5	71.6	.311
169.5	67.2	71.9	.333
226.0	66.9	71.3	.362
282.5	65.9	69.6	.427
339.0	65.4	68.6	.473
452.0	63.2	66.4	.477
565.0	62.5	65.2	.541
678.0	61.9	64.2	.577
904.0	61.2	63.3	.621
1130.0	60.3	61.9	.687
1356.0	60.2	61.6	.727
1582.0	59.7	61.2	.713
1808.0	59.0	60.3	.749
2034.0	58.8	60.0	.760
2260.0	58.3	59.4	.777
2543.0	58.1	58.3	.920

Reproduced from
best available copy.

SEDIMENT: WHITE SAND

CONCENTRATION (MG/L)	RED LIDAR CROSS SECTION		DEPOLARIZATION RATIO
	LIKE(VV,DB)	CROSS(VH,DB)	
1.0	78.6	99.9	.002
5.7	77.00	90.00	.052
11.3	75.90	86.50	.087
17.0	75.60	85.60	.100
22.6	75.00	84.20	.121
28.3	75.00	83.90	.129
28.3	74.80	83.70	.130
34.0	74.60	83.30	.137
39.6	74.50	82.70	.154
45.3	74.20	82.20	.158
50.9	74.10	82.00	.161
56.6	73.90	81.90	.160
56.6	73.80	81.50	.167
71.9	73.50	80.90	.182
87.4	73.10	80.30	.192
101.6	72.90	79.70	.206
115.7	72.70	79.40	.211
131.3	72.50	79.20	.214
131.3	71.90	78.60	.212
145.5	71.90	78.40	.228
160.0	71.80	78.20	.232
173.8	72.00	78.10	.242
188.0	71.80	77.90	.246
203.0	71.10	77.00	.255
231.0	70.90	76.60	.272
260.0	70.70	76.30	.278
287.0	70.60	76.00	.265
316.0	70.40	75.90	.281
348.0	70.20	75.80	.290
348.0	70.30	76.00	.268
417.0	69.90	75.00	.305
560.0	69.00	73.30	.374
560.0	68.60	72.60	.405
560.0	68.50	72.70	.364
631.1	68.30	72.50	.382
730.1	68.00	71.90	.404
871.6	67.30	70.70	.453
871.6	67.30	70.80	.456
1013.1	67.10	70.50	.460
1225.4	65.80	68.30	.561
1437.6	66.10	68.90	.526

SEDIMENT: WHITE SAND

BLUE

CONCENTRATION (MG/L)	LIDAR CROSS SECTION		DEPOLARIZATION RATIO
	LIKE(VV,DB)	CROSS(VH,DB)	
1.0	72.00	84.20	.060
5.7	70.90	79.50	.136
11.3	69.90	77.40	.175
17.0	70.30	77.40	.195
22.6	69.40	76.30	.209
28.3	69.50	76.00	.223
28.3	69.70	76.50	.212
34.0	69.40	76.00	.222
39.6	69.00	75.20	.240
45.3	68.70	74.70	.250
50.9	68.70	74.60	.256
56.6	68.80	74.60	.267
56.6	68.80	74.60	.259
71.9	68.40	74.00	.279
87.4	68.00	73.40	.288
101.6	67.80	73.00	.297
115.7	67.50	72.70	.303
131.3	67.50	72.70	.305
131.3	67.30	72.20	.325
145.5	67.20	72.00	.330
160.0	67.10	71.90	.333
173.8	67.10	71.80	.342
188.0	66.90	71.60	.345
203.0	66.60	71.10	.358
231.0	66.40	70.50	.366
260.0	66.20	70.20	.392
287.0	66.10	70.20	.390
316.0	65.90	70.10	.384
348.0	65.80	69.70	.408
348.0	65.90	70.20	.376
417.0	65.50	69.30	.419
560.0	64.60	67.80	.478
560.0	64.20	67.10	.512
560.0	64.10	67.20	.496
631.1	64.20	67.00	.526
730.1	63.70	66.40	.541
871.6	63.20	65.60	.568
871.6	63.50	66.10	.544
1013.1	63.20	65.70	.556
1225.4	61.80	63.60	.654
1437.5	62.00	64.20	.601

Reproduced from
best available copy.

SEDIMENT: RED SILT (HIGH CONCENTRATION)

CONCENTRATION (MG/L)	RED LIDAR CROSS SECTION LIKE(VV,DB)	RED LIDAR CROSS SECTION CROSS(VH,DB)	DEPOLARIZATION RATIO
1.0	82.8	84.0	.754
14.8	69.00	74.00	.318
29.6	67.80	72.10	.374
44.4	66.90	70.50	.430
59.2	66.10	69.20	.484
74.0	65.50	68.40	.517
88.8	65.10	67.60	.560
148.0	63.60	65.40	.669
185.0	63.10	64.60	.720
222.0	61.80	62.90	.781
296.0	61.30	62.20	.812
407.0	60.60	61.40	.829
555.0	60.10	60.90	.840
703.0	59.90	60.70	.836
814.0	59.80	60.40	.863
962.0	59.60	60.30	.863
1110.0	59.50	60.10	.867
1295.0	59.40	60.10	.863
1480.0	59.30	60.00	.864
1850.0	59.30	60.00	.851
2220.0	59.20	59.90	.848

SEDIMENT: RED SILT (HIGH CONCENTRATION)

CONCENTRATION (MG/L)	BLUE LIDAR CROSS SECTION LIKE(VV,DB)	CROSS(VH,DB)	DEPOLARIZATION RATIO
1.0	77.20	80.00	.525
14.8	64.50	69.80	.295
29.6	63.90	68.70	.329
44.4	63.60	68.30	.336
59.2	63.20	67.30	.365
74.0	62.70	66.80	.394
88.8	62.40	66.20	.410
148.0	61.80	64.90	.432
185.0	61.40	64.50	.465
222.0	60.50	63.20	.535
296.0	60.30	62.90	.554
407.0	60.60	61.00	.554
555.0	60.30	62.80	.558
703.0	60.60	63.10	.557
814.0	60.60	63.20	.559
962.0	60.50	63.00	.552
1110.0	60.40	62.80	.569
1295.0	60.10	62.50	.572
1480.0	60.10	62.40	.577
1850.0	60.30	63.00	.539
2220.0	60.30	62.90	.542

Reproduced from best available copy.

SEDIMENT: RED SILT

	RED		
CONCENTRATION (MG/L)	LIDAR CROSS SECTION LIKE(VV,DB)	CROSS(VH,DB)	DEPOLARIZATION RATIO
1.0	75.30	82.70	.183
3.7	71.70	77.40	.265
7.3	70.60	76.10	.278
11.0	69.90	75.10	.302
14.6	69.30	74.10	.331
18.3	68.90	73.50	.345
22.0	68.50	72.90	.364
25.6	68.20	72.50	.372
29.3	68.00	72.20	.379
32.9	67.70	71.90	.387
36.6	67.70	71.60	.405
45.8	66.80	70.90	.403
54.9	66.60	70.20	.430
64.1	66.40	69.90	.453
73.2	66.10	69.30	.479
82.4	65.80	68.70	.510
91.5	65.30	68.40	.493
100.7	65.20	68.10	.511
109.8	64.90	67.70	.529
119.0	64.60	67.20	.547
128.1	64.60	67.10	.564
146.4	64.10	66.50	.580
164.7	63.90	66.00	.617
183.0	63.60	65.50	.642
201.3	63.40	65.30	.652
228.8	62.90	64.70	.666
256.2	62.70	64.30	.687
283.7	62.40	63.90	.716
329.3	62.10	63.40	.740
393.5	61.70	62.80	.790

SEDIMENT: RED SILT

CONCENTRATION (MG/L)	BLUE LIDAR CROSS SECTION LIKE(VV,DB)	CROSS(VH,DB)	DEPOLARIZATION RATIO
1.0	70.30	80.10	.105
3.7	67.80	74.40	.219
7.3	66.90	73.00	.246
11.0	66.30	72.10	.263
14.6	66.00	71.70	.272
18.3	65.70	71.10	.291
22.0	65.30	70.50	.303
25.6	65.40	70.60	.300
29.3	65.10	70.20	.311
32.9	65.00	70.10	.309
36.6	64.90	69.70	.329
45.8	64.00	68.90	.330
54.9	64.00	68.60	.347
64.1	64.10	68.40	.364
73.2	63.80	68.00	.380
82.4	63.50	67.50	.391
91.5	63.10	67.20	.389
100.7	63.10	67.20	.393
109.8	63.20	67.10	.403
119.0	62.90	66.60	.424
128.1	62.90	66.60	.419
146.4	62.60	66.30	.429
164.7	62.40	66.00	.435
183.0	62.20	65.70	.451
201.3	62.10	65.40	.467
228.8	61.80	65.20	.465
256.2	61.70	64.90	.478
283.7	61.50	64.60	.493
320.3	61.30	64.30	.503
393.5	61.10	64.00	.511

Reproduced from
best available copy.

SEDIMENT: BROWN SILT (HIGH CONCENTRATION)

CONCENTRATION (MG/L)	LIDAR CROSS SECTION LIKE(VV,DB)	LIDAR CROSS SECTION CROSS(VH,DB)	DEPOLARIZATION RATIO
	RED		
35.2	66.8	70.6	.411
70.4	67.00	71.00	.405
105.6	66.4	69.[illegible]	.449
140.8	65.6	68.7	.492
211.2	65.	67.7	.534
316.8	64.00	66.1	.619
422.4	63.3	65.	.66
528.0	63.3	64.5	.746
704.0	62.5	63.8	.731
880.0	62.1	63.4	.734
1144.	61.7	62.9	.758
1408.	61.4	62.6	.756
1760.	61.3	62.5	.766
2200.	61.2	62.4	.770
2640.	61.	62.2	.753
3520.	61.0	62.1	.766
4400.0	60.8	62.00	.762
5280.	60.8	62.1	.745
6160.0	60.7	62.00	.741
	BLUE		
35.2	64.5	70.1	.279
70.4	63.6	69.7	.312
105.6	63.3	69.00	.340
140.8	62.7	67.00	.37
211.2	62.3	66.3	.357
316.8	61.7	65.2	.449
422.4	61.3	64.5	.466
528.0	61.2	64.3	.493
704.0	61.1	64.2	.494
880.0	61.00	63.7	.512
1144.	60.4	63.3	.514
1408.	60.3	63.1	.519
1760.	60.7	63.5	.526
2200.	60.3	63.2	.516
2640.	60.5	63.1	.516
3520.	60.1	63.0	.511
4400.0	60.0	62.9	.511
5280.	60.0	63.0	.504
6160.0	59.8	62.8	.494

SEDIMENT: BROWN SILT

CONCENTRATION (MG/L)	RED LIDAR CROSS SECTION LIKE(VV,DB)	CROSS(VH,DB)	DEPOLARIZATION RATIO
1.00	76.50	85.76	.118
3.9	73.29	80.46	.192
7.8	71.97	78.49	.223
11.6	71.05	77.31	.237
15.5	70.55	76.51	.254
19.4	70.24	75.94	.269
23.3	69.70	75.49	.264
27.2	69.51	75.01	.282
31.0	69.17	74.48	.295
40.7	68.84	73.62	.318
50.4	68.20	72.90	.339
60.1	67.85	72.34	.356
69.8	67.34	71.74	.363
79.5	67.20	71.31	.388
89.2	66.91	70.87	.402
98.9	66.75	70.51	.420
108.6	66.49	70.28	.417
118.3	66.33	69.98	.431
128.0	66.11	69.59	.449
137.7	66.12	69.45	.464
157.1	65.63	68.88	.473
176.5	65.43	68.51	.492
195.9	65.19	68.08	.514
215.3	64.75	67.63	.516
234.7	64.67	67.48	.523
254.1	64.53	67.34	.523
302.6	64.07	66.72	.543
351.1	63.67	66.08	.573
399.6	63.30	65.50	.604
448.1	63.15	64.89	.670
496.6	63.01	64.78	.664
545.1	62.88	64.71	.656
642.1	62.93	64.82	.647
739.1	62.87	64.57	.675

Reproduced from
best available copy.

SEDIMENT: BROWN SILT

CONCENTRATION (MG/L)	BLUE LIDAR CROSS SECTION LIKE(VV,DB)	BLUE LIDAR CROSS SECTION CROSS(VH,DB)	DEPOLARIZATION RATIO
1.00	71.58	82.39	.083
3.9	69.04	76.32	.187
7.8	67.61	74.23	.218
11.6	66.90	73.15	.237
15.5	66.91	72.92	.251
19.4	66.42	72.34	.256
23.3	65.82	71.79	.253
27.2	65.72	71.58	.259
31.0	65.50	71.14	.273
40.7	65.15	70.61	.284
50.4	64.94	70.19	.299
60.1	64.53	69.57	.313
69.8	64.04	69.14	.309
79.5	64.21	69.01	.331
89.2	63.92	68.62	.339
98.9	63.69	68.30	.346
108.6	63.53	68.16	.345
118.3	63.35	67.82	.357
128.0	63.19	67.59	.363
137.7	63.29	67.60	.371
157.1	62.97	67.23	.374
176.5	62.76	66.90	.385
195.9	62.73	66.77	.395
215.3	62.44	66.48	.394
234.7	62.45	66.44	.399
254.1	62.53	66.36	.414
302.6	62.17	65.93	.421
351.1	62.11	65.73	.435
399.6	61.86	65.40	.443
448.1	61.68	65.12	.452
496.6	61.50	64.86	.462
545.1	61.71	64.99	.469
642.1	61.88	65.24	.461
739.1	61.87	65.06	.480

SEDIMENT: ALGAE & WHITE SILT

RED

CONCENTRATION ALGAE (LITERS)	CONCENTRATION SILT (MG/L)	LIDAR CROSS SECTION LIKE(VV,DB)	LIDAR CROSS SECTION CROSS(VH,DB)	DEPOLARIZATION RATIO
1.0	0.0	75.30	82.50	.192
5.0	0.0	75.30	82.90	.175
8.0	0.0	75.10	82.70	.173
10.0	0.0	75.00	82.70	.173
12.0	0.0	75.20	82.70	.179
15.0	0.0	75.70	83.20	.173
18.0	0.0	75.40	83.30	.161
20.0	0.0	75.40	83.20	.169
0.0	21.6	73.90	81.90	.160
0.0	43.2	73.20	80.70	.175
0.0	86.4	71.40	78.50	.197
0.0	129.6	71.00	77.80	.211
0.0	216.0	69.80	75.40	.270
0.0	324.0	69.00	74.10	.310
0.0	540.0	67.30	71.00	.425
		BLUE		
1.0	0.0	70.30	79.10	.132
5.0	0.0	70.80	79.60	.131
8.0	0.0	70.80	79.60	.131
10.0	0.0	71.10	79.90	.131
12.0	0.0	71.50	80.40	.130
15.0	0.0	71.90	81.00	.123
18.0	0.0	71.70	80.50	.131
20.0	0.0	72.00	80.90	.129
0.0	21.6	70.10	77.30	.190
0.0	43.2	69.10	75.90	.205
0.0	86.4	67.40	73.30	.254
0.0	129.6	67.00	72.70	.272
0.0	216.0	65.60	70.40	.334
0.0	324.0	64.90	69.30	.364
0.0	540.0	63.20	66.40	.479

SURFACE: CALM

SEDIMENT: WHITE SILT

CONCENTRATION (MG/L)	RED LIDAR CROSS SECTION LIKE(VV,DB)	CROSS(VH,DB)	DEPOLARIZATION RATIO
1.0	73.79	87.74	.040
30.3	73.77	88.08	.037
90.9	71.76	80.43	.136
151.5	70.64	77.75	.195
303.0	68.78	74.08	.295
454.5	68.15	72.58	.360
SURFACE: MEDIUM			
1.0	73.78	89.07	.030
30.3	73.57	88.03	.036
90.9	71.58	80.26	.136
151.5	70.37	77.48	.194
303.0	68.58	73.97	.289
454.5	67.93	72.38	.361
SURFACE: ROUGH			
1.0	73.56	89.07	.031
30.3	73.92	88.43	.035
90.9	71.26	80.34	.124
151.5	70.01	77.15	.193
303.0	68.37	73.73	.292
454.5	67.69	72.26	.349

SURFACE: CALM

SEDIMENT: WHITE SILT

CONCENTRATION (MG/L)	BLUE LIDAR CROSS SECTION LIKE(VV,DB)	BLUE LIDAR CROSS SECTION CROSS(VH,DB)	DEPOLARIZATION RATIO
1.0	68.71	76.21	.178
30.3	68.14	75.76	.173
90.9	67.02	72.89	.259
151.5	65.90	71.00	.309
303.0	64.30	68.25	.403
454.5	63.92	67.21	.468
SURFACE: MEDIUM			
1.0	68.60	76.27	.171
30.3	70.32	76.16	.156
90.9	66.82	72.85	.249
151.5	65.70	70.91	.301
303.0	64.10	68.10	.398
454.5	63.63	67.06	.454
SURFACE: ROUGH			
1.0	68.29	76.01	.169
30.3	68.69	76.62	.161
90.9	66.39	72.31	.255
151.5	65.46	70.49	.314
303.0	63.83	67.88	.394
454.5	63.30	66.78	.448

SURFACE: CALM

SEDIMENT: RED SILT

CONCENTRATION (MG/L)	RED LIDAR CROSS SECTION LIKE(VV,DB)	CROSS(VH,DB)	DEPOLARIZATION RATIO
8.2	68.62	74.63	.250
40.8	65.06	68.81	.422
122.3	62.26	64.35	.618
203.8	60.89	62.32	.719
SURFACE: CALM			
1.0	68.48	74.24	.265
8.2	68.33	74.27	.255
40.8	65.02	68.81	.418
122.3	62.20	64.32	.613
203.8	60.80	62.46	.683
SURFACE: MEDIUM			
1.0	68.47	74.38	.257
8.2	68.21	74.34	.244
40.8	65.00	68.79	.418
122.3	62.13	64.23	.617
203.8	60.80	62.24	.701
SURFACE: ROUGH			
1.0	68.68	74.69	.250
8.2	68.29	74.33	.249
40.8	64.68	68.53	.412
122.3	61.83	64.07	.597
203.8	60.72	62.26	.701

SURFACE: CALM

SEDIMENT: RED SILT

CONCENTRATION (MG/L)	BLUE LIDAR CROSS SECTION LIKE(VV,DB)	BLUE LIDAR CROSS SECTION CROSS(VH,DB)	DEPOLARIZATION RATIO
40.8	62.22	66.98	.334
122.3	60.58	64.30	.425
203.8	59.98	63.12	.486
SURFACE: MEDIUM			
1.0	64.55	70.71	.242
8.2	64.09	70.32	.243
40.8	62.05	66.88	.329
122.3	60.45	64.10	.432
203.8	59.77	63.06	.470
SURFACE: ROUGH			
1.0	64.40	70.87	.225
8.2	64.16	70.39	.238
40.8	61.62	66.58	.319
122.3	60.11	63.54	.454
203.8	59.53	62.69	.482

SURFACE: CALM

SEDIMENT: BROWN SILT

CONCENTRATION (MG/L)	RED LIDAR CROSS SECTION LIKE(VV,DB)	RED LIDAR CROSS SECTION CROSS(VH,DB)	DEPOLARIZATION RATIO
8.2	69.78	79.66	.103
24.6	67.57	74.50	.203
41.0	66.48	72.45	.253
57.4	65.75	71.10	.291
106.7	64.73	69.35	.345
194.0	63.30	55.72	.455
291.0	62.40	65.39	.503
SURFACE: MEDIUM			
8.2	69.85	80.26	.091
24.6	67.42	74.35	.202
41.0	66.26	72.35	.246
57.4	65.72	71.05	.294
106.7	64.64	69.30	.345
194.0	63.20	66.57	.460
291.0	62.26	65.14	.516
SURFACE: ROUGH			
9.2	70.13	81.31	.074
24.6	67.33	74.10	.210
41.0	66.07	71.96	.258
57.4	65.31	70.88	.277
106.7	64.39	69.09	.339
194.0	63.02	55.37	.463
291.0	62.08	65.04	.505

SURFACE: CALM

SEDIMENT: BROWN SILT

CONCENTRATION (MG/L)	BLUE LIDAR CROSS SECTION LIKE (VV, DB)	CROSS (VH, DB)	DEPOLARIZATION RATIO
8.2	65.81	73.37	.175
24.6	63.54	70.02	.225
41.0	62.79	68.58	.264
57.4	62.28	67.88	.275
106.7	61.58	66.75	.304
194.0	00.00	00.00	.000
291.0	60.53	64.33	.417
SURFACE: MEDIUM			
8.2	65.47	73.20	.169
24.6	63.30	69.89	.224
41.0	62.58	68.61	.249
57.4	62.05	67.97	.257
106.7	00.00	00.00	.000
194.0	00.00	00.00	.000
291.0	60.01	64.19	.382
SURFACE: ROUGH			
8.2	64.80	72.20	.160
24.6	62.83	69.31	.225
41.0	61.99	68.19	.240
57.4	62.26	67.37	.308
106.7	00.00	00.00	.000
194.0	00.00	00.00	.000
291.0	59.61	63.91	.371